THE UNIVERSITY
of EDINBURGH

The Influence of Snow Microstructure and Properties on the Grip of Winter Tyres

Fergus Cuthill

THE UNIVERSITY
of EDINBURGH

THESIS SUBMITTED IN PARTIAL FULFILMENT OF

THE REQUIREMENTS FOR THE DEGREE OF

DOCTOR OF PHILOSOPHY

TO THE

UNIVERSITY OF EDINBURGH

October 2017

Declaration

I declare that this thesis has been composed solely by myself and that it has not been submitted, either in whole or in part, in any previous application for a degree. Except where otherwise acknowledged, the work presented is entirely my own.

Fergus Cuthill

October 2017

Abstract

The friction of tyres on roads has been of practical importance for many years with nearly 80% of terrestrial traffic making use of rubber tyres. Tyres provide the grip required for vehicle acceleration, braking and cornering. In order for a tyre to grip on a snow covered surface friction mechanisms such as “ploughing”, (where sharp tread block edges dig into and break bonds between the snow grains) and fluid film lubrication must be considered. These are not present when a tyre interacts with tarmac. In addition metamorphism of the snow over time can result in variations of the structure and mechanical properties, this can occur rapidly especially when dealing with temperatures close to snows melting point.

When full car-scale outdoor testing is carried out the snow conditions cannot be controlled and vary daily. This means the snow properties must be measured every day so that any observed variations in friction can be attributed to the tyres rather than the snow. At present the simple measurements being carried out on the snow tracks have not proved sufficient to pick up on the variations in the snow. This leads to inconsistent results: one tyre behaves differently on two different days, even though the snow was measured to be the same. This has resulted in the need for further study of the way snow variations influence the grip of winter tyres.

The primary aim of this study is to identify which snow properties contribute to the friction of tyres on snow and be able to estimate the friction from measurements of snow properties. This work is the first comprehensive study to combine: multiple snow properties, microstructure characterisation, measurement of friction behaviour and different snow (both artificial and natural).

In order to study the way snow affects the grip of winter tyres, methods of manufacturing artificial snow with consistent mechanical properties and microstructure are used. A method of blending ice chips (a solid state fracturing process) and

compressing the resulting snow to form a test track was developed during a previous PhD carried out in our group. An alternate snow microstructure was created by using an established process of creating snow by vapour deposition. The process was simplified and downscaled, the resulting snow consisted of large dendritic grains, very different to the blended ice chips. Both snows were pressed in identical manners to create snow testing tracks. In addition, natural snow collected from the field was tested to compare with the artificial snow.

In order to investigate how the variations in the snow affected the friction of tyres extensive testing was carried out in a cold room using a linear tribometer, using procedures established in previous studies. Two analytical rubber samples were used to investigate the friction, a rounded edge sample and a siped sample. Testing was carried out at -10°C at speeds of 0.01m/s, 0.1m/s and 1m/s.

A significant part of this PhD involved the development of new methods and equipment which have not been used to study snow in this way before. In order to characterise mechanical properties, shear testing, compression testing and cohesion testing were carried out. To investigate snow microstructure, surface profilometry, microscopy and X-ray microtomography were used.

Correlating the changes observed in snow characteristics with the changes recorded in the coefficient of friction has allowed the development of an empirical equation. This can be used to predict the coefficient of friction of a given snow based on three relatively simple snow measurements: a compression test to calculate the effective modulus, a roughness measurement to calculate the peak count density and a snow penetration test.

For the first time this study allows us to use the empirical equation to estimate the relative contributions of the ploughing and surface friction mechanisms to the total

friction. This allows the comparison of full car-scale test data as it is now possible to account for variations in the snow test tracks.

Lay Summary

Driving a car on snow in winter can be significantly more dangerous than on dry roads. This is due to the reduced grip the tyres can achieve on a snowy or icy surface. Tyre manufacturers develop specific tread patterns and rubber types for their winter specific tyres in an attempt to maximise available grip.

When designing and testing these tyres it is necessary to understand where any differences in the measured grip come from. This means it is necessary to gain a thorough understanding of how a tyre interacts with a snow surface and what friction mechanisms are occurring to give a tyre its grip. It is also necessary to look at how variations in the snow can influence the friction mechanisms.

The mechanical properties and behaviour of snow can be complex. Snow is made up of thousands of small crystals of ice which can be many different shapes and sizes, from round balls 0.1mm across to large plate shapes over 2cm across. These grains can form bonds between each other; these bonds can be easily broken but will rapidly re-form when a new contact between grains is made. This means that snow properties can vary from day to day. This variation in properties makes it difficult to interpret whether a new tyre design is achieving better grip due to a better design or due to a variation in the snow it is being tested on.

In order to investigate how the mechanical properties of snow influence the grip of winter tyres, artificial snow was created in the laboratory. This provided repeatable snow properties which could be used to investigate the different friction mechanisms and how they relate to the mechanical properties of the snow. In addition natural snow was collected from the field to compare the laboratory results to real and varied snows.

Mechanical testing and imaging of the various artificial snow types was performed and the results compared to the friction of rubber samples on the same snows. By looking for trends in the results it was possible to gain an understanding of how the mechanical properties of the snow influence the grip of the rubber samples.

With this information tyre manufacturers are able to better understand where any variations in their full scale outdoor tyre tests are coming from; improved design or variations in the snow properties.

Acknowledgements

Firstly I would like to thank my first supervisor, Dr Jane Blackford. She has provided incredible support and encouragement throughout both the highs and lows of my PhD, her insights and discussion on the research have been invaluable and I really appreciate all the effort she has put into helping me.

Thanks to Professor Vasileios Koutsos, my second supervisor. He was able to provide clear, concise and focused feedback on my work to keep me on track to achieve my research aims.

The support of Michelin both financially and technically has made it possible to complete this work. The entire team has provided great support, resources and discussions but I would like to give special thanks to Jean-Baptiste Fourrel-de-Frettes for his incredible knowledge and insight into the topic along with all the time you given me with the countless phone calls and visits to Edinburgh for discussions.

I have had many different office mates throughout my time here but I would especially like to thank Dr Tom Barraclough and Dr Tamas Parkani for providing excellent support and input to my work, along with the fun times we had together outside of work and at lunch times.

Last but not least I would like to thank Sophie and Isla for providing never ending encouragement and enthusiasm to get me through even when times got hard and the long hours and weekends at work took time away from us all. I really appreciate it, thank you.

Contents

List of Tables

List of Figures

List of Acronyms

Blended 130	Blended snow prepared with 130 bar compression
Blended 170	Blended snow prepared with 170 bar compression
CT	Computed tomography
CTI	Snow compaction test index
DMP	Dimethyl phthalate
DSLR	Digital single lens reflex camera
FEM	Finite element modelling
FRIMA	Friction-Machine
Natural 130	Natural snow prepared with 130 bar compression
Natural 170	Natural snow prepared with 170 bar compression
PCD	Peak count density
SR	Slip ratio
VD	Vapour deposition
VD 130	Vapour deposition snow prepared with 130 bar compression
VD 170	Vapour deposition snow prepared with 170 bar compression
XMT	X-ray microtomography

List of Symbols

μ	Coefficient of friction
$\mu_{Ploughing}$	Friction contribution from ploughing mechanism
$\mu_{Surface}$	Friction contribution from surface mechanisms
μ_{Total}	Total combined friction from all mechanisms
θ	Internal angle of friction (°)
c	Cohesion contribution to shear strength
s	Shear strength (MPa)
V_x	Vehicle velocity (m/s)
r_{eff}	Effective tyre radius (m)
ω_W	Rotational speed of tyre (rads/s)
V_g	Sliding speed (m/s)
L_x	Contact patch length (length of tyre in contact with road / snow) (mm)
d_x	Sliding Distance (m)
E	Compressive "effective" modulus (MPa)
E_{ice}	Elastic modulus of ice (MPa)
L_0	Length of roughness measurement (mm)
Pa	Arithmetic mean of the surface roughness (µm)
Ra	Arithmetic mean of the surface roughness for unfiltered profile(µm)
Pku	Kurtosis of the surface roughness
Rku	Kurtosis of the surface roughness for unfiltered profile

1 Introduction

1.1 Overview

With the ever increasing reliance on automotive vehicles for transportation people are demanding more and more from their cars. A car is expected to perform in all conditions: hot, cold, wet, dry, snowy. In an ideal setup a vehicle would be able to do this but unfortunately this is not the case. The demands of driving in a hot climate are different to those of driving in a cold, ice and snowy region. The difference in requirements are mainly down to the interface between the car and the driving surface: the tyre. A tyre provides the grip required for acceleration breaking and cornering and as such is vital for safe driving on any road.

Maintaining grip and control while traveling on snow is a difficult task for any tyre. Considerable effort is made by tyre designers to manufacture a tyre which can grip on snow, ice and tarmac. In order to achieve this, iterations of testing and re-design are required. Testing of the tyres can be done in multiple ways, often starting with computer models for the initial designs of the tyre, moving to laboratory testing of tread patterns and rubber compounds and finally with complete tyres mounted to vehicles for full scale testing.

The data from testing the tyres has to be accurate and repeatable if the results are to be used to help design better tyres. However, snow is a variable material which can rapidly change its structure and properties. Changes to the snow structure occur via several processes including melting and sintering processes, resulting in the snow grains altering their shape and often causing clusters of snow grains to coalesce together. Changes in temperature, humidity and sunlight affect how sintering and melting processes progress and thus the structure and properties of the snow.

In the laboratory, these environmental factors are relatively controllable, this means if snow samples are created and tested following a set protocol it is possible to achieve

consistent and repeatable results between samples. When it comes to full car-scale testing in the field, the environment and therefore the snow is rapidly changing, a solution to this is to measure the snow every day in order to take account of the variation in the snow structure and thus friction testing results.

1.2 PhD Aims and Scope

The primary aim of this study is to identify which snow properties contribute to the friction of tyres on snow and be able to estimate the friction from measurements of snow properties. This was work has been made possible by the previous work carried out at the University of Edinburgh by Gerasimos Skouvaklis and Sam Ella, who set up the cold room laboratory and carried out initial studies into the grip of winter tyres on snow and ice. Through the PhD, there was extensive collaboration with Michelin who sponsored the work and whose input, discussion and background knowledge on the topic has been invaluable to the study.

In order to carry out these experiments snow with varied mechanical properties had to be produced, this was done by:

1. Blending ice chips to a powder. A process developed during a previous PhD at Edinburgh University by Gerasimos (Skouvaklis, 2010)
2. Making snow using a vapour deposition process, much more similar to the process which occurs in nature. This process was adapted from the process described by (Schleef et al., 2014)
3. Collecting natural snow in the field.

Next, the different snows had to be tested, both to characterise the snows and to measure the friction of analytical rubber samples. The characterisation was done using:

density testing, shear testing, compression testing, surface profilometry, optical microscopy and X-ray microtomography (CT Scanning). Extensive work has been done on basic snow mechanics and is summarised well by (Mellor, 1975) and (Butkovich, 1956) which proved useful in designing tests for this study. Less work has been done on X-ray microtomography and surface profilometry but the work by (Coléou et al., 2001), (Schleef et al., 2013) and (Ella, 2014) has proved to be excellent background for designing the experiments.

The friction testing was done using a large linear tribometer and two rubber samples; a rounded edge sample to measure surface effects and a siped sample to measure ploughing effects. Finally, the snow characterisation and friction measurements are brought together in an effort to understand how and why the snow properties effect tyre grip on snow.

1.3 Thesis Structure

This thesis contains seven chapters. Chapter 2 sets out the fundamentals of rubber friction on snow and reviews literature on the current methods used to characterise snow and measure snow properties.

Chapter 3 details the experimental methods used throughout the research, beginning with a description of the cold laboratory where the majority of the testing was carried out, and then explaining how the artificial snow was created and the processes and procedures which were followed in order to complete the comprehensive testing plan which included measurement of: friction, density, compaction, surface roughness, shear strength, compression strength, cohesion, X-ray microtomography and finishing with the imaging of snow using optical microscopy.

Chapter 4 presents the results gathered from all the mechanical testing and characterisation of the snow which was carried out, except the friction data.

Chapter 5 presents the results of all the friction testing of all the snows. The volume and complexity of the friction data required extensive analysis and as such merits a separate dedicated chapter. Friction tests were carried out on different snows using both siped rubber samples and smooth rubber samples in order to investigate different friction mechanisms. The raw data from each individual friction measurement was examined individually in an attempt to identify where subtle differences in the friction measurements were resulting from.

Chapter 6 presents the process of drawing together the considerable amount of data on both friction and snow characterisation with the aim of correlating the variations observed in the properties and characteristics of the snow with the differences recorded in the coefficient of friction. This was done through the development of an empirical formula which relates measured properties of the snow to the coefficient of friction.

Using three individual measurements of the snow properties (compressive strength, surface roughness & snow compaction) it was possible to predict the expected coefficient of friction of a rubber sample on that snow.

Chapter 7 presents conclusions which could be drawn from this research, as well as recommendations for future work.

2 Literature Review

Summary

This chapter begins with an introduction to the fundamentals of snow and ice friction, moving to look more specifically at rubber friction mechanisms on snow. This leads into the various properties and characteristics of snow which may have an influence on friction. And finally looking at the established methods for testing snow properties, concentrating specifically on those methods which have been used to test high density snows which are the subject of this study.

2.1 General Background

2.1.1 Snow and ice friction

The study of friction on snow and ice has been of interest to the scientific community for more than 100 years, originally it was thought that the low friction observed on ice was due to a liquid layer forming between the ice and the object sliding which was caused by pressure melting. More recently it has been proved that pressure melting does not cause a meltwater layer until temperatures rise above -2°C (Barnes et al., 1971). Instead the theory of frictional heating suggested by (Bowden et al., 1939) has become the accepted reason for the meltwater layer which has been observed. This meltwater layer acts as lubrication for materials sliding on snow or ice giving its characteristically low coefficient of friction. Other general trends seen in snow and ice friction are: an increase in coefficient of friction as temperature decreases (Bowden et al., 1939, Marmo et al., 2005, Bäurle et al., 2007). Secondly a decrease in friction is seen as speed increases while sliding on ice due to the increase in frictional heating (Bäurle et al., 2007, Blackford et al., 2012). Other studies have noted the importance of surface roughness on the coefficient of friction and its influence on real area of contact (Lang et al., 1982, Skouvaklis, 2010, Ella, 2014). (Mellor, 1975, Colbeck, 1992) provide detailed reviews of the various features of snow and ice which influence the friction, providing a useful insight into what tests have been done to measure the influence of various property changes such as snow wetness or grain size.

2.1.2 Rubber Friction

Rubber tends to exhibit a relatively high coefficient of friction because of the way it behaves. Firstly a viscoelastic material such as rubber exhibits hysteresis (internal energy dissipation). This means that stress and strain are out of phase. A perfectly elastic material would have stress and strain perfectly in phase and a completely perfect fluid would have stress and strain 90° out of phase. Rubber lies somewhere in the middle and it is this phase lag between stress and strain which means rubber does not recover immediately from a deformation which gives it a lateral reaction force to a vertical indentation (Ella et al., 2013).

Secondly the rubber can deform around protrusions, both macroscopic and microscopic, resulting in a higher real contact area giving a higher coefficient of friction. Although the general material properties of rubber intrinsically give it a high coefficient of friction, when considering tyre friction on snow the sculpture of the tyre tread must be taken into account. The addition of tread blocks and then adding sipes to these tread blocks drastically alters the grip behaviour of a tyre, to the point where the majority of the friction effects observed on snow are coming from the sculpture rather than the rubber properties (Ripka et al., 2009, Ella, 2014).

2.1.3 Mechanical Properties and Structure of Snow

Tyre friction on snow is different to tyre friction on tarmac. The dominant friction mechanism changes from adhesion and indentation of the rubber to ploughing and edge effects of the tread blocks digging into the snow. Due to the fact that so much of the tyre grip comes from the ploughing and edge effects of tread blocks and sipes (Ripka et al., 2009) determining the snow characteristics which influence these edge effects is important for understanding the overall grip of a winter tyre. Further work looking into

the interactions during ploughing is required; one source of information regarding the ploughing interaction and the properties of snow that influence ploughing friction is from those groups who carry out finite element modelling of snow friction. Their models need to be based on mechanical properties of snow and as such, they make mechanical tests on snow to determine these properties and validate their models.

The following is a list of properties of snow, some of which will have a large influence on the friction of rubber on the snow.

1. Density
2. Elastic Properties
    a. Young's modulus
    b. Shear modulus
    c. Bulk modulus
    d. Poisson's Ratio
3. Shear Strength
4. Compressive Strength
5. Tensile Strength
6. Fracture Toughness
7. Hardness
8. Creep Resistance

Much work has been done determining various mechanical properties of snow (Butkovich, 1956, Mellor, 1964, Mössner et al., 2013) provide details of studies they have carried out and their methods. (Mellor, 1964) gives an excellent review of other studies. The most common tests are uniaxial strength tests, compression, tension and shear. Some of the main studies using these tests are summarised in Appendix 8.1.

Snow has a complex structure which is influenced by many factors such as time, temperature and humidity. These external factors can cause changes to the snow structure both during formation and once the snow is settled on the ground, the main characteristics influenced by these external factors are:

1. Grain Size
2. Grain Type
3. Intergranular bond area
4. Surface Roughness
5. Moisture Content

The grain size, type and intergranular bond area will all have an influence on the measureable properties listed above. The surface roughness is a result of many things including grain size and type along with how the surface was formed (scraping or air flow across the surface for example). The moisture content of the snow can be important when considering friction on snow, especially near the melting point, due to the formation of a meltwater layer and potentially reaching a fully lubricated state.

To illustrate some of the different microstructures possible Figure 2.1 shows two of the more extreme types. A round ball shape ice crystal and a dendritic snow grain. Both of which are artificially created in the lab but both types can also be found in nature.

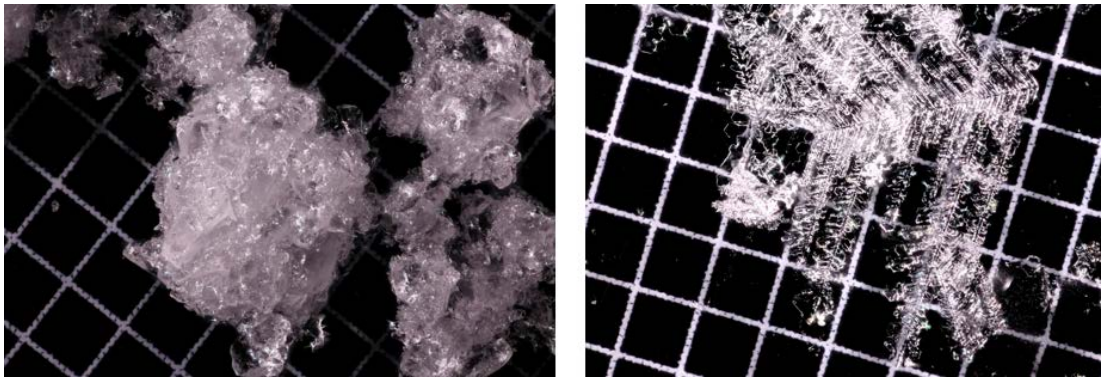

Figure 2.1 - Different snow microstructures. Left - Rounded ice balls. Right - Dendritic snow grain. (Both artificial) (1mm square reference background)

Snow grain sizes can vary from below 0.1mm to greater than 20mm across. This grain size can have a large influence on the density of freshly fallen snow, which can be in the range of 100kg/m^3 to 400kg/m^3. Once the density rises above 700kg/m^3 it can be considered more like ice than snow. Figure 2.2 below shows some of the possible ice grains which are found in nature and the humidity and temperature conditions in which they can be found. This is useful to understand the extended range of snow grain shapes and sizes which are possible both in nature and the lab.

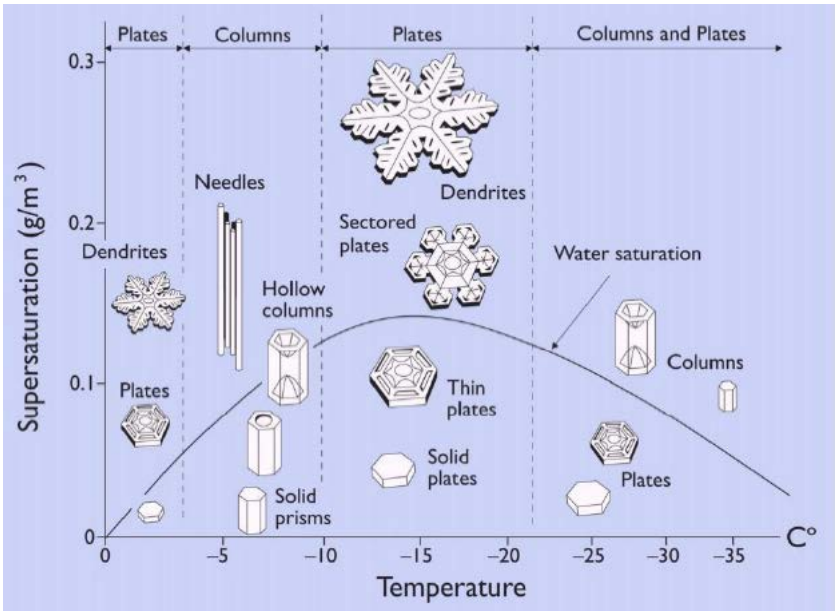

Figure 2.2 - Nakaya Supersaturation curve detailing the types of ice grains generally found in certain humidity and temperature ranges. (Taken from (Libbrecht, 2005))

2.2 Friction Mechanisms

During the PhD of Sam Ella at The University of Edinburgh, extensive work was done to investigate the different friction mechanisms that may occur in tyre-snow friction. The following is a summary of the main mechanisms resulting in energy dissipation, causing friction on snow. The influence of each mechanism on the grip of a sample will depend on the different parameters of the test such as temperature, test speed as well as the particular snow characteristics.

2.2.1 Adhesion of rubber

Adhesion is the formation of van der Waals bonds between the rubber surface and the snow. In the situation of a tyre rolling the bonds are formed, stretched and then broken (Figure 2.3) (Ella et al., 2013). Adhesion applies mostly when materials are similar in molecular structure, macroscopically smooth and have time to bond (Rabinowicz, 1984). This means that during sliding, the friction from adhesion is very small as there is very

little time for the bonds to form and the surfaces are so different that bonds do not readily form.

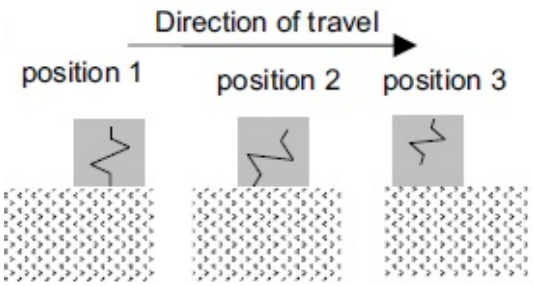

Figure 2.3 - Rubber adhesion from van der Waals bonds forming (position1), stretching (position 2) and breaking (position 3) (Ella et al., 2013)

2.2.2 Indentation of Rubber

Friction from indentation of the rubber occurs as a result of rubber's viscoelasticity as described in section 2.1.2. Figure 2.4 illustrates the forces applied to a rubber sample as a result of indentation. For indentation to occur there does not need to be any adhesion, however, if there is adhesion of the surface the indentation increases. A combination of indentation and adhesion form the two main mechanisms of grip on dry roads (Michelin, 2001). At low temperatures (below -10°C) where there is less possibility of the snow forming a fluid film, indentation may have a significant role in the grip of winter tyres especially on higher density snow (>600kg/m^3) where ploughing may not be so prominent and the surface profile of the snow is rough enough to cause rubber indentation.

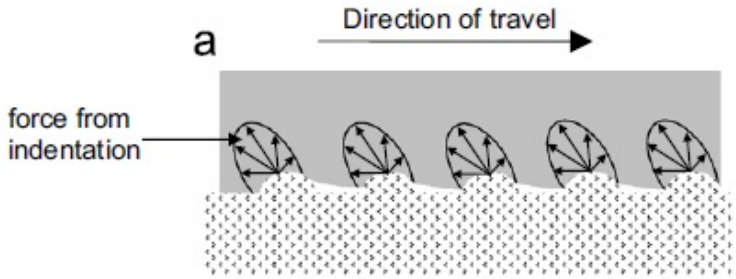

Figure 2.4 - Frictional force from indentation of rubber resulting from rubbers viscoelasticity (Ella et al., 2013)

2.2.3 Ploughing

Ploughing friction results partly from the expenditure of energy in the compacting of the snow beneath the slider and partly from shearing snow at the front and edges of the slider (Mellor, 1964). However it does not appear to be a simple shear process which is occurring at the leading edge of the sipe, instead a combination of compression, fracture and shearing (Figure 2.5). As the tread block plunges into the snow the contributions

of each part of the ploughing mechanism are likely to change with a higher dependence on the compressive strength the deeper the block goes.

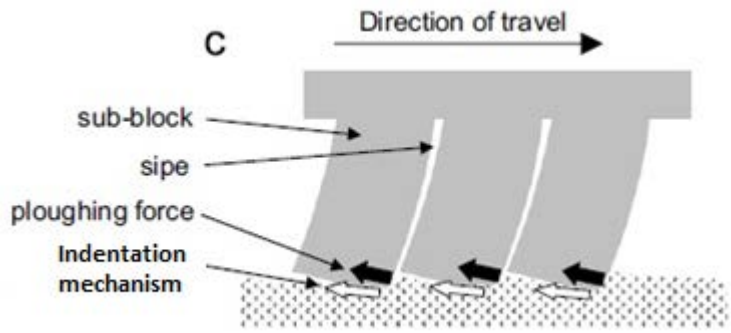

Figure 2.5 - Ploughing force from compaction and shearing of the surrounding snow. Black and white arrows represent forces being applied to the rubber from both the ploughing and the indentation respectively. (Ella et al., 2013)

2.2.4 Lubrication – Friction Melting

The presence of a meltwater layer as the reason for snow and ice's characteristically low friction has been proven by (Bowden et al., 1939). Figure 2.6 illustrates the presence of the meltwater layer. The frictional heating of the snow surface causes a small amount of the snow surface to melt and provide fluid film lubrication. The exact details of the fluid film and its formation are still a key focus of many investigations but further evidence confirming its existence has been gathered by (Fowler, 1993, Bäurle, 2007 & Makonnen, 2014)

Fluid film lubrication it is likely to have less of an effect when a siped sample is ploughing into the snow as the ploughing process constantly refreshes the snow surface

with the passing of each sipe, this means there is less time for the snow to melt and form a fluid film layer.

(Colbeck 1988) investigated lubricating film thickness on snow, although it was difficult to measure, Colbeck found the film thickness to be in the region of 0.2µm – 1.2µm. (Colbeck 1988) also concluded that the water was removed by shearing and even if a separate source of water was added the film thickness did not increase dramatically due to increased removal rate.

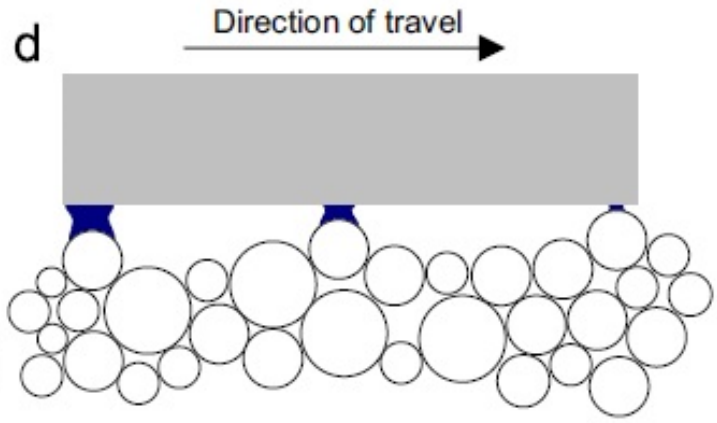

Figure 2.6 - Lubricating melt water layer (not to scale) (Ella et al., 2013)

2.3 Mechanical testing used for finite element studies

"Density is the most important parameter to characterise snow but it is insufficient due to the effects of snow microstructure on the mechanical properties of snow" (Lee, 2011). Both (Nakajima, 2003) and (Mellor, 1964) agree with this statement, both specifying a critical density in the region of 400kg/m^3 below which the snow's mechanical properties seem to depend mainly on microstructure (Mellor, 1964). This is due to the very porous grain structure with very angular snow grains in fresh low density snow (ca. 200kg/m^3).

The high porosity and angularity of the grains means there are not as many contact points between the grains to form sintered bonds.

When force is applied to small and rounded grains this may result in a behaviour similar to that of sand. If the grains are large and dendritic the dendrites may lock together to provide some mechanical strength (Mellor, 1964). In higher density snow the grains are more closely packed giving much more opportunity for intergranular bonds to form and provide strength. As a result, many studies into the mechanical properties of snow tend to relate the snow properties being tested (e.g. shear or compressive strength) to the density of the snow so that there is some common ground on which to base comparisons of different snow types.

In recent years the advances in computational power have allowed teams to carry out computer simulations of the friction of tyres on snow (Shoop et al., 1999, Nakajima, 2003, Shoop et al., 2006, Lee, 2009, Lee, 2011, Choi et al., 2012). In order to carry out the simulation of the snow, the snow properties had first to be determined. All of the above studies modelled the snow as low density (200-250kg/m^3) fresh powder snow except (Choi et al., 2012) who, in addition to the low density 200kg/m^3 also modelled a middle density snow at 350kg/m^3 and a higher density snow at 500kg/m^3.

The Young's modulus and Poisson's ratio in Shoop's model were estimated from data from (Shapiro et al., 1997) and show a strong correlation with density but for the model, was set to a value equivalent to snow in a density range 300-400kg/m^3 as snow at densities less than this have minimal elastic contribution.

All of the studies take into account the increase in density of the snow as the tyre passes. With final densities varying from 500kg/m^3 (Shoop et al., 2006) to 800kg/m^3 (Nakajima, 2003). Although the density increases, none of the studies shear tested higher density snow in order to have data for the changes in snow characteristics available

within the model, instead they used the plate sinkage test (see section 2.3.2) to extrapolate property changes as the density increases throughout a simulation. This is illustrated in Figure 2.7 where 3 different measurements were made of snow with different densities; the grey box represents the data the model has generated as an extrapolation of the inputted snow properties.

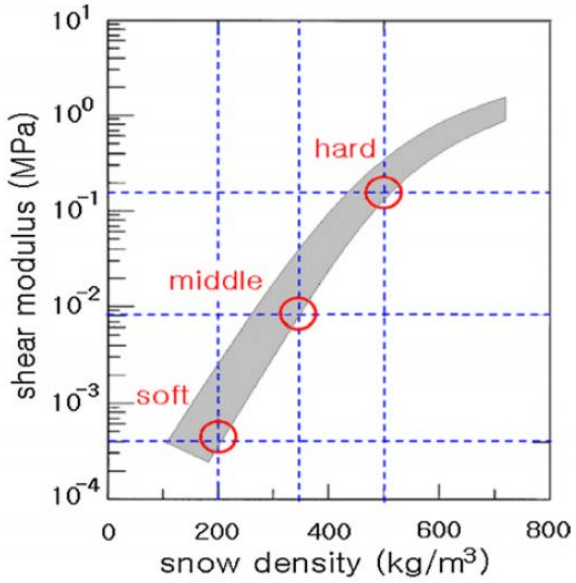

Figure 2.7 - Relation of snow density to shear modulus (Choi et al., 2012)

The main characteristics used to describe the snow in these studies are the density, the shear strength and compressibility (plate sinkage test into an appropriately large volume of snow as opposed to an unconfined compression test, see section 2.3.2) as these provide enough information for a model to calculate the sinkage of a tyre into the snow.

Snow density is measured by simply weighing a known volume of snow; this can be done in the field or in the lab.

2.3.1 Shear Tests

(Nakajima, 2003) discusses how the shear strength of the snow is proportional to density at values lower than the critical density (400kg/m^3), while the shear strength sees a rapid increase beyond this critical density due to the formation of intergranular bonds. The critical density is "the density where the structure of the snow changes because of the connection of snow particles" (Mellor, 1964). (Mellor, 1964) goes on to explain how this critical density is the point at which fresh snow develops strong intergranular bonds which would explain the rapid increase in shear strength around this density. (Nakajima, 2003) goes further to point out that in addition to being related to the density, the shear strength is also related to the storage time, the structure/type of snow particles and the humidity, but density is the best indicator of shear strength. However (Nakajima, 2003) decided to simplify his model by assuming that snow characteristics are a function of only density.

(Lee, 2011) carried out simulations which show both positive and negative shear stresses present on the snow surface, with shear in different directions depending on the slip ratio (negative shear stress between base of the tyre and the snow surface during acceleration and positive shear force observed when braking). All of the simulations carried out by (Shoop et al., 1999, Nakajima, 2003, Shoop et al., 2006, Lee, 2009, Lee, 2011, Choi et al., 2012) showed similar levels of shear dependence within their simulations.

Shear testing of granular materials which exhibit cohesion must be split into 2 components: firstly, the strength due to the cohesion of the grains, secondly, the friction between the grains. This can be expressed using the Coulomb Equation (Equation (1))

$$s = c + \sigma \tan\theta \quad (1)$$

Where s is the shear strength, c is the cohesion, σ is the normal pressure acting on the plane and θ is the angle of internal friction (the angle measured between the normal force and the resultant force at the moment failure occurs from a shearing stress (Figure 2.8). Once the initial shearing has taken place and the strength of the cohesive bonds has been overcome, the normal force being applied will have an influence on the strength as the grains move past each other.

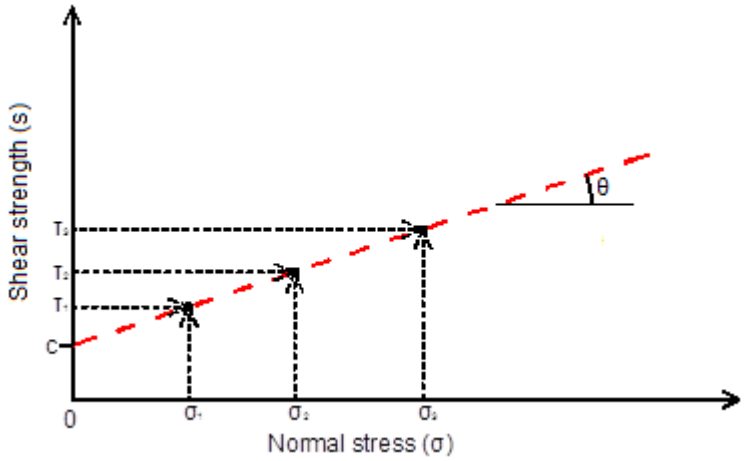

Figure 2.8 - Determining the internal angle of friction for a granular material from experimental results (Steiakakis, 2013)

2.3.2 Plate Sinkage Test

The second main parameter used in FEM studies to characterise snow is penetration resistance. This is a form of compression test confined within a block of snow. These tests are performed using either rigid rectangular plate (Nakajima, 2003) (Figure 2.9) or circular plate (Shoop et al., 2006), forcing them into a specific volume of snow with a solid base at a constant speed and measuring the force required to do so.

Figure 2.9 shows data used by (Nakajima, 2003) and produced by (Muro et al., 1980) using the rectangular plate test. The Labels D0, D1, D3, D7 & D14 refer to the snow type in this case D represents an artificial snow and the number referring to the number of days the snow is stored before tests are carried out. The snow is shown to behave elastically initially but becomes plastic at penetrations larger than a few millimetres.

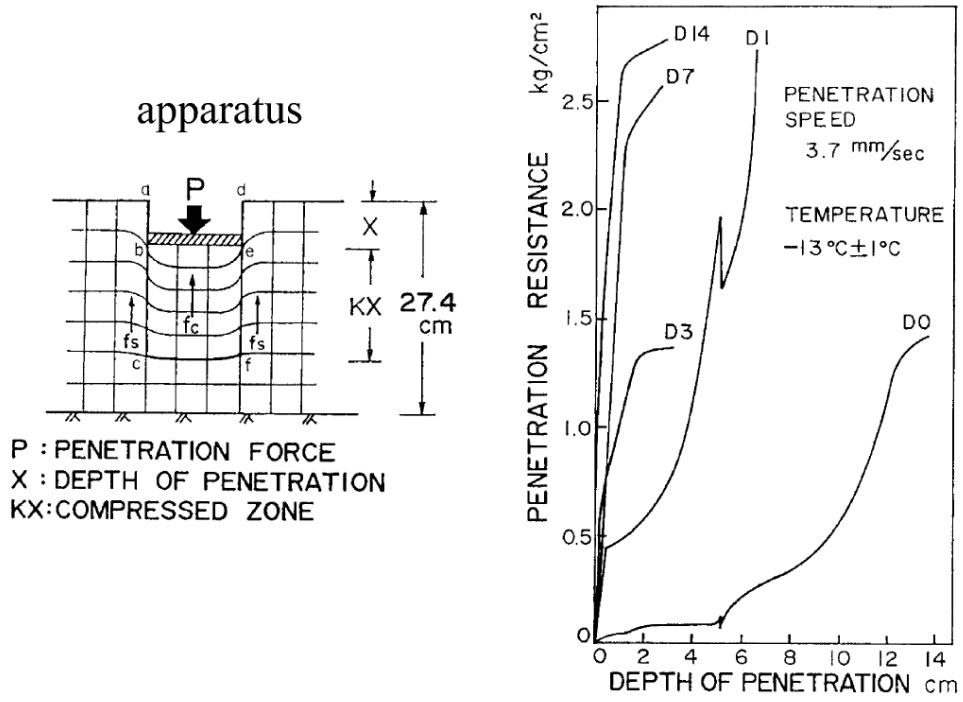

Figure 2.9 - Snow characteristics in compression using rectangular plate loading test (Nakajima, 2003)

A plate sinkage test is carried out until the force being applied corresponds to the equivalent contact pressure of a vehicle tyre is reached. From this data a Young's modulus and Poisson's ratio can be estimated which can then be input into the finite element model (Nakajima, 2003). Both Shoop and Nakajima comment on the rate dependence of the snow when performing these sorts of tests, so tests should be performed at a rate equivalent to the rates expected to be seen during the simulations

in order to obtain relevant results. Both studies also go further to talk about the additional shear force seen at the edges of the penetration plate and take steps to ensure their models take account of these forces.

2.3.3 Applicability of FEM studies

From examining the parameters recent studies have used to characterise snow for simulation, none of them have taken into account surface interactions; adhesion, indentation and fluid film formation. This is likely to be because their simulations begin with low density snow which rapidly deforms meaning there is no time for the rubber to adhere to the snow. This rapid deformation also means there is very little force from the snow surface to indent the rubber until the density of the snow increases. In the simulations the majority of energy dissipation for friction comes in the form of sinkage of the tyre into the snow causing an increase in density of the snow within the voids (void shrinkage (Nakajima, 2003)) resulting in higher shear strength and the shearing providing the majority of the grip (on new snow ca. 200kg/m^3).

However this does not seem to take into account one of the key features of snow friction, the surface melting at the interface. The meltwater layer was first proved to exist by (Bowden et al., 1939) and later confirmed by others such as (Evans et al., 1976, Kennedy et al., 2000, Marmo et al., 2005). However in the case of low density snow interacting with a winter tyre at relatively low temperatures (-10°C) there may be very little melt water due to the sipe edges refreshing the surface meaning little direct sliding on the surface. Studies of the surface profile of snow in the lab will provide indirect data about whether surface melting is occurring during siped sample testing.

2.4 Mechanical Testing and Investigation Options

The following describes the testing options which have been considered for use on snow to identify the snow characteristics related to winter tyre grip. Justifications are given why or why not these tests are appropriate for this work.

2.4.1 Shear Testing

Lee, (2011) noted that there are both positive and negative shear forces observed during tyre-snow interaction. There are shear forces between the base of the sipes and the surface of the snow, the edge of the sample (or tyre) and the edges of the trench that forms and there is a complex mechanism at the leading edge of the tread block involving both shear and compression. The amount of shear interactions taking place makes it important to know what characteristic is allowing the snow to provide a reaction force and thus enable winter tyre grip.

Several methods currently exist for measuring the shear strength of snow; the vane-cone or rotary vane apparatus (Muro, 1980) Figure 2.10 & Figure 2.11, and the shear frame apparatus (Perla, 1982) Figure 2.12. These methods feature intermediate fins spaced evenly either around a cone or within a frame. These allow the frame to grip the snow rather than compress or simply slide around the snow. These methods have proved successful and shown by (Perla et al., 1982) to correlate well with each other. Although it is noted that the shear frame cannot be used on higher density (>530kg/m^3) snow, due to the higher forces involved that cannot be applied by hand (>1000N). Mechanical application of force would make the method applicable again.

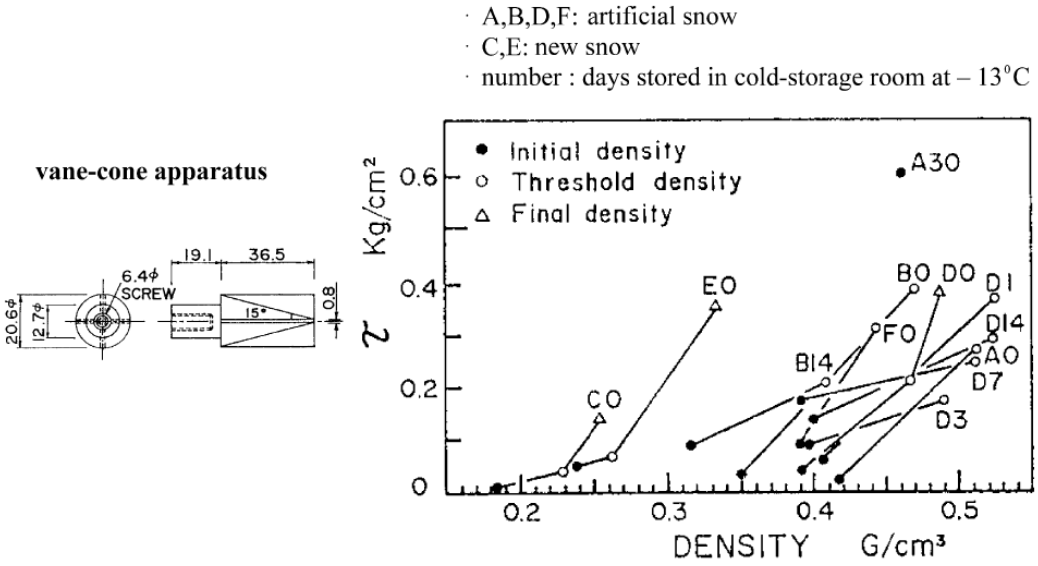

Figure 2.10 - Shear strength of snow vs density using vane-cone shear test (Muro et al., 1980)

Figure 2.10 shows how the shear strength of the snow varies with density, unfortunately (Muro et al., 1980) was published in Japanese so determining the exact protocol for the test and how the "Threshold density" (critical density) was determined was not possible. The threshold density appears to be the point at which a rapid rise in strength is observed and is therefore the critical density for that particular type of snow.

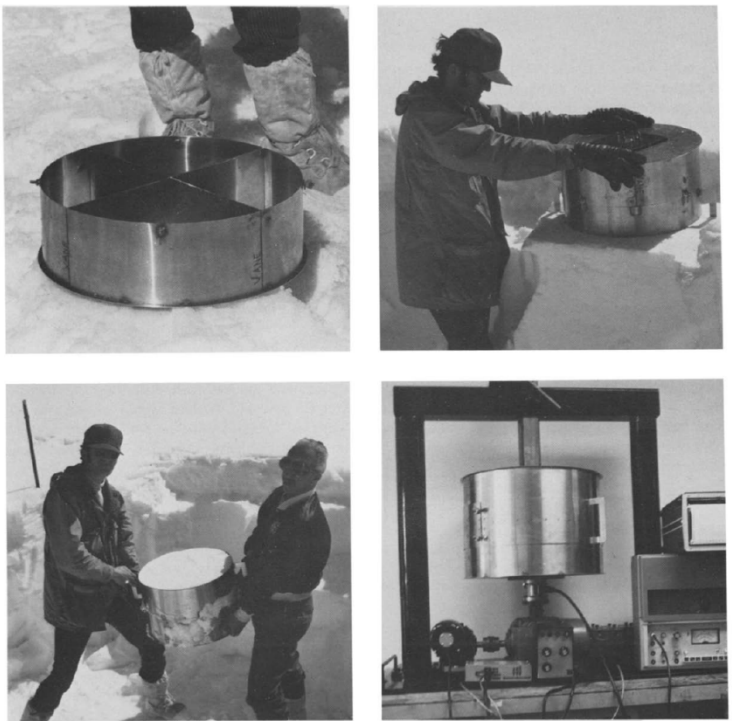

Figure 2.11 - Rotary Vane Apparatus (Perla et al., 1982)

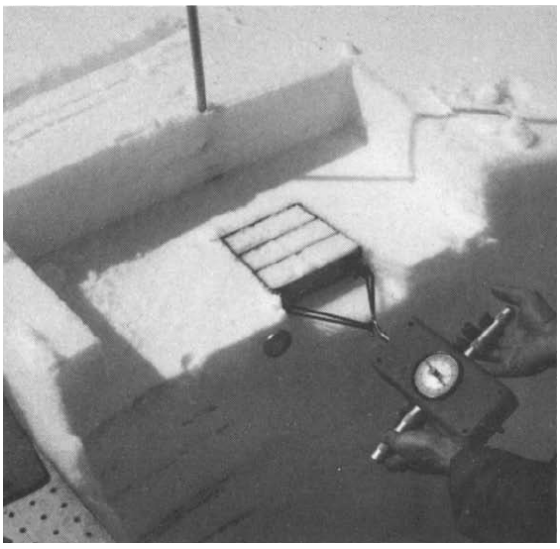

Figure 2.12 - Shear frame apparatus used in the field (Perla et al., 1982)

(Perla et al., 1982) found that the shear frame test was an extremely useful test for determining material properties of snow and the shear strength of the snows correlated very well with snow density (Figure 2.13). However, Perla further tried to correlate the shear strength with both the crystal size and the temperature of the snow but the correlation was extremely erratic and was not able to draw any valid conclusions from the results. This suggests that there is an additional effect influencing the shear strength of the snow which is related to the grain structure of a particular snow which is not completely understood.

Density and shear index data

Crystal type	Density (kg m^{-3})				Shear index (Pa)			
	Min.	Max.	Mean	S.D.	Min.	Max.	Mean	S.D.
+	18	139	82	27	35	668	217	178
⅄	72	321	146	37	96	10600	937	1410
●	139	427	280	72	511	19500	6280	4810
□	142	457	332	61	128	44400	8350	5380
○	306	531	452	40	2950	20800	9560	3610
V	102	369	222	88	126	6680	2290	1670
All	18	531	308	108	35	44400	6930	5400

Temperature and crystal size data

Crystal type	Temperature (°C)				Crystal size index (mm^2)			
	Min.	Max.	Mean	S.D.	Min.	Max.	Mean	S.D.
+	−15	−0.5	−6.94	3.68	--	--	--	--
⅄	−23	0	−8.08	6.34	–	–	–	–
●	−24	0	−6.07	3.86	1/8	4	0.54	0.49
□	−25	0	−3.88	3.68	1/8	16	2.25	2.25
○	-- 2	0	−0.52	0.30	1/4	8	2.42	1.49
V	−10	0	−5.47	2.70	--	--	--	–
All	−25	0	−4.37	4.31	–	–	–	–

No. of samples	Symbol	Morphology
27	+	Newly fallen
66	⅄	Initially metamorphosed (transition)
118	●	Granular and rounded (without melting)
341	□	Granular and faceted
89	○	Granular with melting and refreezing
17	V	Surface hoar

Figure 2.13 - Data from shear frame testing (Perla et al., 1982)

2.4.2 Compression Testing

Compression tests are an important method for determining material properties, the tests can be relatively easy to carry out and can provide a lot of information about the failure of the material.

Shear testing results in failure through a pre specified plane in the material. This means that a strength value higher than those seen in different tests such as compression or tension (where failure occurs on the weakest plane) can be observed. When carrying out a compressive test on a cohesive granular solid, the material may fail by a shear mechanism on internal faces rather than in pure compression (Figure 2.14) (Butkovich, 1956, Murthy, 2002) . This can give a better estimation of the realistic shear strength of the material, as it is free to fail through its weakest plane rather than a pre-specified one.

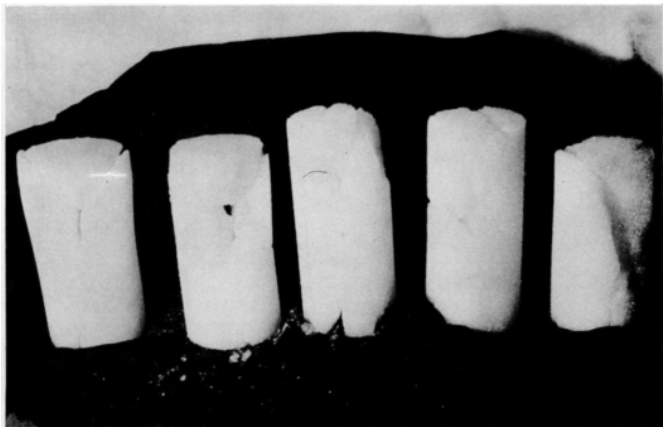

Figure 2.14 - Shear failure observed in compression test samples (Butkovich, 1956)

A compression test will give an insight into failure mechanisms of the snow, which can then be applied to the analysis of the complex behaviour at the leading edge of the sipes and also has the advantage of providing additional mechanical data for comparison to the shear test results and calculating elastic properties of the snow.

2.4.3 Flexural Tests

Flexural tests are extremely hard to carry out on a granular material such as snow (Mellor, 1975) due to the stress concentrations around the loading points resulting in rapid fracture through the beam (Lintzen, 2013). Also the lower tensile strength (around half of the compressive strength for snow in the density range 500-600kg/m^3 (Mellor, 1964) results in fracture initiation and propagation from the face being subjected to tension. The way (Lintzen, 2013) attempted to get round this problem was to use a 4 point bending setup with load distribution plates. Even with this setup limited tests were possible due to the beams failing as they were loaded into the test rig.

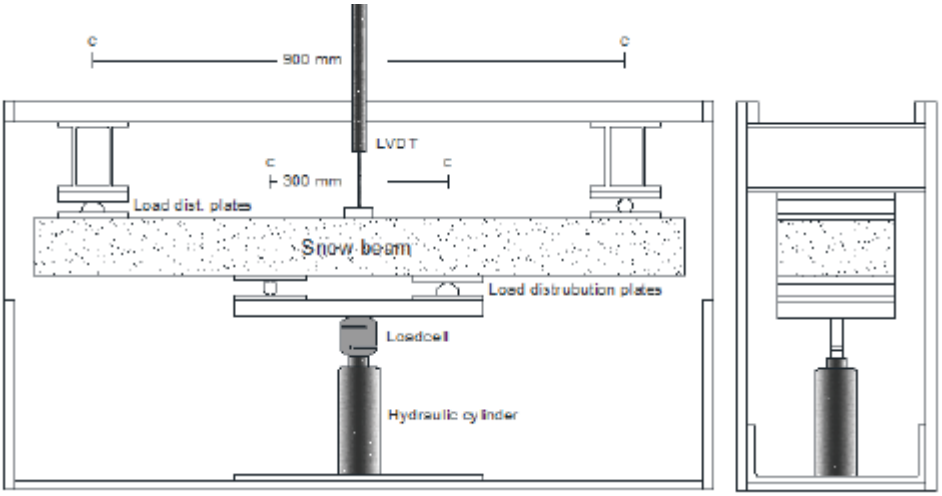

Figure 2.15 - Four point load test setup (Lintzen, 2013)

No other studies carrying out flexural tests on snow were found. In general studies tend to concentrate primarily on compressive and shear testing of snow with some recent tests looking at tensile strength of snow (Hagenmuller et al., 2014) as these test provide more useful and applicable data on the mechanical properties of snow. As (Mellor, 1975) says “The most un ambiguous determinations of strength are obtained from direct uniaxial stress tests in tension or compression”. No literature has mentioned that a bending test can provide additional information related to friction of tyres on snow that

cannot be better represented using a more direct uniaxial test. For this reason bending tests will not be investigated any further.

2.4.4 Surface Roughness Testing

Several studies have made note of the effects of surface interactions (adhesion, rubber indentation and formation of meltwater layer) on snow friction (Bowden et al., 1939, Bowden, 1953, Colbeck, 1992, Ella et al., 2013). The surface roughness of both the rubber and snow will have an effect on the real area of contact between the snow and the slider. Methods for measuring surface roughness can be a physical measurement using a contact profilometer or optical measurements calculated using microscopy. (Ella, 2014) also developed a method of stabilising the snow structure using dimethyl phthalate, which allowed the snow to be sectioned. The surface profile could then be traced by hand, this proved to be a very time consuming method with the potential for a lot of human error so will not be used in this study.

2.4.5 X-ray Microtomography (XMT)

X-ray Microtomography of snow is a method of visualising snow using computed tomography to generate a series of X-rays of the snow structure which can be assembled to form a 3D image of its microstructure. XMT has been around since 1917 when the mathematics behind the system were worked out. It wasn't until 1970 that a commercial CT system became available with modern CT systems becoming ever more advanced and are now able to achieve resolutions as low as 400nm (Bruker, 2011).

Where XMT differs from regular X-ray imaging is that a 3D visualisation can be produced and analysed, providing far more in depth and robust information about the 3D structure of a material. In order to produce a good quality visualisation of a material there needs to be a good contrast between densities of the object being scanned. Air, snow and plastic containers used to house a snow sample all have relatively low

densities. In order to maximise the density sensitivity the lowest X-ray energy must be used (Ketcham et al., 2001). Figure 2.16 is an example of the sort of 3D visualisation which can be achieved using this technique.

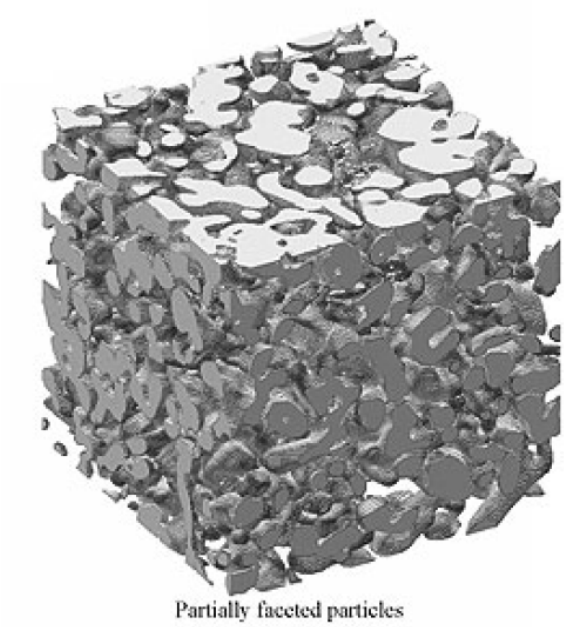

Figure 2.16 - Subsample of XMT scan of "partially faceted particles" after one month storage at -20°C (300^3 voxels)(Coléou et al., 2001)

Many characteristics of snow can be determined using XMT. The porosity can be determined by looking at the ratio of snow grains to void space in the 3D model and can give a good indication of mechanical properties (Coléou et al., 2001, Lee, 2011) as it is related to the density of the sample. The grain curvature can give you information about snow type and metamorphism. At its most basic showing that fresh dry snow generally has very faceted grains and old or wet snow generally has much more rounded grains.

2.5 Summary of the Mechanical Properties of Snow

The mechanical properties of snow are extremely varied and are influenced by many different features from density to grain size. The following is an overview of compressive strength, elastic modulus and shear strength for a range of snow types which have been identified in various studies. Compression and shear testing are the two main methods for characterising snow's mechanical properties, both of which are closely linked to a snows density. Flexure and tensile testing have been attempted but the results are very inconsistent and the tests are very difficult to carry out so will not be discussed here.

As no two studies are testing exactly the same snow, the density of the snows are given along with the relevant mechanical property so as to provide some context for comparison.

2.5.1 Compressive Strength

Several studies into the compressive strength of snows have been carried out, with the first large studies being carried out in the 1950s. (Butkovich, 1956) carried out extensive compressive testing on snows taken from various depths of a 100ft deep pit made in the northern Greenland ice cap. The strength was found to vary from 0.07MPa for snow of density 354kg/m^3 to 2.6MPa for snows at 641kg/m^3. A graph of crushing strength vs density for these snows can be seen in Figure 2.17 which shows a linear relationship between compressive strength and density for snows over 400kg/m^3.

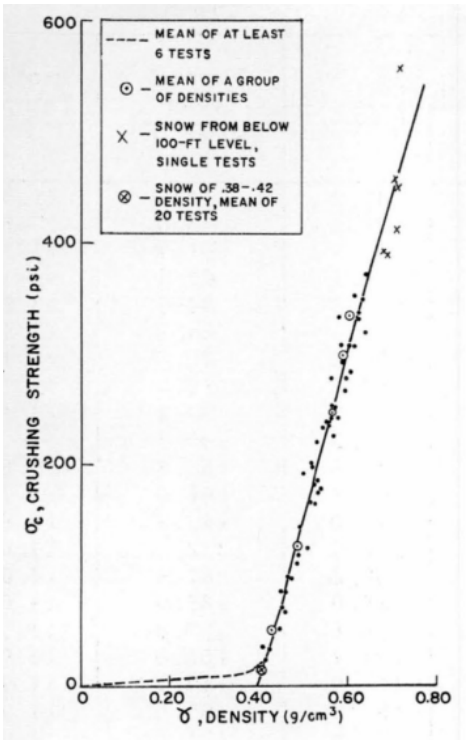

Figure 2.17 - Crushing strength vs density for snow from Greenland Icecap (Butkovich, 1956)

Further studies into the compressive strength of snows were carried out by (Jellinek, 1958), (Salm, 1982), (Ramseier, 1963) and (Mellor, 1964). Between them, snows ranged between 200kg/m^3 and 700kg/m^3 were tested, giving compressive strengths from 0.16MPa to 1.56MPa. All studies agreed that below approximately 400kg/m^3, the strength of the snows was very low and did not follow the linear relationship with density which is noted above 400kg/m^3, as shown in Figure 2.17.

2.5.2 Elastic Modulus

The elastic modulus of snow can be calculated from any mechanical test where a force and displacement can be measured. Figure 2.18 by (Sigrist, 2006) brings together the results from several different studies looking at the elastic modulus of snow. The modulus was calculated by quasistatic compression testing (Scapozza et al., 2004), uniaxial compression and tension experiments (Mellor, 1975), high frequency flexural

vibration testing (Mellor, 1975) and finally the dynamic torsional shear tests performed by (Camponovo et al., 2001). As can be seen in Figure 2.18, the tests were all performed on snow of relatively low density (220kg/m^3 - 350kg/m^3), with the elastic modulus varying from 1.3 MPa up to 50 MPa. Interestingly, all of the calculated modulus values were from snows under 400kg/m^3 which, as mentioned in section 2.5.1 above, is below the point where snow begins exhibiting a much higher mechanical strength. None of the studies looking at the compressive strength of higher density snows attempted to calculate the elastic modulus.

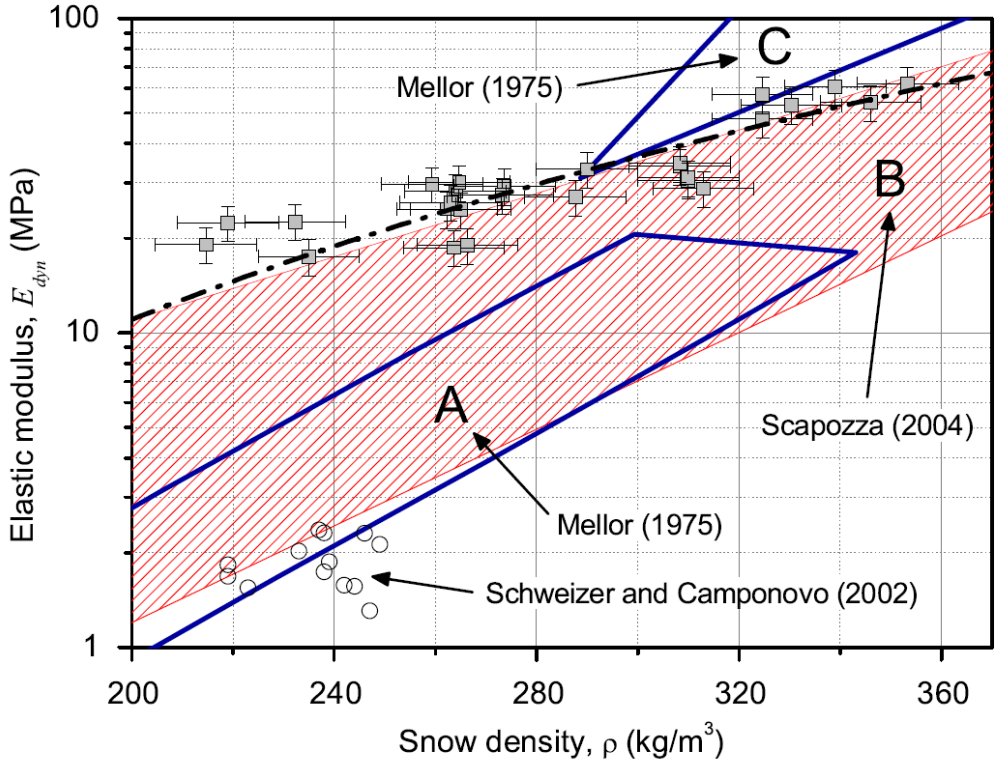

Figure 2.18 - Dynamic Young's Modulus results compiled by (Sigrist, 2006). "The dash dot line represents the best fit of Sigrist's data. The dashed area (B) represents the range of Young's Modulus found by (Scapozza et al., 2004) in quasistatic compression experiments. (A) are uniaxial compression and tension experiments compiled by (Mellor, 1975) and (C) pulse propagation or flexural vibration tests at high frequencies, also compiled by (Mellor, 1975). Additionally, the results of the dynamic torsional shear experiments of (Camponovo et al., 2001) were converted to Young's Modulus (circles)."

2.5.3 Shear Strength

The majority of shear testing which has been carried out on snow has been in the form of field tests making use of shear frames and rotary vanes as shown in Figure 2.11 and Figure 2.12. One of the larger studies of snow shear strength was carried out by (Brun et al., 1987). The study took in multiple snow types of different densities and grain type, a plot of the resulting shear strength vs density can be seen in Figure 2.18.

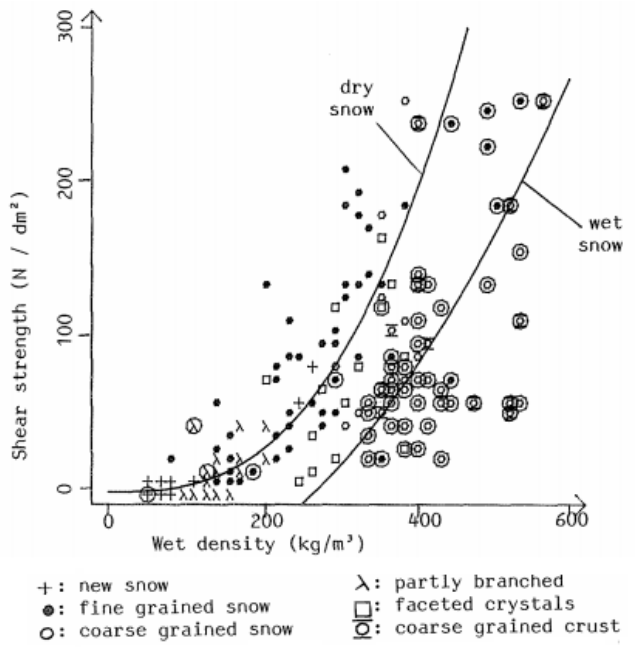

Figure 2.19 - Shear Strength vs Density for multiple alpine snow types (The points surround by a circle were measured at 0°C and are considered wet). (Brun et al., 1987)

The study found that snow with a low density (under 200kg/m^3) exhibited almost no shear strength, above this, there is a significant spread of results with a wet snow of approximately 550kg/m^3 having the highest shear strength of approximately 260 N/dm^2 (26 kPa). The results from other studies match closely with what was found here with (Domine et al., 2011) measuring shear strengths as low as 20 Pa for powder snow and (Perla et al., 1982) measuring up to 44.4 kPa for snow of density 500kg/m^3.

2.6 Conclusion

This chapter has examined the literature relating to the friction fundamentals for rubber friction on snow. It has been shown that there are multiple friction mechanisms occurring simultaneously (adhesion, indentation, ploughing and fluid film lubrication). The friction mechanisms can be extremely complex and can vary with both the rubber and the snow properties. In addition, the exact process going on in both the ploughing mechanism and the formation and dissipation of the fluid film is not well understood.

In order to investigate how the properties of snow relate to the grip of winter tyres, the current state of the art in mechanical testing of snow has been examined. From this, it has been possible to decide which tests are to be carried out within this study.

The mechanical tests to be carried out on the snow are:

1. Shear Testing
2. Compression Testing

The non-mechanical tests to be carried out on the snow are:

1. X-ray Microtomography
2. Surface Profilometry
3. Density Testing

3 Development and implementation of experimental method

Summary

This chapter presents the working environment of the cold room laboratory along with the methods for making artificial snow and collecting natural snow. This chapter also discusses the process of developing new experimental methods and describes the final protocols which were used during the testing. To collect friction data a linear tribometer was used. Mechanical testing was done by compression testing and shear testing. In addition, the snow was characterised using density measurements, optical microscopy, surface profilometry and X-ray microtomography.

3.1 Introduction

The following chapter details the testing methods carried out throughout the course of the PhD along with the rationale behind each test. A considerable amount of time in the initial stages of the PhD was devoted to identifying which testing methods could best be utilised to identify the properties of snow which could be related to the frictional behaviour of the rubber on it. After much discussion of how the tests and measured values relate to the friction mechanisms on snow, it was decided that compression testing, shear testing and compaction testing (CTI) would be used to characterise the mechanical properties of the snow. Additional properties and features would be identified by density testing, surface profilometry microscopy and X-ray microtomography. The aim was then to link the measured properties of the snow to the rubber friction as tested on a linear tribometer in order to determine the relationships between snow structure and tyre grip.

3.2 Cold Room and Lab setup

In order to carry out testing on snow, a controlled environment was required. As the work required using relatively large volumes of snow on multiple different machines it would not have been possible to use individual environmental chambers for each machine. Firstly, because transferring the snow between machines through the air at temperatures above 0°C would have rapidly altered the snow structure. Secondly, the machines used, specifically the linear tribometer (FRIMA) is too large to have an individual environmental chamber built around it.

The tests were carried out in a full cold room laboratory setup. This allowed a constant temperature to be maintained between all testing systems and during transfers between testing systems. The cold room was constructed in 2010 during the PhD of Gerasimos Skouvaklis, it consists of 3 rooms, an entranceway to restrict warm air from entering the rest of the rooms, the main room where the linear tribometer and snow press are

housed and a smaller secondary room where all auxiliary equipment and testing systems are housed.

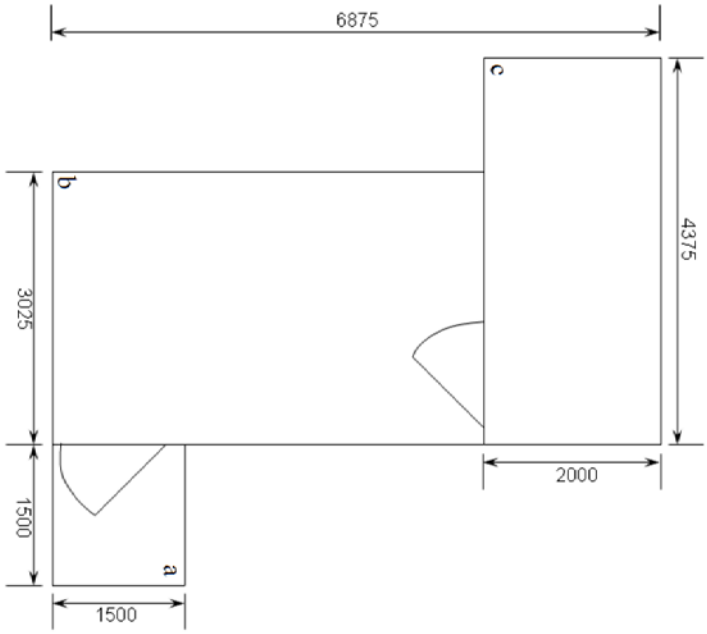

Figure 3.1 - Cold room laboratory floor plan, set up during PhD Skouvaklis (2010). Room a is the small entrance room, b is the main room where the linear tribometer and snow preparation equipment is kept, room c is the secondary testing room for all other equipment

The temperature in each room can be individually controlled with a range of 0°C to -18°C in 1°C increments. Humidity in the laboratory was controlled by the temperature of the evaporator, with excess humidity from sublimation or respiration being deposited on the evaporator, and subsequently disposed of during the automated defrosting. This has the overall effect of maintaining a relative humidity close to 80%. Figure 3.2 shows the measured values of temperature and relative humidity within the back room (room c) over a 24 hour period with a temperature set point of -10°C. Excluding the defrost cycles the average temperature variation is approximately ±0.5°C.

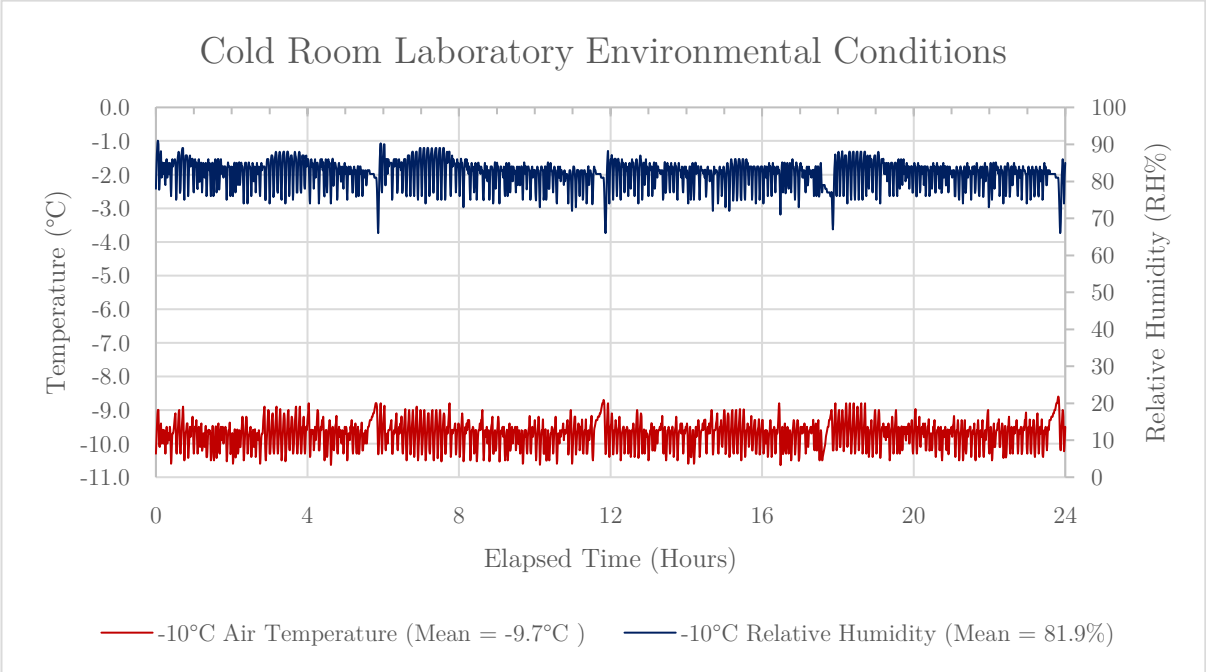

Figure 3.2 - Cold Room Environmental Conditions measured over a 24 hour period. Note the defrost cycle every 6 hours.

3.3 Testing Plan

With the aim of investigating the relationship between snow properties and friction on snow, a comprehensive testing plan was designed in order to maximise the number of different tests which could be carried out on a specific volume of snow and also to minimise the time taken to carry out the testing. It was essential that all tests could be completed within one day (8 hours). if the snow was left overnight the metamorphism of the snow would have altered the structure and properties of the snow and the results would not be comparable to the results from the previous day.

After much consideration it was decided that the following tests would be the most appropriate for the characterisation of the snow and measurement of the mechanical properties:

1. CTI Testing (9 measurements across the area of the testing tray)
2. Density testing (5 measurements before and 5 after snow is formed into testing tray)
3. Friction Testing (2 rubber samples, 3 speeds 3 test repeats)
4. Surface Profilometry (20 measurements in different areas of a prepared test track)
5. Shear Testing (4 measurements)
6. Compression Testing (3 different compression test rates, 5 samples tested at each speed)
7. X-ray microtomography (sample was taken and stored at -80 until scanner was available)
8. Optical Microscopy (imaging of snow structure before and after tray preparation was carried out)

Each of these tests is explained in detail below in sections 3.4 to 3.13. In order to aid understanding of how these tests were carried out on a snow tray Figure 3.3 shows an approximate layout of the tests on a testing tray. The snow area is 700mm x 350mm.

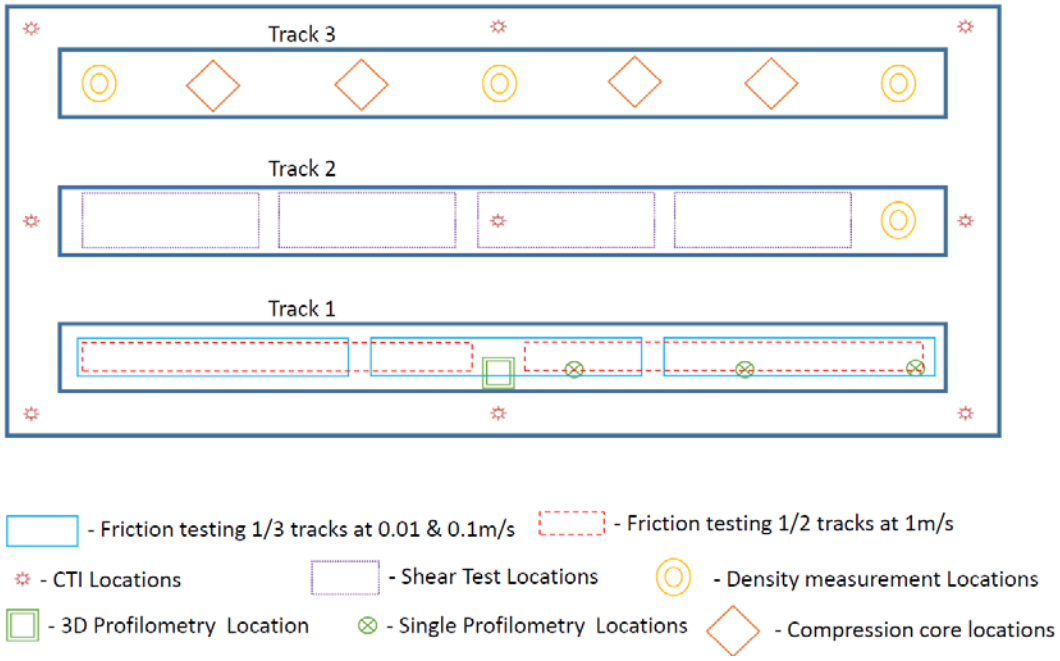

Figure 3.3 - General layout of tests on a snow tray in plan view. Actual locations and the exact number of test repeats which were carried out vary from tray to tray. Tray size = 700mm x 350mm.

3.4 Friction Testing

3.4.1 Linear Tribometer: FRIMA

Friction testing is a key part of this research, extensive work has previously been carried out by Sam Ella and Gerasimos Skouvaklis during their PhDs along with Michelin personnel to develop the most effective and consistent friction testing method. This has been followed closely in order to ensure good quality friction data was collected. In order to do this, a large linear tribometer (also referred to as FRIMA) was installed by Michelin during the PhD of Gerasimos Skouvaklis. The tribometer is capable of carrying out friction tests at speeds from 0.005m/s to 2m/s while applying loads of 0.25kN to 1.5kN. In order to achieve this, a pneumatic piston applies the normal force to the sample. The movement of the test sample is controlled using an electromagnetic motor system which can achieve accelerations up to $20ms^{-2}$.

In order to measure the forces generated during a test, the snow is prepared in an aluminium tray which is bolted to a Kistler 9253B22 3D force measurement platform. This system allows the logging of the force in all 3 axis. The measurement range is ±15kN in the X and Y direction (X is in the horizontal plane in the direction of movement, Y is in the horizontal plane perpendicular to the direction of movement). In the vertical Z direction Fz can be of the range -15kN to 30kN. The layout of the testing area can be seen in Figure 3.4.

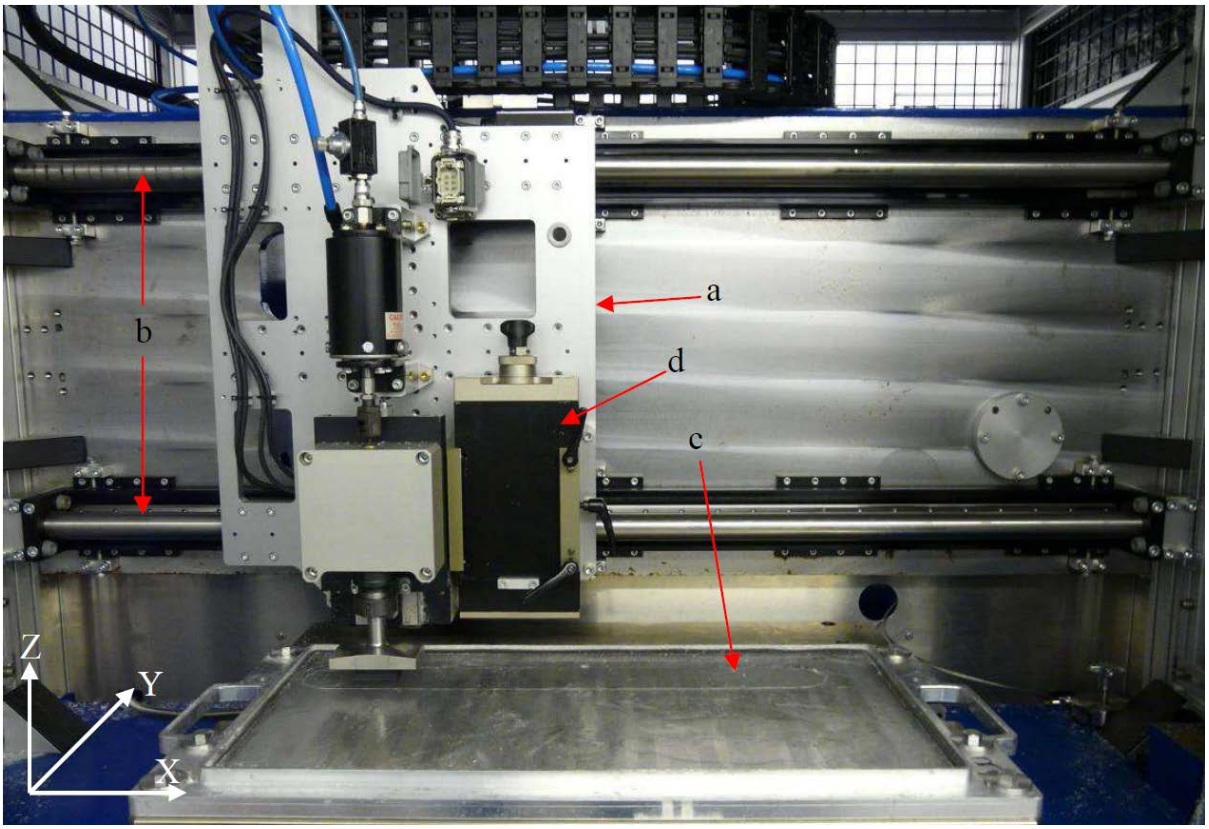

Figure 3.4 - Testing area of FRIMA. (a) Moving sample holder mounted on electromagnetic rails. (b) Electromagnetic rails. (c) Kistler force measurement platform with sample tray bolted on top. (d) Mounting location for auxiliary tools

In addition to logging the forces applied in the X, Y and Z directions the system also logs the Z position of the rubber sample, this allows the depth which the sample penetrates into the snow to be recorded.

3.4.2 Rubber Samples and Friction Testing Procedure

The details of how the snow trays are prepared and testing tracks created are detailed in section 3.5.1 & 3.5.4. This section describes the rubber samples which were used for friction testing and the procedure which was followed in order to achieve consistent results. Two main rubber samples were used for the friction testing, a 4 siped sample and a rounded edge sample. The two samples were provided by Michelin, both were

made using the same rubber compound (the exact details of the compound have been kept confidential by Michelin) with the only difference between them being the geometry of the sample. Images of the two samples can be seen in Figure 3.5. These samples were chosen so the 4 siped sample could be used to investigate the ploughing mechanism and the rounded edge sample could be used to investigate the surface friction mechanism (indentation, adhesion and fluid film lubrication), full details of the mechanisms can be found in Section 2.1.

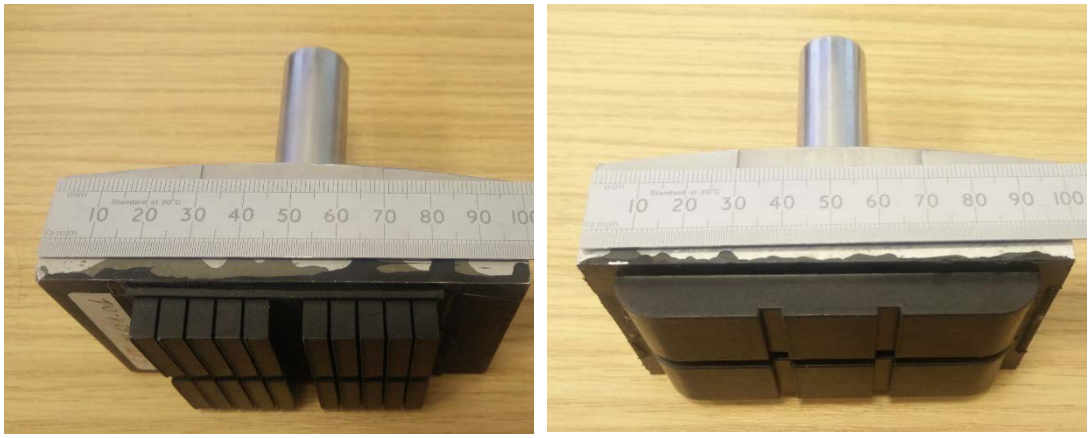

Figure 3.5 - Rubber samples. Left: 4 Siped sample. Right: Rounded edge sample. Both mounted to 100mm sample holders designed to mount into FRIMA.

Friction testing was carried out at 3 different speeds: 0.01m/s, 0.1m/s and 1m/s. A snow track on the testing tray is approximately 600mm long. In order to maximise the use of this space 3 tests were carried out across the length of the track when testing at 0.01m/s and 0.1m/s. When testing at 1m/s a larger space was required in order to reach the required speed and still have space to decelerate. For this reason, only 2 tests were possible on a snow track at 1m/s.

Once the snow tray has been prepared (as detailed in section 3.5.4) the following test method can be followed to carry out friction testing:

1. Testing track is prepared using scraping tool to ensure consistent testing surface(Figure 3.6)
2. Loose snow is gently brushed away from track surface
3. Rubber sample is loaded into FRIMA sample holder
4. Normal force is applied to the sample. The force used for all tests was 0.82kN
5. Test is carried out at selected speed
6. Sample is cleaned to remove loose snow and build up between sipes
7. Procedure is repeated

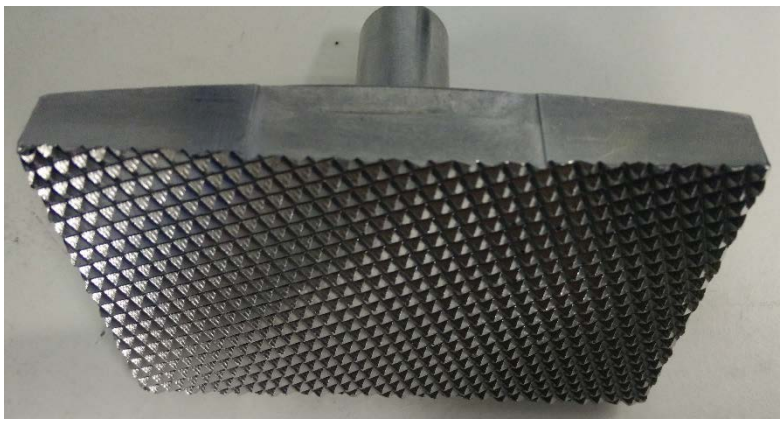

Figure 3.6 - Snow track preparation scraping tool. Dimensions: 100mm x 60mm

Each test speed is repeated 3 times (twice for tests at 1m/s) for each sample. This was the maximum number of tests it was possible to carry out on a single snow tray due to the ploughing process and the track preparation process removing snow volume.

3.5 Artificial Snow Making and Natural Snow Collection

In order to compare the way snow microstructure and properties affect the grip of winter tyres, it was necessary to be able to create snows with different microstructure and properties. In order to achieve this a previous method developed by (Skouvaklis, 2010) and further refined by (Ella, 2014) of creating artificial snow by blending ice chips was used. This resulted in a snow made up of rounded ice particles. In order to create a snow with a completely different microstructure a method of making snow by vapour deposition was used. This method was initially developed by (Schleef et al., 2014) and was modified for this research. This created a snow made up of large dendritic grains. In addition to testing artificial snow, it was important to test natural snow to confirm that the results achieved in the lab are applicable to what is found in nature. To achieve this a procedure was developed to allow the collection of natural snow which could be brought back to the lab for testing.

3.5.1 Blended Snow Making

The procedure for creating snow by blending went through considerable development during the PhD of (Skouvaklis, 2010). The following is a brief overview of the procedure. Ice flakes are taken from a commercial ice maker (Scotsman Ice Flaker AF80AS-6), placed in Cordura bags and frozen in stages, a minimum of 24h at -30°C followed by a minimum of 24h at -80°C. At this point the bags of snow are taken out of the freezer, they are smashed with a large hammer in order to break up the larger chunks of ice that will not fit in the blender. The ice is then blended for a total of 42s, the ice is now considered to be snow. The snow is left covered in the cold laboratory until the temperature of the snow reaches the ambient temperature (-10°C), approximately 3h. Figure 3.7 shows the change the ice goes through and the resulting snow grains.

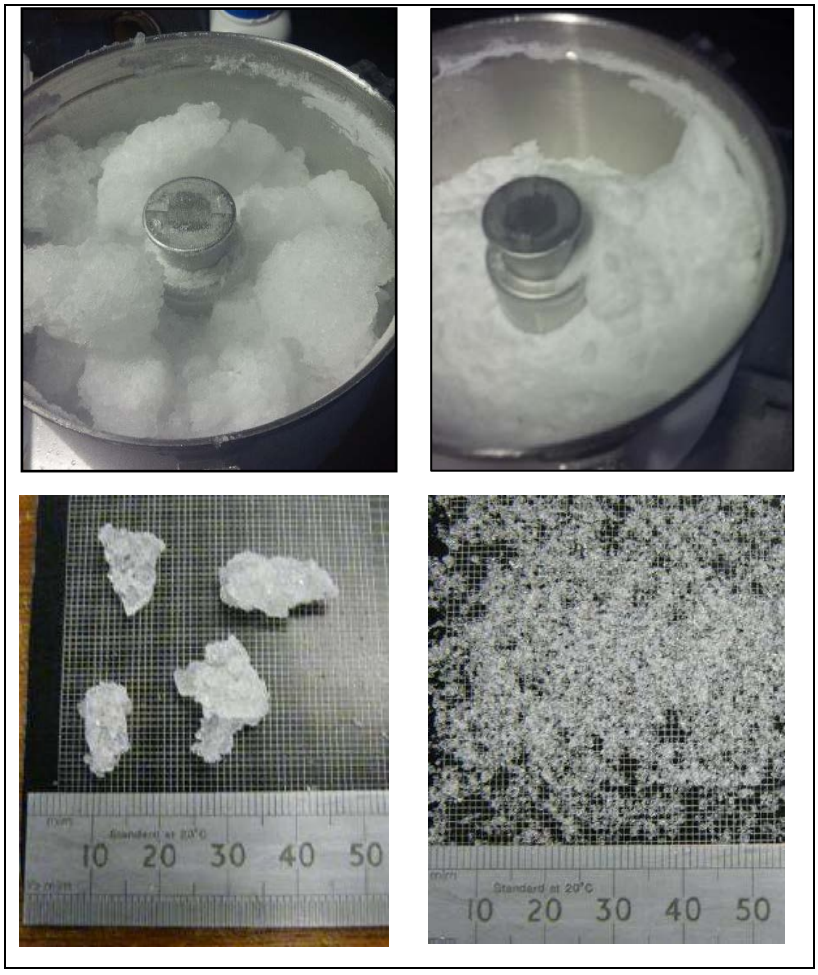

Figure 3.7 - Top Left - Ice flake clusters before blending. Top Right - Snow formed after blending. Bottom Left - Individual ice flakes before blending. Bottom Right - Snow grains after blending

3.5.2 Vapour Deposition Snow Making

The procedure used by (Schleef et al., 2014) to create artificial snow by vapour deposition involved some very large equipment kept in a cold room. The set up in the cold laboratory meant there was no space for such a setup here. Instead, the procedure was altered to fit within a standard domestic chest freezer which could be kept outside the cold room. The procedure used a heated water bath to provide water vapour, a fan to circulate the vapour throughout the deposition area, a series of wires to provide points for the nucleation and growth of new snow grains and a collection area where the

snow could be gathered to allow space for more snow to form. The layout of the simplified setup can be seen in Figure 3.8.

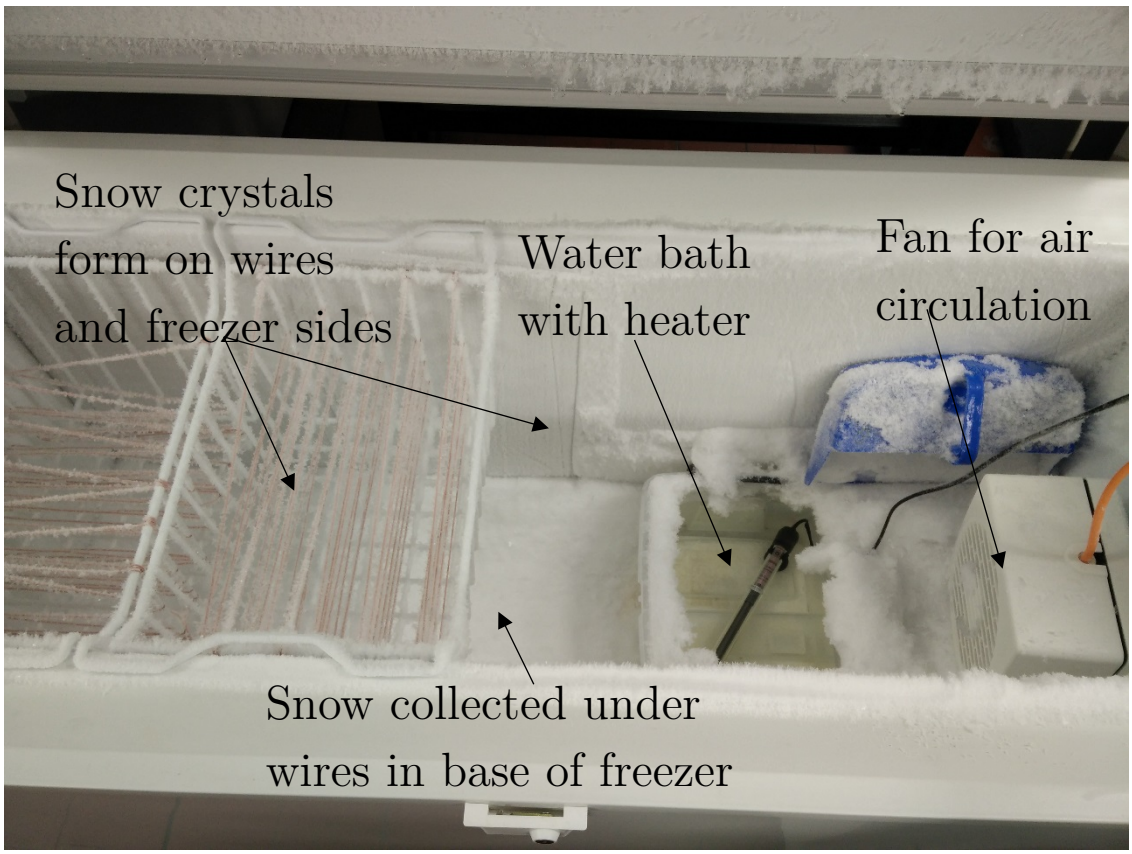

Figure 3.8 - Layout of vapour deposition snowmaking equipment

Figure 3.9 shows the temperatures of different areas within the vapour deposition freezer. The freezer has a set point of -40°C however as seen in Figure 3.9 no area of the freezer reaches this temperature due to the presence of the water bath which is being held at a temperature of approximately 27°C

The snow grains which form by this process can vary in structure and size but the majority of the grains are large dendrites or plates as shown in Figure 3.10. The grain size varies from 0.5mm to 30mm. The dendrites are extremely fragile so many smaller grains were created by fracturing the larger ones during manipulation of the snow.

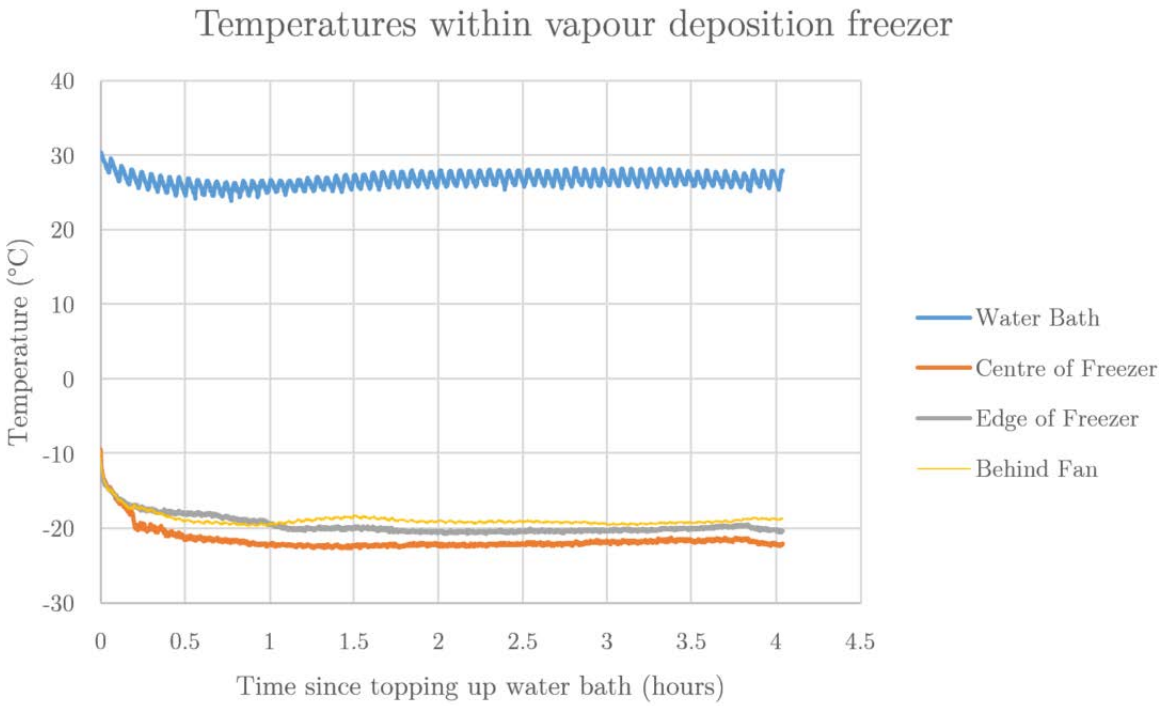

Figure 3.9 - Environmental conditions within the vapour deposition snowmaking freezer

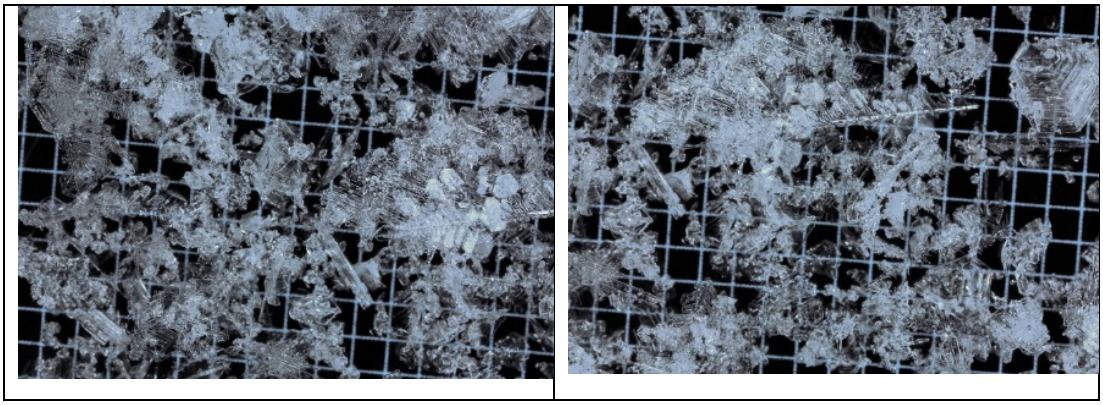

Figure 3.10 - Example vapour deposition snow grains on 1mm² reference background

Once enough snow has been collected in the base of the freezer it is transferred to the cold laboratory in polystyrene containers and left covered until the snow reaches the ambient temperature of -10°C.

3.5.3 Natural Snow Collection

Collecting natural snow in Scotland can be very challenging. The air temperature rarely drops below -5°C for extended periods of time except on the highest mountain summits. As large quantities of natural snow were required for testing (approximately 10kg of snow per tray) it would be impractical to attempt to collect snow from high on mountains. The only other option was to rely on the weather and be ready to go and collect snow as soon as the conditions were favourable. In order to do this, it was necessary to rent a freezer van which could be driven to some of the highest roads in Scotland in an attempt to collect snow at as low a temperature as possible. Other methods were considered such as using a generator and a chest freezer in the back of a car or large volumes of dry ice and polystyrene boxes but these methods proved very impractical for collected the volumes of snow which were required. Figure 3.11 shows the van which was used, the rear load area was extremely well insulated so it could maintain a temperature of -25°C during travel so would keep the collected snow as stable as possible.

Figure 3.11 - Ford transit custom freezer van. Van was capable of maintaining a temperature of -25°C in the rear compartment.

In order to collect snow which would be as natural as possible large drifts were found. These were cut out so a FRIMA testing tray could be placed in the drift at 20cm below the surface. The snow was then cut to the size of the testing tray and the snow would fall into the testing tray. The top layer could then be cut off to be level with the top of the tray, a cover was placed on the tray and it was placed back inside the van. It was possible to collect 4 trays of snow this way as that was the number of aluminium trays available. In addition, large volumes of snow were collected in a similar way in polystyrene boxes so the snow could be placed in the trays back in the cold laboratory.

During the winters of 2014/15 & 2015/16, there was very little snowfall which lay at a low enough altitude to drive to without the ambient temperature rising above 0°C during the day. This meant only 4 trips were made to collect natural snow, this first year was to experiment with collection procedure and investigate if the tray preparation and testing would need to be altered. The second year only one collection trip was very successful, (Figure 3.12 shows the conditions on the unsuccessful trip) and enough snow

was collected from Cairngorm Mountain Ski Centre in order to carry out the testing required.

Figure 3.12 - Author looking for suitable natural snow for collection on an unsuccessful trip

Figure 3.13 shows the structure of the natural snow which was used during the testing plan. As can be seen, the grains resemble those of the blended snow however extensive sintering has occurred resulting in the much smoother appearance of the grains and also the coalescing of many grains to form a smaller number of larger grains. This natural snow is an example of one extreme type of snow and is very useful to compare to the artificial to see how it compares to an extreme case found in the field.

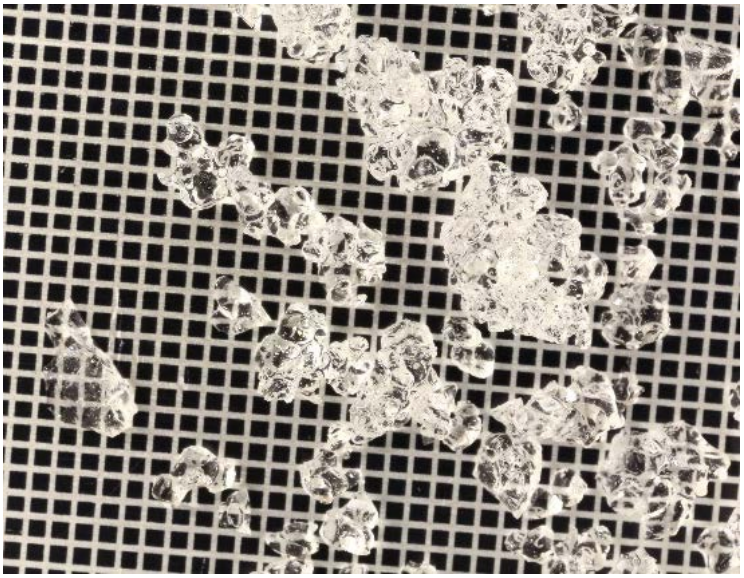

Figure 3.13 - Natural snow on 1mm² reference background

3.5.4 Snow Tray Preparation

In order to achieve the most consistent snow characteristics, all the snows were formed into testing trays in very similar ways. There are slight differences between the blended and vapour deposition snows, this was done in an attempt to preserve the larger grains of the vapour deposition snow.

Blended snow was prepared by sieving the snow material into a testing tray using a sieve with apertures of 1.56mm. This meant any ice chips which were not properly blended during the preparation process were not included. Next, the snow was compacted in a specifically designed snow press (Figure 3.14). Two different pressing procedures were used in order to create snow with different mechanical properties. From this point onwards they are referred to as 170 preparation and 130 preparation; these numbers refer to the pressures used in the hydraulic cylinder in bar (not the pressure applied to the snow surface).

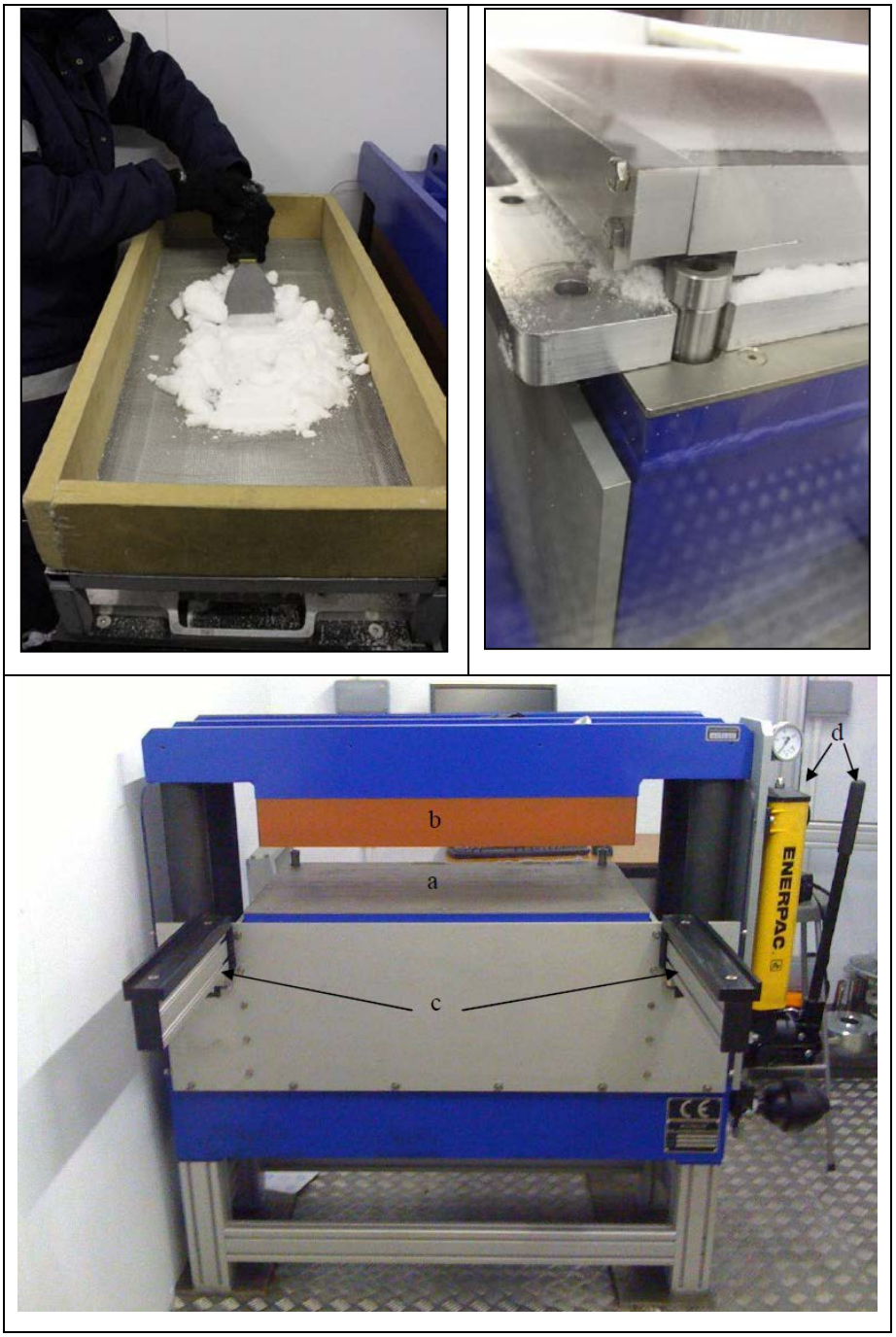

Figure 3.14 - Top Left - Sieving blended snow into the testing tray. Top Right - Prepared blended snow tray about to be pressed. Bottom - Snow Press, (a) moving press table, (b) Teflon coated pressing surface, (c) supporting arms for tray preparation, (d) Hydraulic pump

The 170 bar preparation corresponds to the pressure the snow would experience if cars were driven over the top of it. This pressure is maintained for 20 hours at which point the pressure is released, the snow is covered and left to mature for a further 20 hours. For the 130 procedure, the snow is pressed until the cylinder reaches 130 bar, this creates a much softer and weaker snow than when it is pressed to 170 bar. In addition to the lower pressure, the pressing time is reduced to 5 hours. The time for the snow to mature before testing is kept constant at 20 hours. These parameters are illustrated in Figure 3.15.

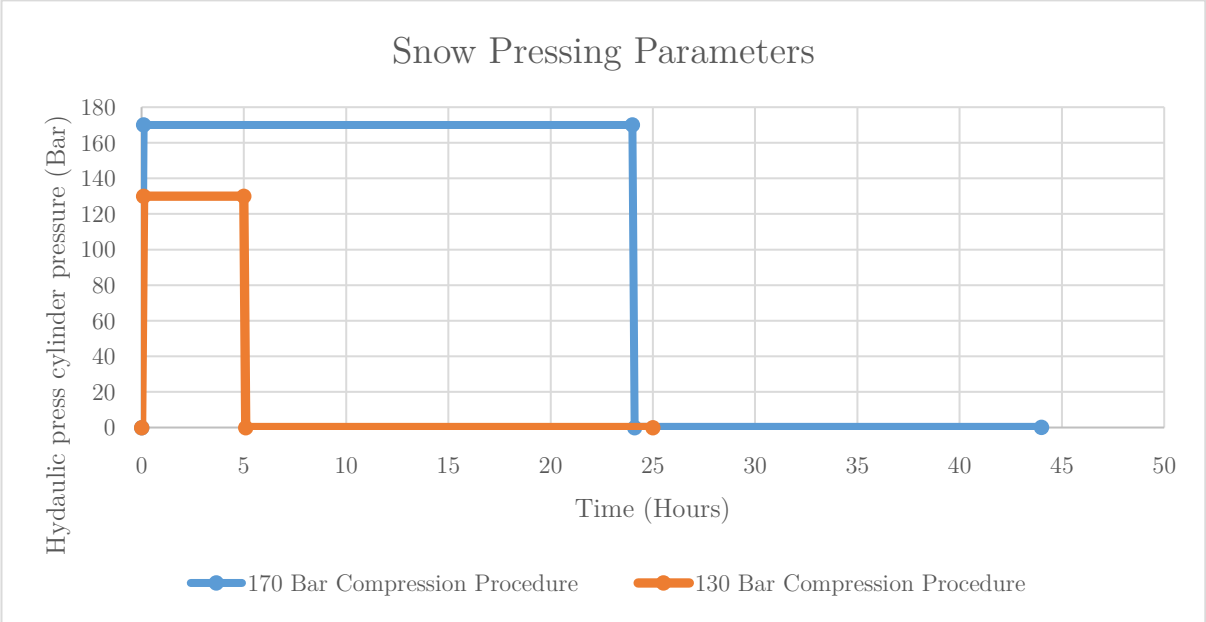

Figure 3.15 - Snow pressing parameters

The vapour deposition snow is pressed in an identical way however the snow is not sieved into the tray, it is instead spread as evenly as possible by hand. This ensures the microstructure of the snow is kept as similar as possible to the as-vapour deposited state, and as different as possible to the blended snow rather than sieving to achieve the same grain size as the blended snow. It should be noted that the lower density of the vapour deposition snow meant a larger volume of vapour deposition snow was

required than the blended snow (but a similar mass). This was achieved by adding larger edges to the testing tray to contain the snow before compression. If this was not done the snow would be compacted so much that there would not be enough volume to carry out tests on.

The natural snow was pressed in the same way as the other two snows. The snow was collected in the trays directly from the field as described in section 3.5.3 so no sieving was required.

These preparation procedures resulted in 6 different snow testing trays. Blended 170, Blended 130, Vapour Deposition 170, Vapour Deposition 130, Natural 170 & Natural 130. These are the names which will be used throughout the rest of the thesis to refer to the different snows which were used during testing.

3.6 Density Testing

The snow density was measured immediately before the tray preparation process began, by taking samples of the snow from the buckets. Measuring the density of the snow after sieving was attempted but measuring the volume of the sieved snow proved to be difficult so it was decided to keep the method consistent between snow types and measure the density of the starting material before anything had been done to it. In addition to the starting density, the density of the snow after compaction was also measured. This gives data on the snows compaction by examining the change in density before and after compression.

3.6.1 Density testing before snow compression

The density of the snow was measured before compression using a specific snow density measuring kit (Taylor-LaChapell density kit, manufactured by Hydro-Tech), designed for use in the field. It consists of a 200cm^3 scoop with an edge cutter to achieve a known volume. Immediately before the snow is sieved into the testing tray the density is

measured by pushing the scoop into the snow, removing the excess and measuring the mass of the scoop and snow combined, the mass of the scoop could subsequently be subtracted to allow calculation of the density of the snow. The snow scoop can be seen in Figure 3.16. The density was measured 5 times in order to have an average.

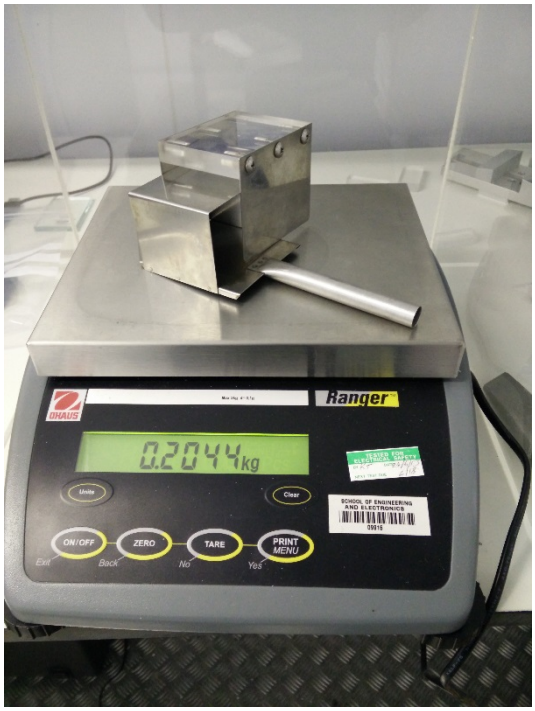

Figure 3.16 - 200cm³ snow scoop for measuring the density of uncompressed snow

3.6.2 Density Testing After Compression

Density testing after compression was significantly harder to carry out than testing on the uncompacted snow. This is because the compressed snow is more like ice, being hard to the touch and not possible to push a scoop into. This meant that snow samples had to be cut from the testing tray on the day of testing. They could then be cut down to a cuboid shape using a Leica SM2010 R Microtome. This allows the samples to be cut with parallel sides meaning the dimensions could be accurately measured using callipers and the volume calculated. The mass of the snow was then measured and the density could be calculated. An example density measurement can be seen in Figure 3.17.

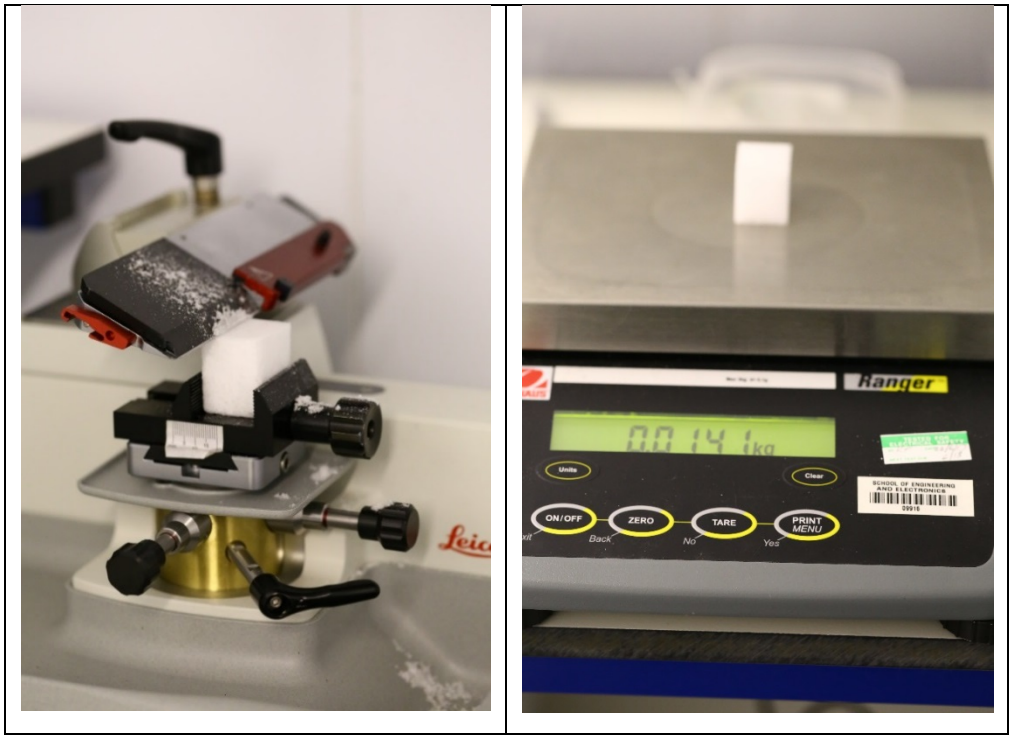

Figure 3.17 - Left - Leica SM2010 R Microtome being used to create a cuboid of snow. Right - Cuboid of snow being weighed

3.7 Snow Compaction Measurement (CTI Testing)

Snow compaction is measured using a snow penetrometer. By measuring the indentation of a spike into the snow surface it is possible to have an understanding of the snow's compaction. This is one of the measurements used to characterise snow for tyre traction testing as specified in ASTM F1572-08. It is a unitless measurement between 50 for very soft snow and 92 for extra hard packed snow. Above CTI 92 the snow is considered to be ice (Shoop, 1993). The CTI is measured using an impact test by dropping a weighted spike onto the snow from a set height and measuring the penetration, Figure 3.18 shows the CTI measurement device. Nine measurements across the area of the testing tray were made in order to measure an average compaction for the entire tray.

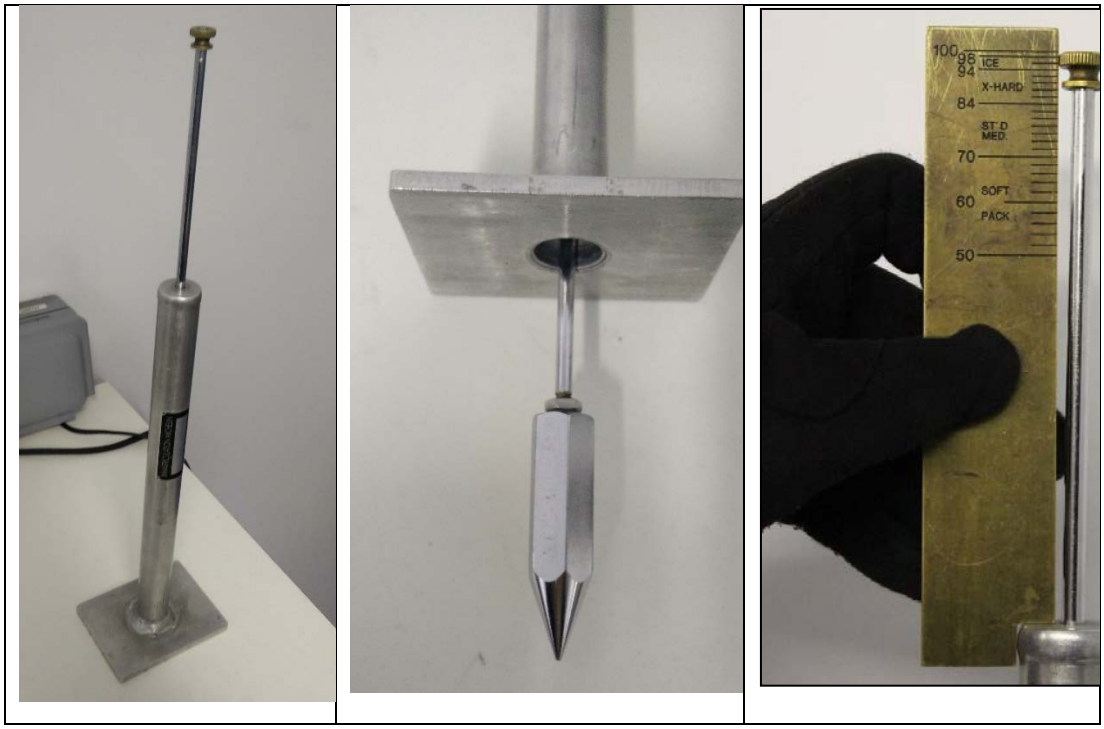

Figure 3.18 Left - CTI Tester. Middle - Weighted measurement spike. Right - CTI measuring gauge.

3.8 Profilometry

Measurement of the roughness of the snow surface was a key parameter to be studied. Previous attempts to investigate snow roughness were very labour intensive, involving infiltrating a snow sample using dimethyl phthalate (DMP), sectioning the sample using a microtome, imaging the cross section and manually tracing the profile (Ella, 2014). Part of the work of this PhD has been to investigate the use of a contact profilometer to measure the surface roughness of the snow directly. The use of a contact profilometer drastically reduces the labour required to carry out a measurement and allows multiple measurements to be carried out in different locations to reach an average roughness for the snow tray. The profilometer chosen is the Mitutoyo Surftest SJ-412. This profilometer is capable of measuring roughnesses in the range of ±800µm with a resolution of 0.0125µm with increased resolution at lower ranges. The measurement

stylus used a 2µm tip meaning measurement of some of the finest details was limited as shown in Figure 3.19.

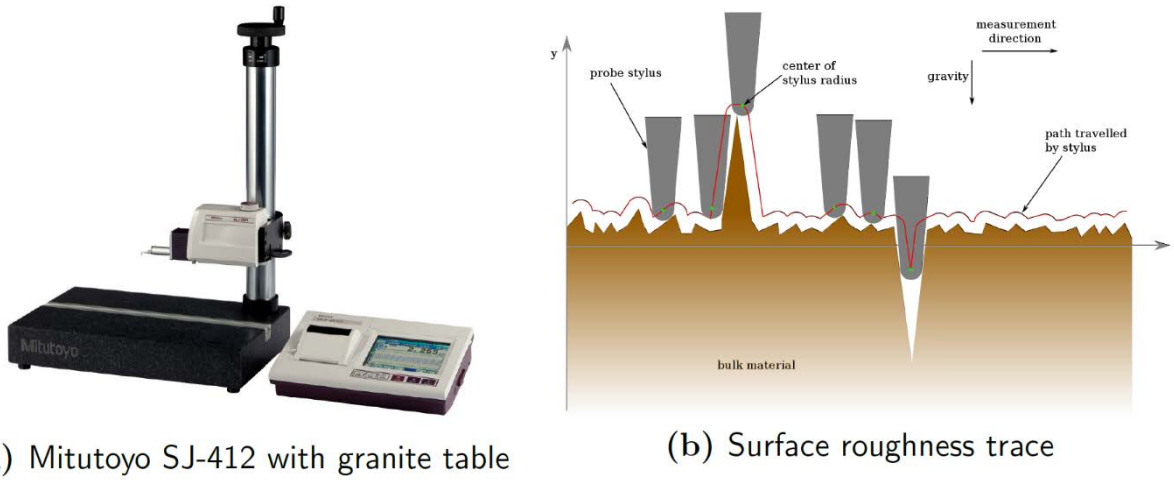

a) Mitutoyo SJ-412 with granite table

(b) Surface roughness trace

Figure 3.19 - a) Mitutoyo SJ-412 contact profilometer. (b) The limitations of the measurement profile. A contact profilometer trace is limited by the size of the stylus tip. A larger tip may be unable to pick up features smaller than the size of the stylus tip on the actual surface. (Suga, 2016)

The surface roughness of the snow was measured on a scraped track immediately before friction testing. This allowed the measurement of the surface which was about to interact with the rubber. Instead of using a separate mount for the profilometer as shown in Figure 3.19 the system was mounted directly to FRIMA via the slot design for auxiliary equipment as shown in Figure 3.20. This allows the measurement of the snow roughness at different locations along the testing track without having to place the instrument on the snow surface, thus preserving the snow track for friction testing.

The roughness profiles were 10mm in length, this measurement was enough to take in a representative number of snow grains (average grain size approx.1mm).

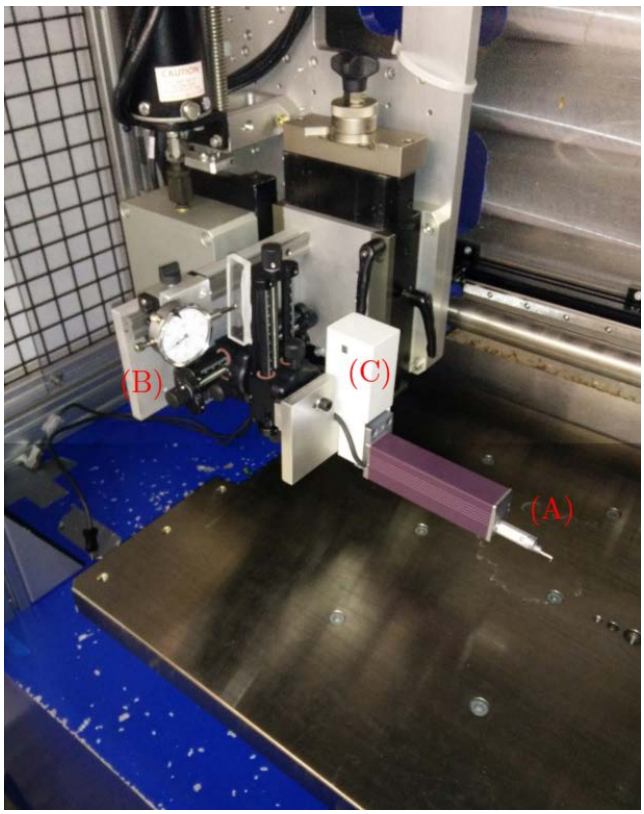

Figure 3.20 - Contact profilometer mounted to FRIMA auxiliary equipment holder. (A) - profilometer tip, (B) - lateral position adjustment, (C) - Autoset unit to position profilometer vertically on the snow surface

A minimum of 20 different roughness measurements were made at approximately 5 different locations along the test track length. At each of the 5 locations, 4 measurements were made next to each other (profilometer manual offset using mounting jig). The roughness could be quite variable so many measurements were required so that a binning process could be carried out where the measurements were examined by eye and if there are large sections where no data is recorded (a trough too deep for the profilometer tip to reach) the measurement is discarded.

In addition to the individual measurements of surface roughness spread across the snow tray, an attempt was made to generate a 3D surface profile of the snow. This was done by using the lateral position adjustment (B) in Figure 3.20, to move the tip sideways from the previous measurement. This lateral movement was measured with a dial gauge allowing movements as small as 0.01mm. The 3D profiles were created by taking 100 measurements of 5mm in length with a gap of 0.05mm between them. This gives a 5mm x 5mm image of the surface which makes it easier to visualise the surface and identify grain shapes and structure then looking at an individual roughness trace.

3.9 Shear Testing

Shear testing is a well-established mechanical testing method for use on snow (Muro et al., 1980), (Perla et al., 1982)). Even so, it is still a difficult technique to use to get good quality repeatable results. The main issue is how to grip the snow without fracturing it during a test. In order to achieve this on the highly compacted snow used in this research extensive experimentation was required, looking into different testing apparatus, different snow preparation processes, different snow sample sizes and different shear rates. Several months were spent designing, building and testing different shear box designs, altering the parameters of the testing (speed, acceleration, normal force), altering the preparation protocol for preparing the shear samples and finally choosing the size of the shear sample. All of these were selected in order to achieve the most consistent shear failure mechanisms where the entire block would shear across its base simultaneously in order to achieve the best consistency of results.

The shear testing method which was used throughout the testing plan was carried out on FRIMA as the system already had all the data logging equipment and it was easier

to prepare the snow for a test then removing the snow from a test tray and shearing using other equipment. The processes of carrying out a shear test are as follows:

1. An initial section of snow is milled out so there is a clear area to shear the snow into. This was milled to 11mm depth (Figure 3.21 (A)).
2. A shear box with metal blade edges (internal width 55mm, blade depth 10mm) was used to mark the area of the snow which is to be sheared(Figure 3.21 (B)).
3. The marked area of the snow is cut out using an electric router (Dewalt D26203 Plunge Router with 5mm diameter straight cut bit) (also milled to 11mm depth) (Figure 3.21 (C)).
4. Any excess snow left behind by the cutter is removed using compressed air
5. The shear box is pressed into the cutout area. The blade edges of the shear box are 10mm deep so do not touch the snow below, instead, a load is applied directly to the top surface of the snow to be sheared
6. The shear test is carried out. The test is carried out at 0.1m/s and the load applied to the shear block was 0.2kN. The shear block measured 30mm x 55mm (Figure 3.21 (D)).

Figure 3.21 shows example images of the stages of carrying out a shear test. Steps 1, 2, 3 & 6 refer to images A, B, C & D respectively.

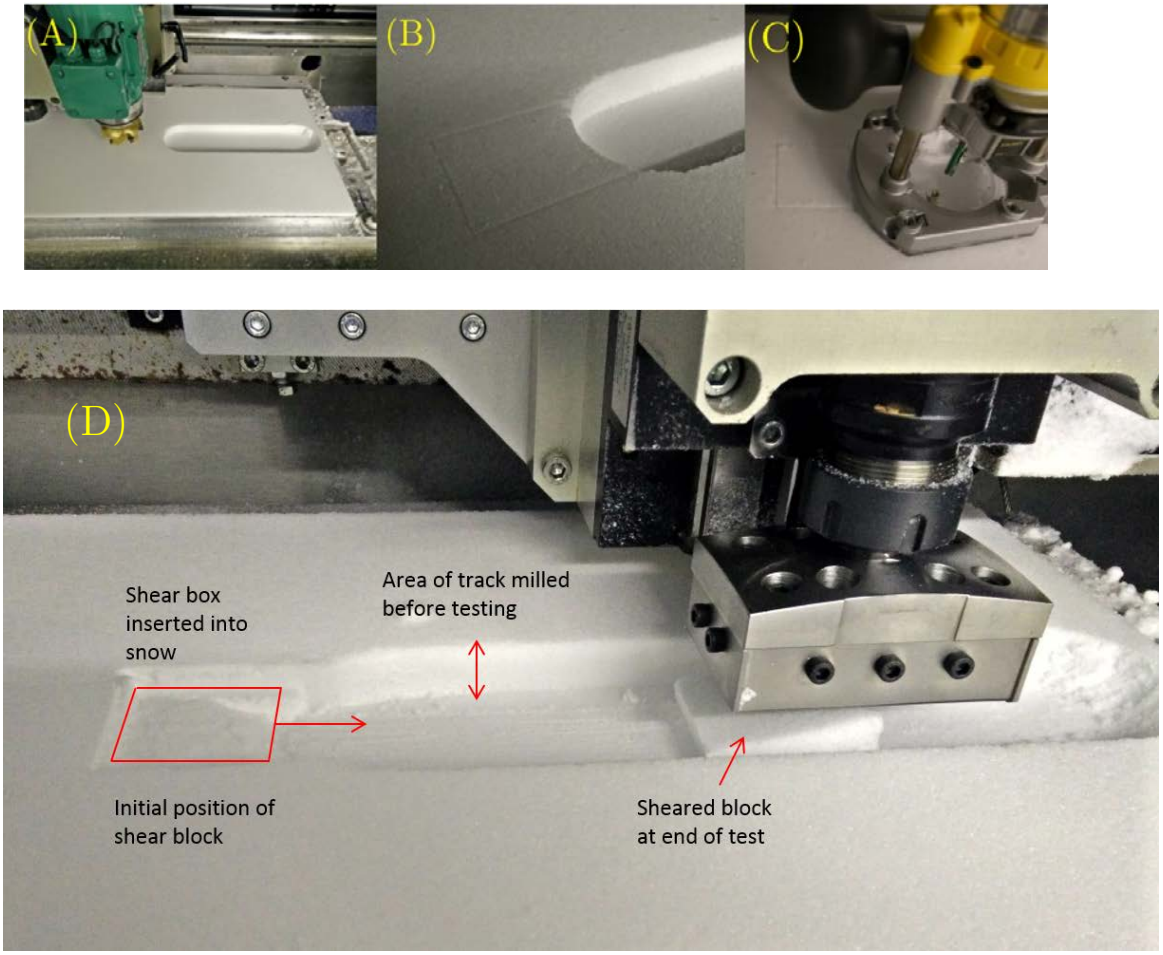

Figure 3.21 - (A) - Milling snow before the shear test. (B) - Marking out area to be prepared for the shear test. (C) - Milling out snow around the shear block. (D) - Example process for carrying out shear test

Five tests were carried out on each tray this number provided enough repeats to calculate an average shear strength but left enough unused snow in the tray for the other testing. Occasionally the snow would not shear cleanly but would instead collapse, in these cases the test data was discarded as other failure processes are occurring rather than basic shearing.

3.10 Compression Testing

Unconfined compression testing of snow in the laboratory was carried out using a commercially available universal tester, specified and procured during this project. The tester used in this study is a Tinius Olsen 50ST model (Figure 3.22). In order to ensure universal tester operated correctly in the cold laboratory at -10°C, special ball screws were supplied with the compression system. In addition, the load cell had to be calibrated while at -10°C.

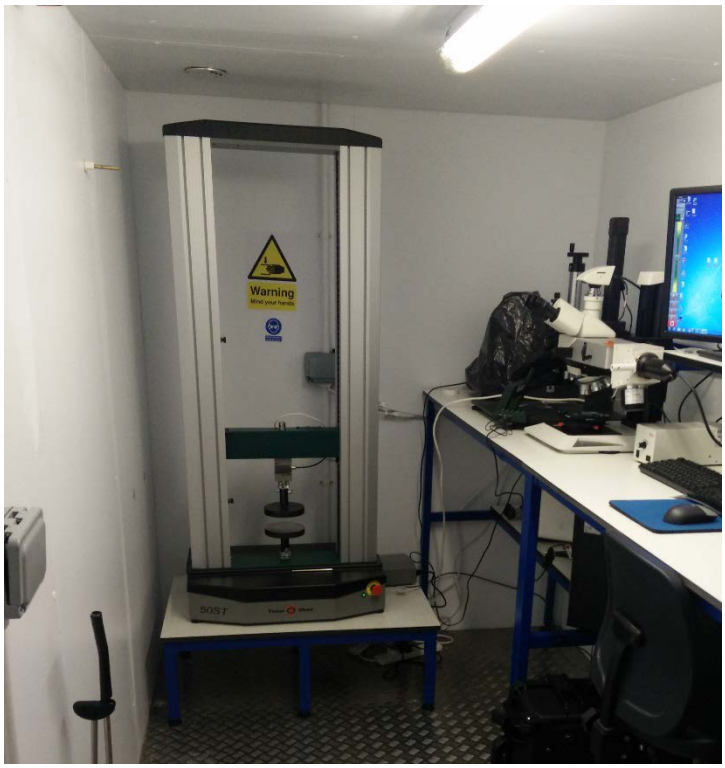

Figure 3.22 - Tinius Olsen 50ST universal tester in place in cold laboratory

With this system set up, it was possible to use a core drill to extract samples of snow (Figure 3.23) from the testing tray, these samples were then prepared on the same microtome used to prepare the snow samples for density testing (Figure 3.17). This

allowed the snow samples to be cut down to have parallel sides in order to achieve even load application during the compression test.

Figure 3.23 - Core drill. Left - bimetal core drill with quick release chuck. Right - Example use of core drill during the development of the testing protocol.

The snow samples all varied in height and diameter so each sample was individually measured using a digital vernier calliper, by using a 60mm core drill the size of the compression test samples were approximately 55mm∅ x 40mm height, example test specimens can be seen in Figure 3.24. As with all the testing procedures, a careful balance of the number of samples and sample size had to be found in order to achieve consistent mechanical testing results while leaving enough material for the other testing methods. Three different size core drills were initially used (40mm, 60mm & 100mm) the 40mm drill produced samples which would fail erratically and were harder to handle. The 100mm drill used up too much of the snow tray in order to extract enough test samples so the 60mm drill was chosen.

Figure 3.24 - Left - Core samples before microtome preparation. Right - Example core sample in place in compression platens (for illustration only, ends have not been prepared to be parallel).

Compression tests were carried out at 3 different speeds: 5mm/min 50 mm/minute and 500mm/minute. Snow compressive strength is strain rate dependent so it was important to test at multiple different speeds in order to investigate how the snow strength varies and also to investigate snow above and below the brittle/ductile transition which is present in snow.

500mm/minute was chosen because it is the highest rate the compression system could achieve, this would give test data as close as possible to the speeds tests were being carried out on FRIMA (friction tests carried out at 0.01m/s (600mm/min)). 5mm/minute was chosen as it was a low enough speed that all the snows behaved in a ductile manner, no cracks were seen to propagate through the material when testing at this speed, instead, the snow compressed in the manner of a foam. 50mm/minute was chosen as an intermediate speed between the two extremes. Examples of ductile and brittle failure can be seen in Figure 3.25. Each test speed was repeated 5 times for each snow type, a total of 15 compression test samples had to be extracted from each test tray.

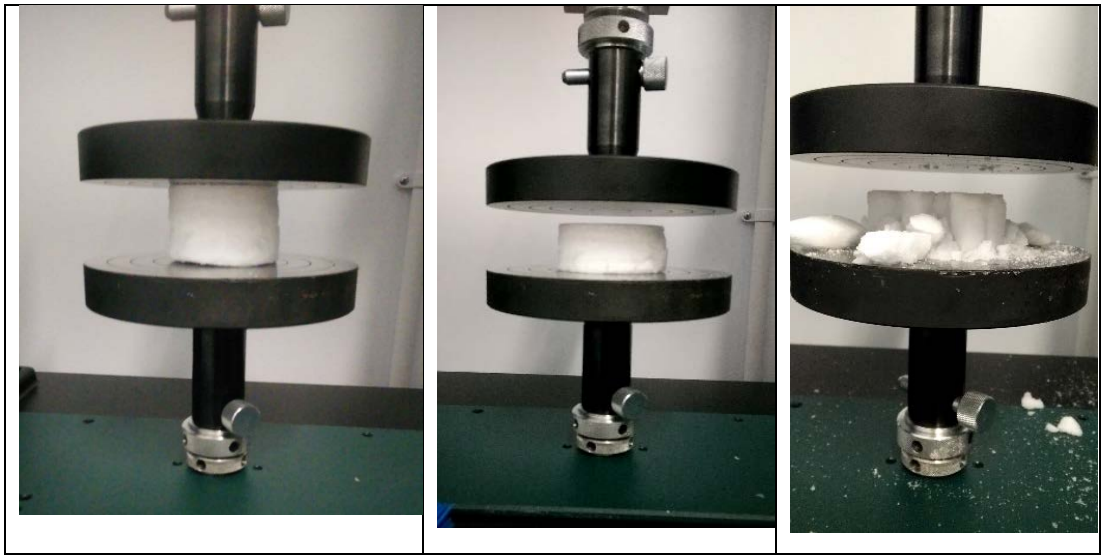

Figure 3.25 - Left - Example snow sample in place before compression test begins. Middle - Ductile failure of snow sample after testing at 5mm/minute. Right - Snow sample after testing at 50mm/minute

3.11 Cohesion Testing

Cohesion testing is a method of measuring the forces required to break apart the snow structure by forcing a blade through the snow at a constant speed. There is a lot of different interactions going on within this test, not just shear or compression, the test was developed by Michelin in an attempt to rapidly characterise snows, it was carried out during this PhD as a method of rapidly confirming the similarities between snow tray repeats and also as a method to compare to the previous snow trays characterised using this method ((Ella, 2014)).This test is carried out on FRIMA, on a snow track which is prepared the same way as a snow track to be used for friction testing (track prepared with scraping tool).

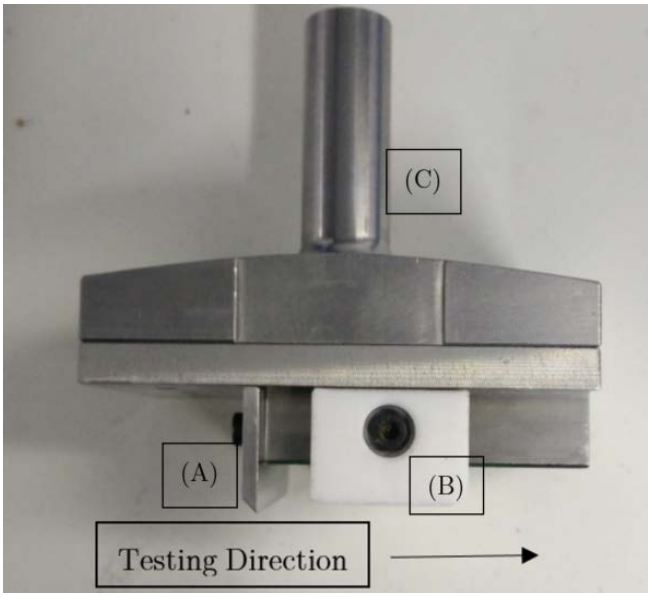

Figure 3.26 - Cohesion testing tool. (A) - metal blade to penetrate 2mm into the snow, (B) - polymer slider to reduce friction, (C) - FRIMA sample holder.

Figure 3.26 shows the cohesion measurement tool which was used for this test. It is used by forcing the metal blade 2mm into the snow until the polymer slider contacts the snow surface. The normal load on the tool is then reduced to 0.1kN and a test is carried out by using FRIMA to force the blade laterally through the snow at 0.1m/s and measuring the force required to do so. The test is repeated 3 times in order to calculate an average cohesion force.

3.12 X-ray Microtomography

X-ray microtomography was carried out in collaboration with Dr Ian Butler of the University of Edinburgh Geoscience department. Ian has built a custom XMT system designed to be adaptable to take different types of sample stage and different sizes of samples. The system is set up within a concrete reinforced laboratory originally designed for blast testing and is rated to contain up to 20 Kilobar blasts. Setting up the XMT system in a room such as this allows large samples and axillary equipment to be placed in close proximity to the X-ray source without being constrained by a small X-ray analysis system as is more normal. An image of the test area can be seen in Figure 3.27.

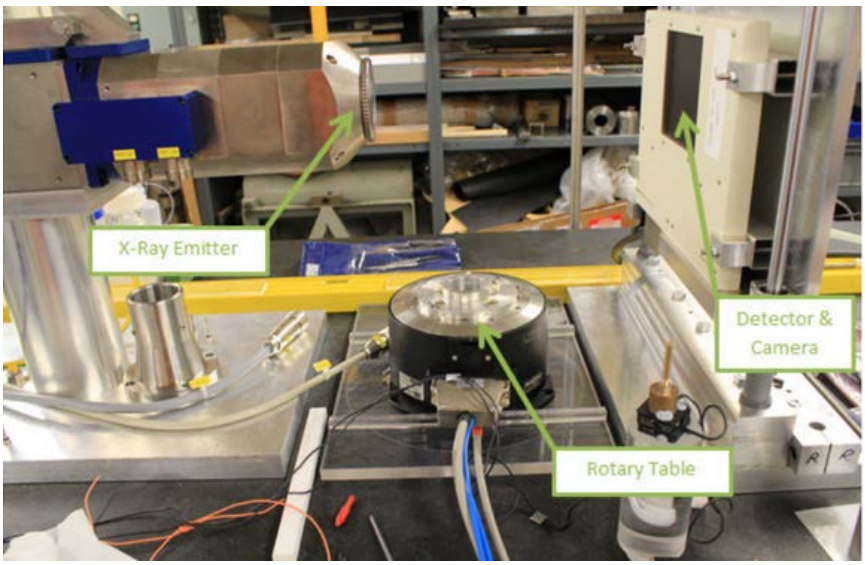

Figure 3.27 - X-ray Microtomography Test Area

In order to examine snow microstructure using this XMT system, a cold stage had to be designed which would contain the snow samples, maintain a temperature of at least -10°C for several hours and be able to rotate 360° to allow full imaging of the sample. In addition, the chamber walls had to have as low an X-ray attenuation as possible in order to gather as much data as possible from the snow sample held within.

Initial designs for this stage made use of a Peltier thermoelectric cooling plate along with liquid cooling components designed for use with computers. A rendering of this design can be seen in Figure 3.28.

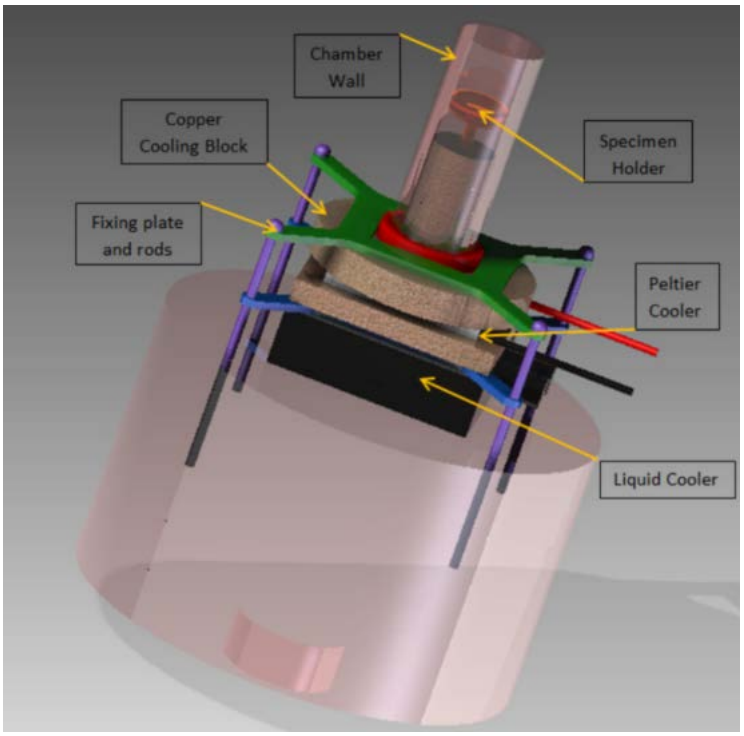

Figure 3.28 - Cold stage concept design for use with XMT system

The design was tested and improved over many iterations, however, it never achieved the performance and temperature stability required to achieve good quality imaging. The decision was taken to invest in a commercially available cold stage which could be modified for use with the XMT system. The system was supplied by Deben, the technical drawing of the stage design can be found in Appendix 2 (Section 8.2). The design utilized a double walled sample chamber constructed from polystyrene which exhibits very low X-ray attenuation. The chamber could hold snow samples up to 5mm x 5mm x 5mm cubes and could maintain a temperature of -20°C indefinitely, by making use of Peltier thermoelectric cooling. An image of the stage in place immediately before an X-ray scan is taken can be seen in Figure 3.29.

Figure 3.29 - Deben cold stage in place immediately before X-ray scanning. Snow sample can be seen polystyrene chamber.

As time on the XMT system had to be booked in advance it was not always possible to test snow samples on the same day which the other tests are carried out. Instead, snow samples were taken from the trays on the day of testing, cut to be approximately 5mm x 5mm x 5mm cubes on the microtome, then stored at -80°C until the XMT system became available.

On the day of testing, the sample holder was cooled to -20°C for one hour to ensure the system was stable. The snow was then placed inside the double walled chamber while the whole system is within the cold room. The entire cooling system was then

transported on a trolley to the Geoscience department while making use of a portable mains power supply (APC Smart-UPS 1500VA Uninterruptable Power Supply), to ensure cooling was maintained during transport. The stage could then be installed in the XMT system, aligned and then scanned.

Scans times were between 50 minutes and 3 hours depending on which settings were used and how many images were taken. A typical scan consisted of 1500 images with the X-ray source at 60kV and a power of 2.8W. This achieved a resolution of approximately 13.7µm per voxel, however, all of these values were slightly different for each scan as alterations were made based on previous results. An example 3D visualisation of the snow microstructure can be seen in Figure 3.30, the full process of analysing these images and interpreting results is discussed in section 4.8.

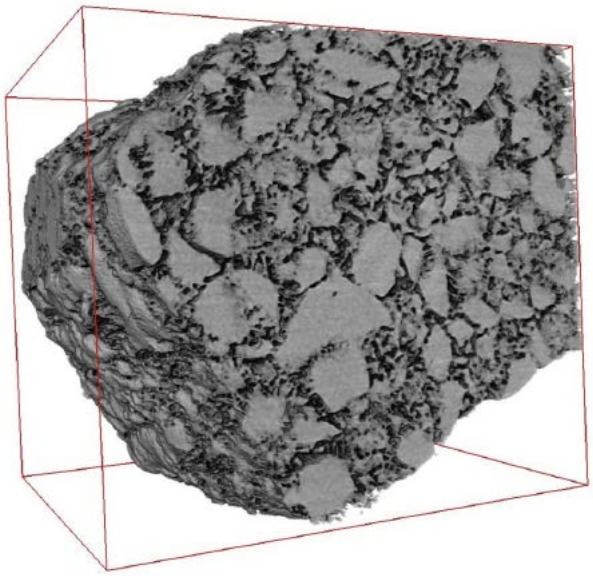

Figure 3.30 - Greyscale 3D visualisation of XMT scan of Blended 170 snow (approx. dimensions 5mm x 5mm x 5mm).

3.13 Microscopy

In order to identify the different microstructures seen in the different snow types imaging was used. Optical imaging of the snow was carried out on the snow before it was compressed into testing trays and also on the samples of snow removed from the testing tray after compression. Imaging was done using either a Canon 6D DSLR camera and a Canon MP-E f2.8 1-5x macro lens or using a Leica materials microscope using objective lenses from 5x to 100x magnification as shown in Figure 3.31. The snow samples were placed on a reference 1mm^2 background (snow crystal card) and the images taken. This proved to be a more reliable method for comparing the images from the microscopy and the photography as it was difficult to get accurate scaling information using a DSLR without this. Example DSLR images can be seen in Figure 3.32.

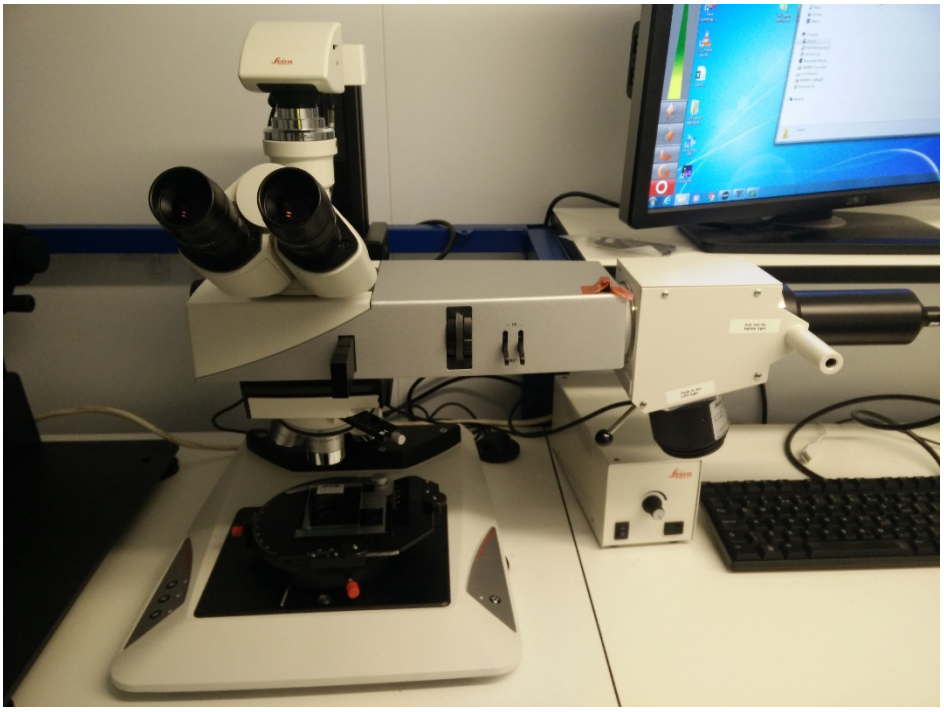

Figure 3.31 - Leica microscope in place in cold laboratory

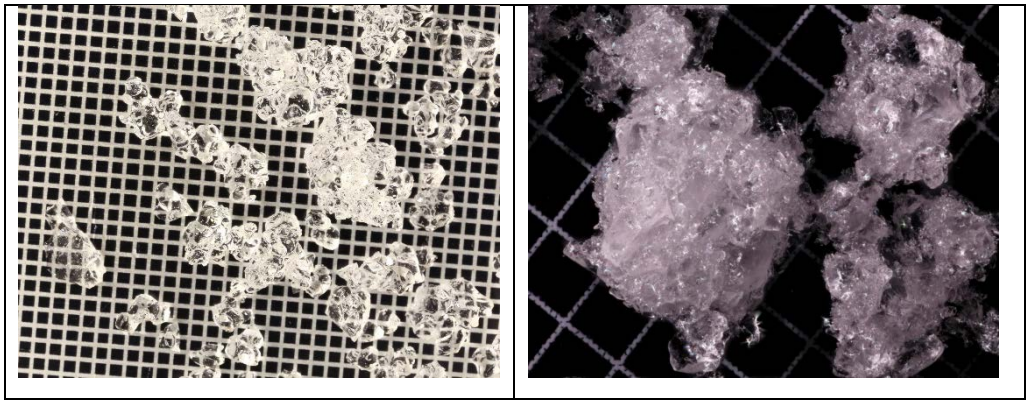

Figure 3.32 -Example images of snow taken using DSLR. Left - Natural Snow. Right - Blended Snow. Reference background of 1mm² squares.

3.14 Summary

Extensive work has been carried out to develop new methods for testing and characterising snow in the laboratory. No previous investigation into the mechanical properties of snow has used all of the methods listed above in order to attempt to characterise snow. When combined with the friction testing program, the results can be used to investigate which snow properties and characteristics have the greatest influence on rubber friction on snow.

4 Snow characterisation results and discussion

Summary

This chapter presents the mechanical testing and characterisation results from the testing of the different snow types. Each of the tests was repeated between 3 and 20 times so a binning process of discarding failed tests could be carried out for some measurements in addition to calculating average values. In addition to presenting the raw data, analysis has been done to investigate and determine values that can be extracted from the data. For example, calculation of the kurtosis and peak count density from the surface profiles and evaluation of the yield point and compressive modulus from the compression test data.

4.1 Introduction

In order to identify differences within the available snows that may lead to variations in friction, a carefully selected set of tests were carried out on the snows. The tests were chosen to allow fundamental mechanical analysis of the snow in addition to the established tests used by Michelin such as cohesion and penetration testing. The testing methods and instrument capabilities are described in chapter 3. The following is the presentation and discussion of the results gathered during the testing.

With these results, the differences between the snows can be found which contribute to the variations in friction seen during the friction testing. If some of the results do not provide a strong difference or conclusions about the snow, the results are still to be used to look for how the measured properties effect friction, even if only in a very subtle way.

4.2 CTI Testing

CTI testing is a measure of snow compaction by measuring the penetration resistance of the snow. A shaped mass is dropped on onto the surface of the snow and the penetration is measured. The results are unitless and can vary from 50 for soft powder snow to 92 for extra hard packed snow, above 92 the material is considered to be ice. CTI testing was carried out in 9 locations across a snow tray to ensure a consistent material before proceeding to the other tests. CTI measurement results for all snow trays and tray repeats can be seen in Figure 4.1.

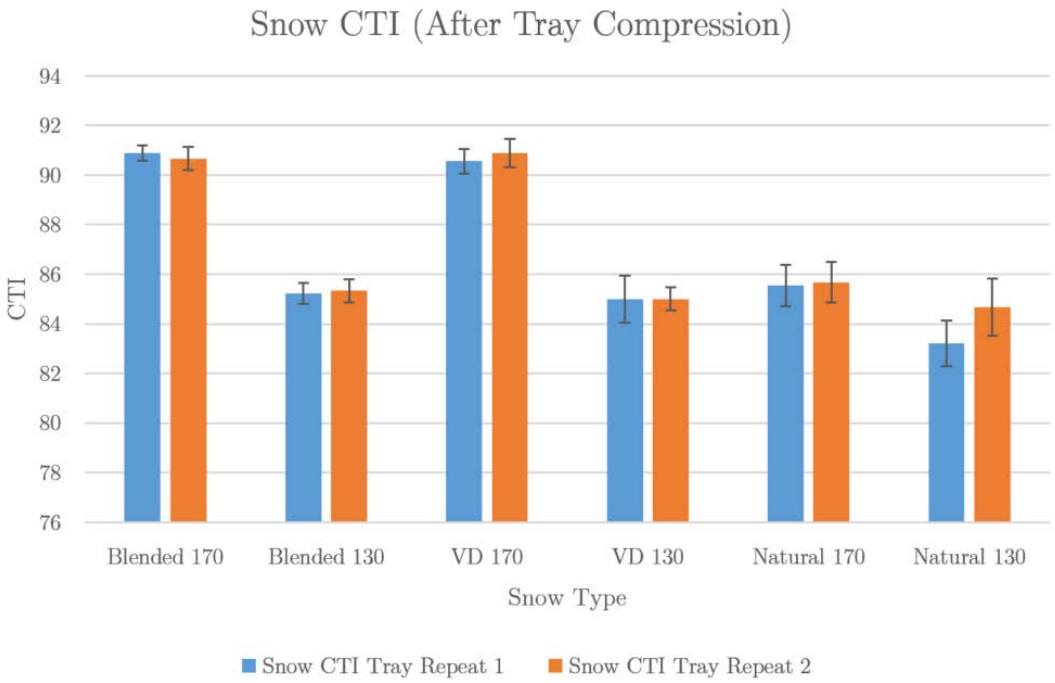

Figure 4.1 - Average snow tray CTI measurements. Orange bars represent tray repeats. Error bars represent the standard deviation of nine CTI measurements across the tray.

From examination of Figure 4.1, it is possible to see that the CTI measurement is a very consistent measurement with the standard deviation across a single tray and tray repeats giving close and consistent results. In general, the preparation procedure is the main influence on the CTI of the snow. The 170 procedure produced vapour deposition and blended snow with a CTI of 91 and the 130 procedure produced snow with a CTI of 85. The natural snow did not respond as consistently as the other two snow types with the 170 procedure only producing snow at CTI 85 and the 130 procedure producing snow at CTI 84. This is most likely due to the larger grain size of the natural snow resulting in lower packing density during the tray preparation process. This leaves a lot more air between the grains which allow the penetrometer to enter further into the snow.

It should be noted that the Blended 170 and VD 170 snows have a CTI of 91 which is on the verge of being considered ice.

4.3 Density Testing

In the initial testing plan, only one measurement was made per testing tray. During the second testing plan, five density measurements were made before the snow was compressed into the snow tray, a further five measurements were made once the snow had been compressed. This allowed measurements to be taken across the snow tray in order to confirm that the density is consistent across the entire snow tray.

The average results from the density testing carried out in the secondary testing plan along with the standard deviations are presented in Table 4.1

Table 4.1 - Density Testing Results - Tray repeats are listed separately (2 of each snow type at each compression level)

	Blended	Blended	Blended	Blended
Compression Level	170	170	130	130
Density Before Compression (kg/m³)	427.8	420.4	425.3	435.6
Standard Deviation	11.7	15.7	7.6	5.2
Density After Compression (kg/m³)	577.6	592.0	524.5	531.3
Standard Deviation	18.4	15.5	33.8	22.2
	VD	**VD**	**VD**	**VD**
Compression Level	170	170	130	130
Density Before Compression (kg/m³)	152.0	168.9	164.0	160.3
Standard Deviation	11.3	9.1	4.1	2.3
Density After Compression (kg/m³)	534.5	500.1	419.5	421.1
Standard deviation	24.1	9.4	7.4	16.1
	Natural	**Natural**	**Natural**	**Natural**
Compression Level	170	170	130	130
Density Before Compression (kg/m³)	430.5	499.8	481.1	501.5
Standard Deviation	24.7	7.2	8.9	2.9
Density After Compression (kg/m³)	475.1	559.4	407.6	518.9
Standard Deviation	11.8	8.7	21.4	16.4

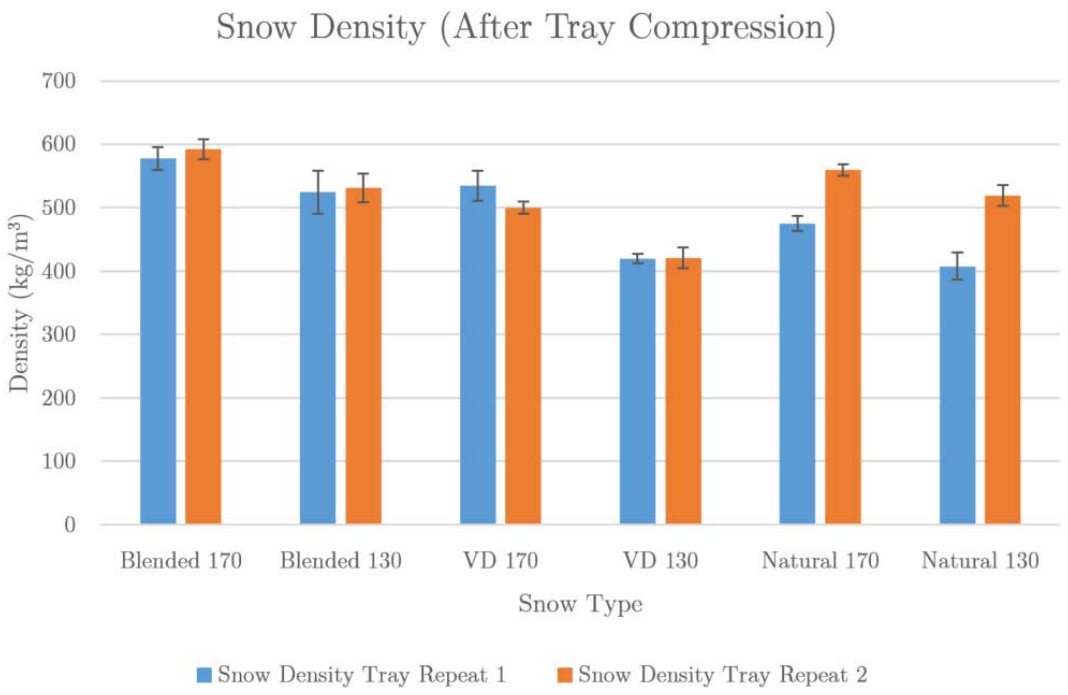

Figure 4.2 - Density of all snows in testing plan 2. Orange bars represent tray repeats. Error bars represent the standard deviation of 5 density measurements across the tray.

Figure 4.2 shows the average tray densities measured in the middle of the testing day (immediately after the friction testing has taken place) in order to be as consistent as possible with the timing of these measurements.

These measurements are useful to understand some basic differences between the snows. Blended snow has a higher density then vapour deposition snow with the compression parameters having a distinct effect on the density of the snow for the blended and vapour deposition snows. The 170 compression procedure makes blended snow of ~580kg/m^3 while the 130 procedure makes blended snow of ~528kg/m^3, a difference of 52kg/m^3. For the vapour deposition snow, the 170 procedure makes snow at ~517kg/m^3 and the 130 procedure makes snow at 420kg/m^3 a difference of 97kg/m^3. The reason

there is a bigger difference in the density of the two procedures for the vapour deposition snow compared to the blended snow is most likely due to the fragility of the dendritic vapour deposition snow resulting in more fracture and thus achieving a tighter packing than the blended snow.

The natural snow is interesting as it still exhibits the same effect of having a lower density when the compression is lower. When the date at which these tests were carried out is taken into account it is possible to see the tray repeats (shown here in orange, were carried out 6 to 8 weeks later than the original tests) have significantly higher densities than the initial tests. During the time between tests, the snow was stored as it was collected from the field in cardboard boxes at -40°C. This time has caused the snow to sinter and the grains to grow, resulting in the higher density measurements as shown.

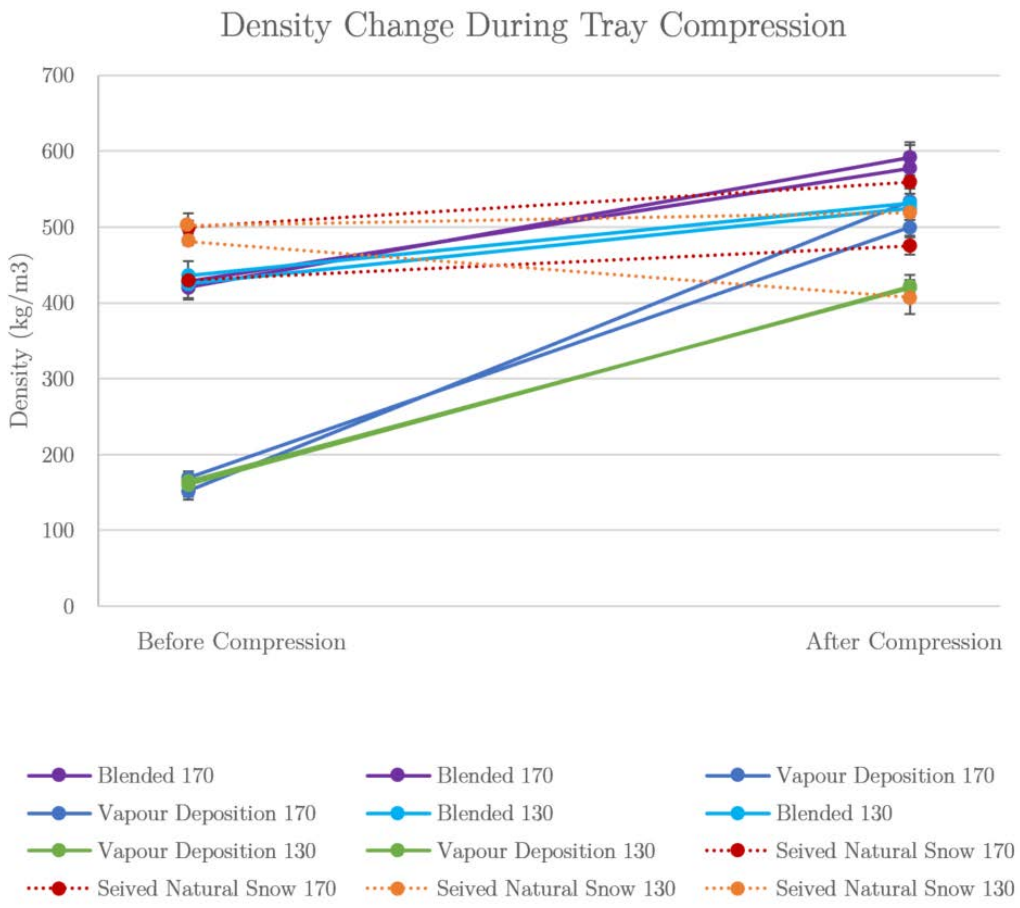

Figure 4.3 - Density data, initial density measurements before compression on the left, final density measurements on the testing day on the right. Pairs of coloured lines represent tray repeats.

From an examination of Figure 4.3, it is possible to see that there are three distinct clusters of starting density. The lowest density is that of the vapour deposition snow, this is consistent with the examination of the microstructure by eye. The large dendritic grains are very fine and pack very loosely with adjoining grains. All measurements of vapour deposition starting snow are within the margin of error of the density of each other, showing that starting material has remained relatively constant over the testing period.

The next cluster of snow of the same starting density is the blended snows. Again, all blended snows start at similar densities meaning that it is a consistent starting material.

The highest starting densities are from the natural snow. However, there is also a natural snow measurement included with the blended snow cluster. This was the first natural snow which was tested. The density was measured on the same day it was collected from the Highlands. The other natural snows were tested several weeks later after being stored in a -40°C freezer. This additional time allowed the natural snow to sinter further and thus densify.

When looking at the densities of the snows after compression, on the day of testing some general trends are obvious. The lower compression preparation gives a lower density snow then the high compression. The vapour deposition snow has a lower density than the blended snow for almost all cases.

4.3.1 CTI and Density

When the CTI values are considered the low compression snows all had approximately the same CTI of 84-85 but had a large range of densities. It was initially assumed that the CTI and density would correlate (which they do if only considering one snow type e.g. blended). The same is seen for the high compression snows except that the natural snow does not have the same CTI as the others (85 for the natural compared to 91 for vapour deposition and blended). These differences are likely due to the packing of the grains and their response to the impact of the CTI tester. A graph of CTI vs Density can be seen in Figure 4.4 which helps to visualise some of the discussions above.

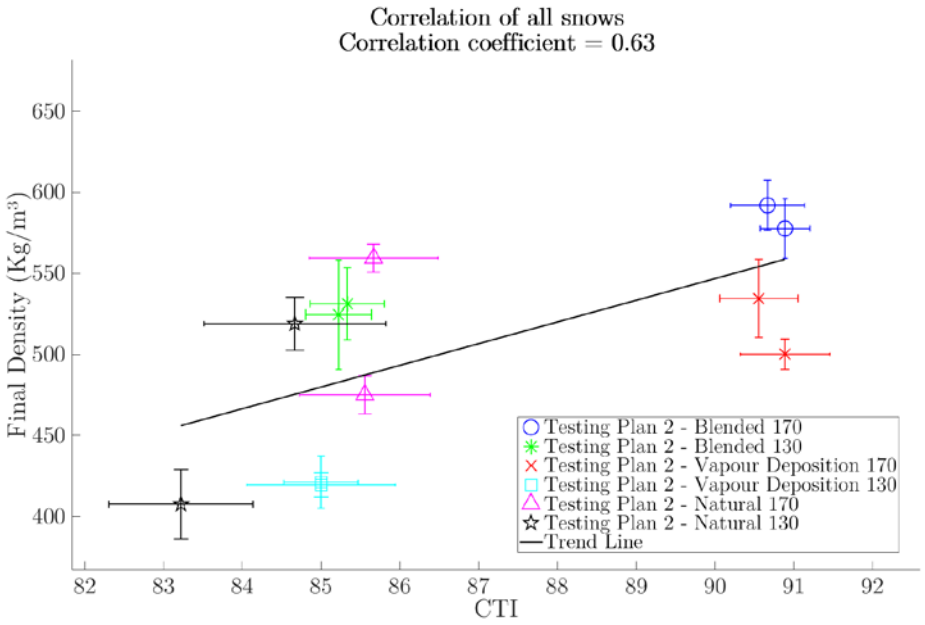

Figure 4.4 - CTI vs Density for all snow types

One major anomaly is present in the results. One of the natural snows had a lower density after compression then the starting material. The only explanations for this are an effect of the sintering during the maturation process or human error during the measurements. Each measurement was repeated at least 3 times giving the same value. This indicates that there is another process going on during the compression and maturation of the snow. In certain cases, sintering can cause a reduction in density, but further investigation to repeat the effect and identify the cause would be required to say conclusively what occurred with this sample.

4.4 Cohesion Testing

Cohesion testing is a relatively simple measurement to take on the snow trays. It gives a good estimation of the strength of the snow. Although there are many different mechanisms going on during the test (shear, compression, and intergranular bond fracture) it is very useful for quickly identifying differences between snow trays.

Cohesion testing was carried out on FRIMA along with the main friction measurements. This meant the data could be analysed using the same software that Michelin provided for the analysis of friction data.

Due to the limited space on the snow tray, there was no room for multiple tests at multiple speeds. For this reason, it was decided that several repeats of one speed would be the most useful way of measuring cohesion. The speed chosen was 0.1m/s and the test was repeated 3 times. The average force measurement was taken over the range 50-80mm to ensure there was a constant speed.

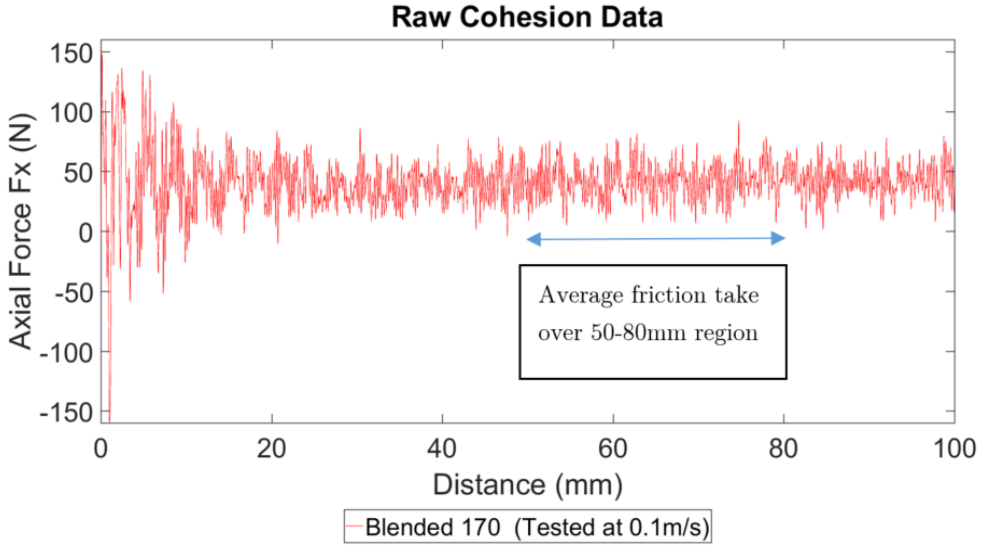

Figure 4.5 - Raw data from cohesion test for blended 170 snow, tested at 0.1m/s. Axial force, Fx refers to the force measured on the x-axis resisting the movement of the blade through the snow.

Figure 4.5 gives an example raw data trace from a cohesion test on blended snow. The noise within the data comes as a result of the thrust tube motor system being used to power the FRIMA testing system. An average value was taken over the range 50-80mm. This gives a value for cohesion which is comparable to the other snows.

From looking at the average cohesion values in Figure 4.6 it is possible to see some basic trends. The high compression (170) have higher cohesion strength than their low compression equivalents. Natural snow has the lowest cohesion, this is most likely due to the larger grain size of the starting material so they were less well packed resulting in a lower coordination number (number of points where one grain contacts other grains) and thus fewer intergranular bonds were able to form. There is an especially large standard deviation of the cohesion results for VD 130 tray one, this is most likely due to an inconsistency in the preparation of the snow tray. It is assumed that the true value for VD 130 snow should be much closer to that seen in the tray repeat, which has an extremely low standard deviation.

This cohesion data can now be used to interpret where the differences in friction arise from when investigating the correlation of μ with mechanical properties in chapter 6. During this process, the values for the two tray repeats are averaged together to achieve a single value for the cohesion of each snow type.

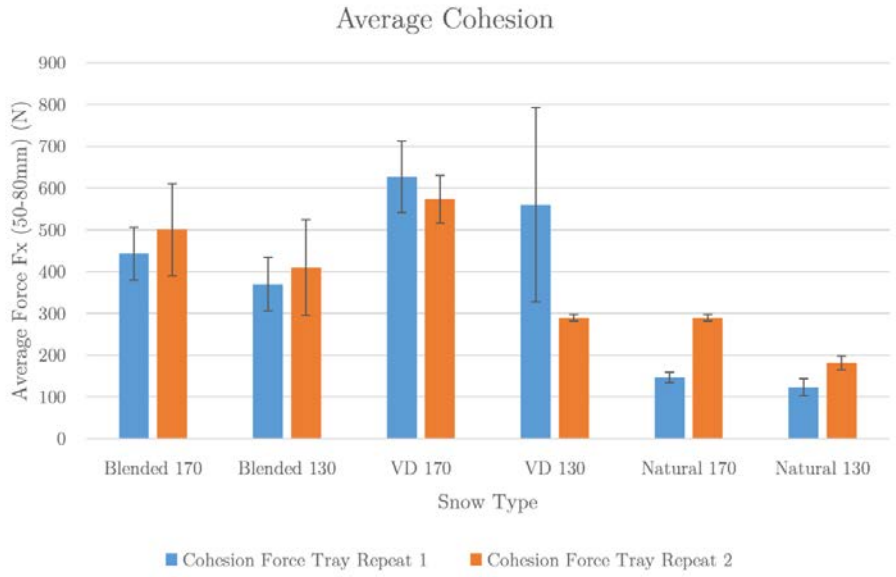

Figure 4.6 - Average cohesion values for all snows, tested at 0.1m/s, error bars represent the standard deviation of the results

4.5 Shear Testing

Shear testing was carried out on the snows trays on FRIMA. Therefore it was possible to use the same software provided by Michelin to analyse the results as with the cohesion and friction testing. It was decided that the most important data to get from the shear tests was the peak shear stress. Analysis of the shear modulus was attempted but there was too much variation in the results resulting from both electrical signal noise and the difficulty in creating parallel sides of the shear block.

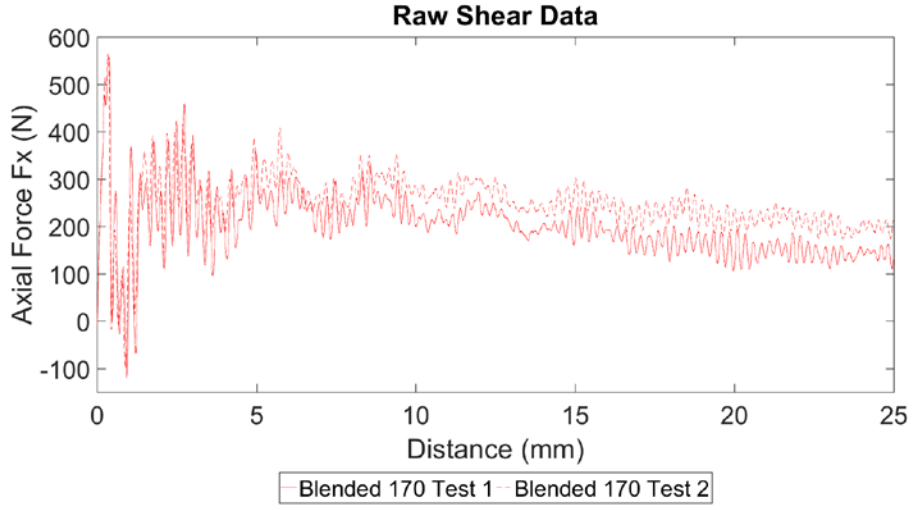

Figure 4.7 - Raw shear test data for blended 170 snow. Two repeats are included

Two example raw data sets from shear testing on blended 170 snow can be seen in Figure 4.7. There was space for 5 shear tests to be carried out on each snow tray, however, the snow would sometimes collapse during the testing rather than shearing cleanly. In order to investigate the fundamental mechanical properties of the snow, it was only possible to use the results which exhibited a clean shear failure. When collapse of the block occurred, other mechanisms influenced the results. This necessitated

discarding the collapsed block data as it presented more like a cohesion test rather than a shear test. For this reason, there were generally between 2 and 4 good quality tests on each snow tray.

Once the raw data was collected it was then converted to stress using the measurements taken of the dimensions of the shear block taken before each test. With the data in the form of stress, it was then possible to find the peak shear stress by selecting the peak stress value before a significant drop was observed. In the case illustrated in Figure 4.7, this is straightforward as there is a very distinct drop with very little noise being obvious in the lead up to the peak at around 1mm distance. Sometimes it is difficult to identify the real shear peak from the noise generated by the testing system. In an attempt to avoid this difficulty a 100 point averaging filter was applied to the trace using Matlabs Signal Processing Toolbox. An example of this can be seen in Figure 4.8.

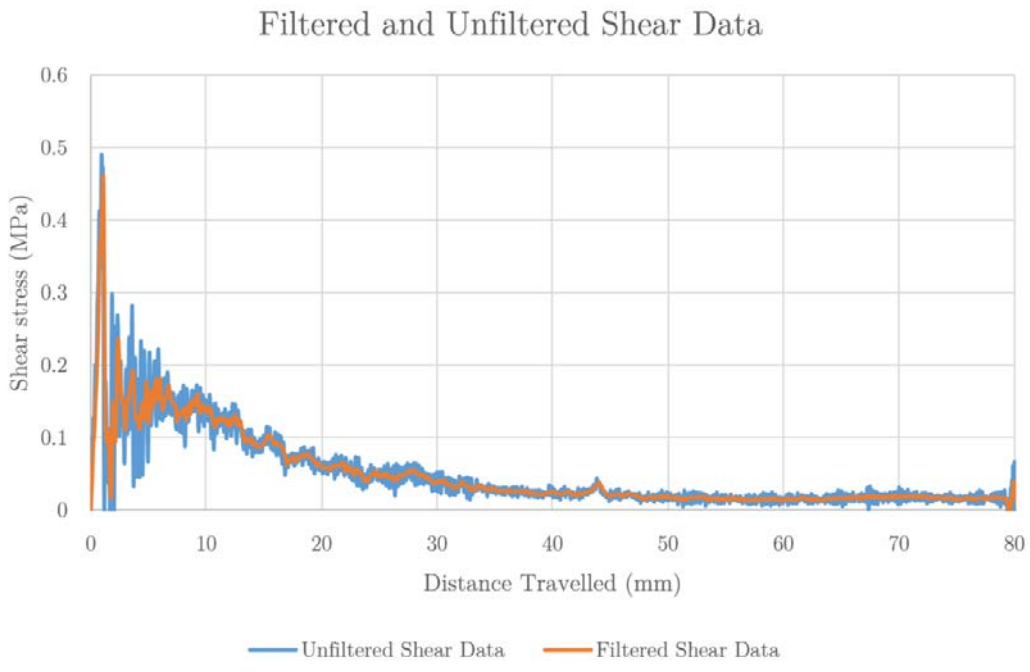

Figure 4.8 - Example of applying a 100 point averaging filter to raw shear data (Raw data from Blended 170 snow)

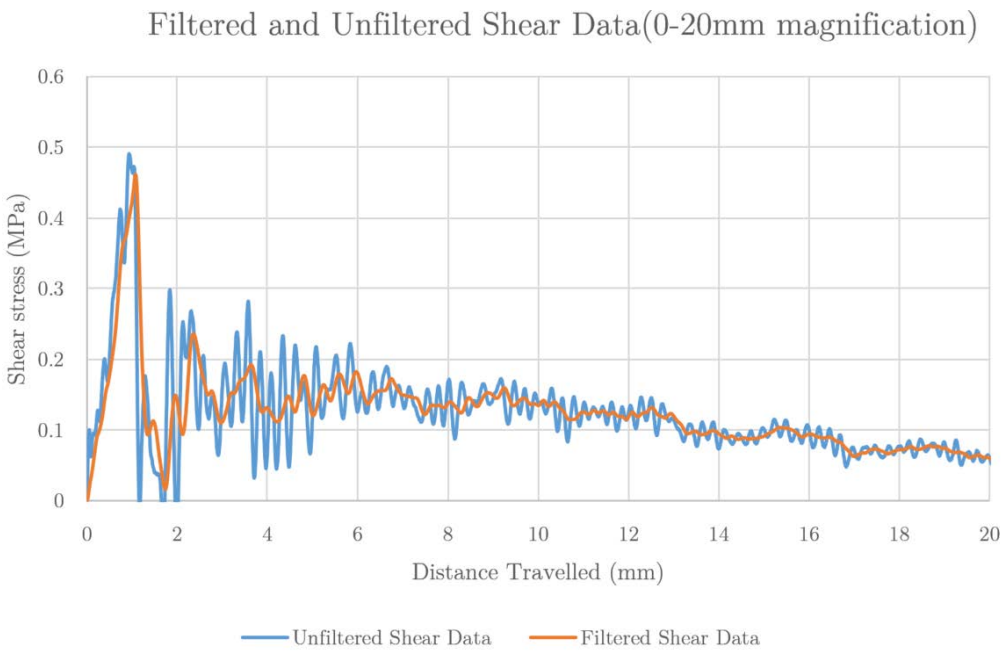

Figure 4.9 - Magnification of Figure 4.8 over the region 0-20mm

Filtering did remove a significant proportion of the noise, however, it was found that in some cases the filtered trace yielded significantly different values for peak shear stress than when the peak is identified by eye. For this reason, the filtering was not used for extracting the peak stress from the raw data, it was selected by eye so that consistency could be ensured.

Average values for peak shear stress are presented in Figure 4.10. The shear test results show a very distinct difference between the low compression and high compression snows. It is not possible to identify differences in strength between the high compression snows as they are all very similar (approximately 0.3MPa). Error bars for these snows are large in relation to the difference between the peak values for the snows.

The same is true for the low compression snows, except for natural snow which appears to have a lower peak shear stress of 0.16MPa compared to the other two low compression snows with peak shear stress of 0.22MPa. The reason for this is likely to be as a result

of the weaker intergranular bonding seen in the natural snow as discussed when investigating the cohesion results.

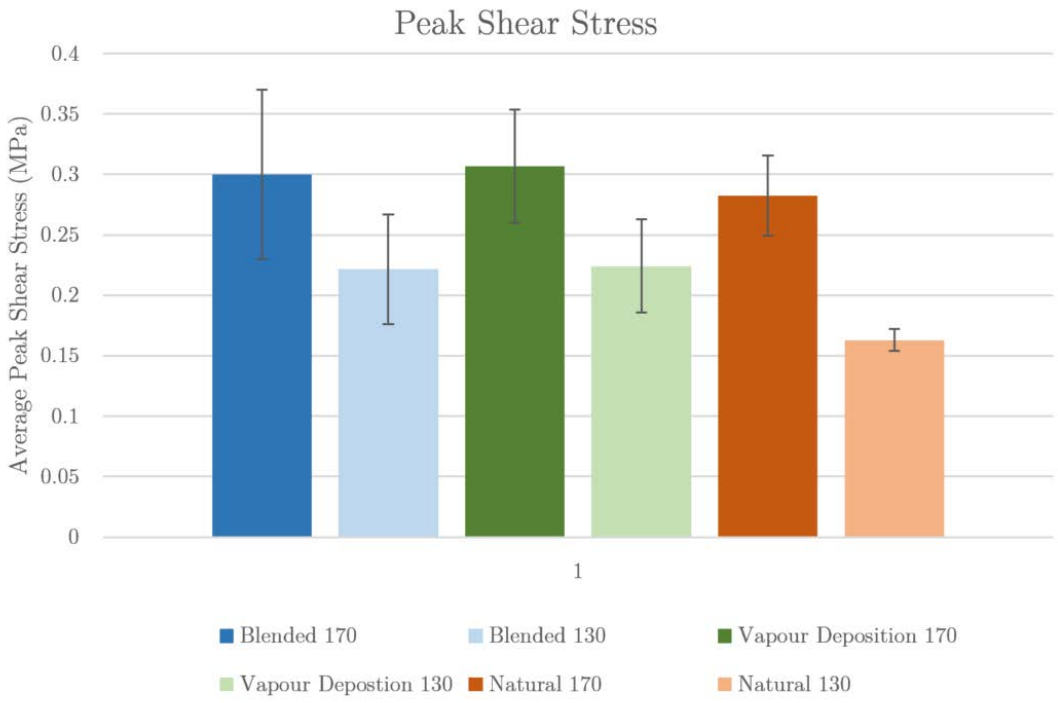

Figure 4.10 - Average peak shear stress listed for all snows, error bars represent standard deviation of results

4.6 Compression Testing

Compression testing was carried out on all snow trays. Three difference speeds were used for the compression testing 5mm/min, 50mm/min and 500mm/min. For each speed 5 samples were tested.

The different speeds used gave different failures. When testing at 5mm/min the strain rate was low enough that the snow did not fracture but compressed in a more ductile way, at 50mm/minute a brittle failure occurred. At 500mm/minute brittle failure also occurred, this is the limit the machine could reach and the speed was chosen to be as close to the strain rates being used during the friction testing. Examples of each of these failures can be seen in

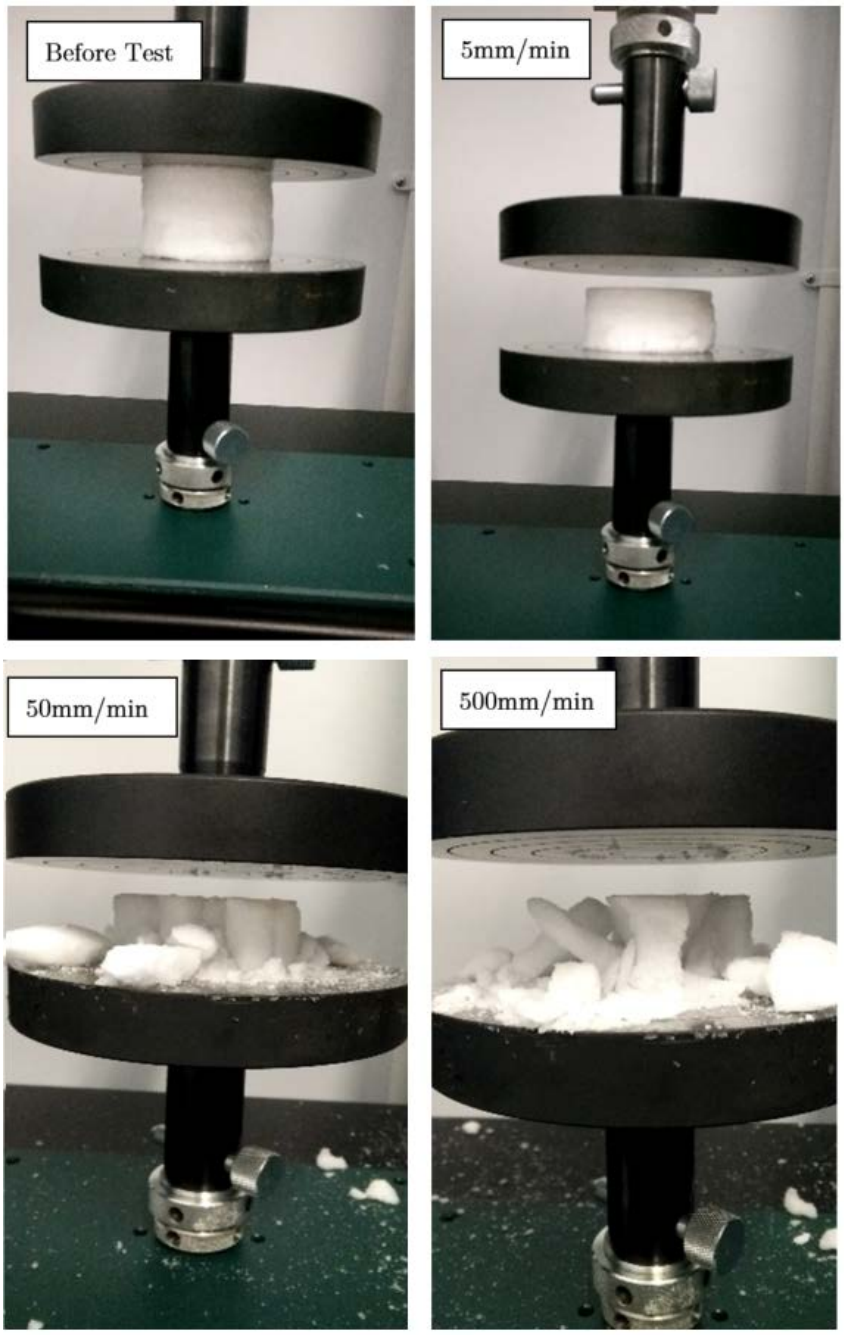

Figure 4.11 - Example compression test images. Top left -Snow sample before compression, Top Right - Snow sample after compression at 5mm/min, Bottom Left - Snow sample after compression at 50mm/min, Bottom right - Snow sample after compression at 500mm/min

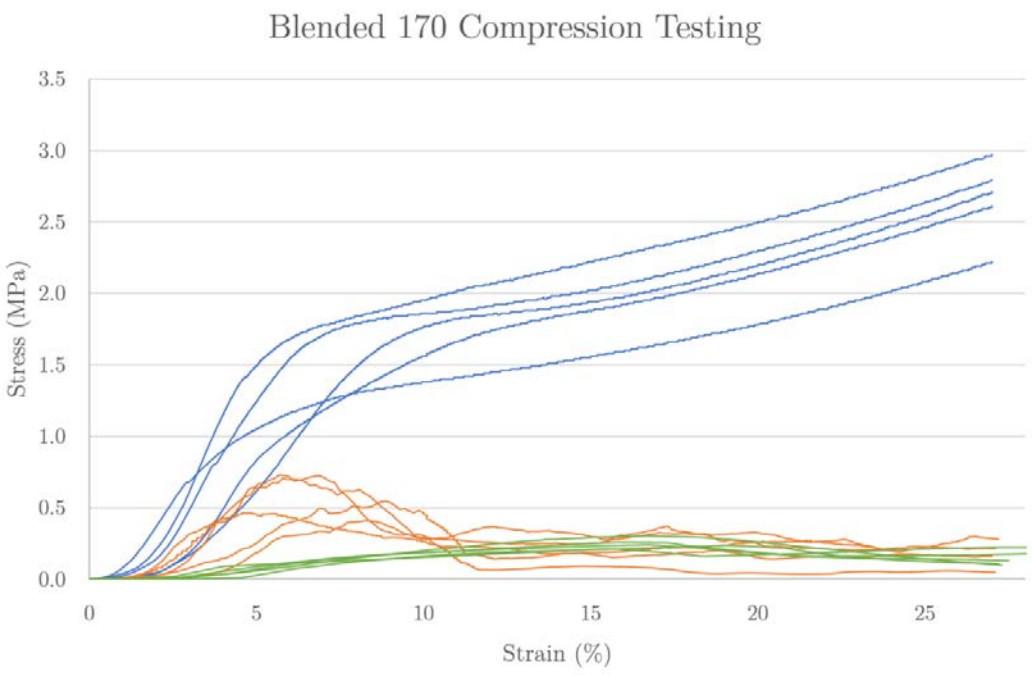

Figure 4.12 - Raw data curves for compression testing of blended 170 snow. Blue lines represent tests at 5mm/min, orange lines represent tests at 50mm/min, green lines represent tests at 500mm/min. 5 repeats of each.

Once the raw data had been used to calculate the stress-strain curves the yield strength and the Young's modulus were determined. In order to calculate the yield point the 0.2% offset method was attempted. However, the gradient of the linear region of the curve was not always constant. This lead to unreliable results when attempting to use the 0.2% offset method.

The chosen solution was to select the yield point by eye. To do this a Matlab program was used which displayed each of the curves in turn and asked the user to click on the most appropriate yield point. The program would then cycle through all of the curves for all of the snows, repeating each test twice. This gave two values for each test which were averaged to give a value for each test. All 5 tests for each snow at each speed were

then averaged to give a value for the yield strength of the snow at the selected speed. The average values for yield strength are presented in Figure 4.13

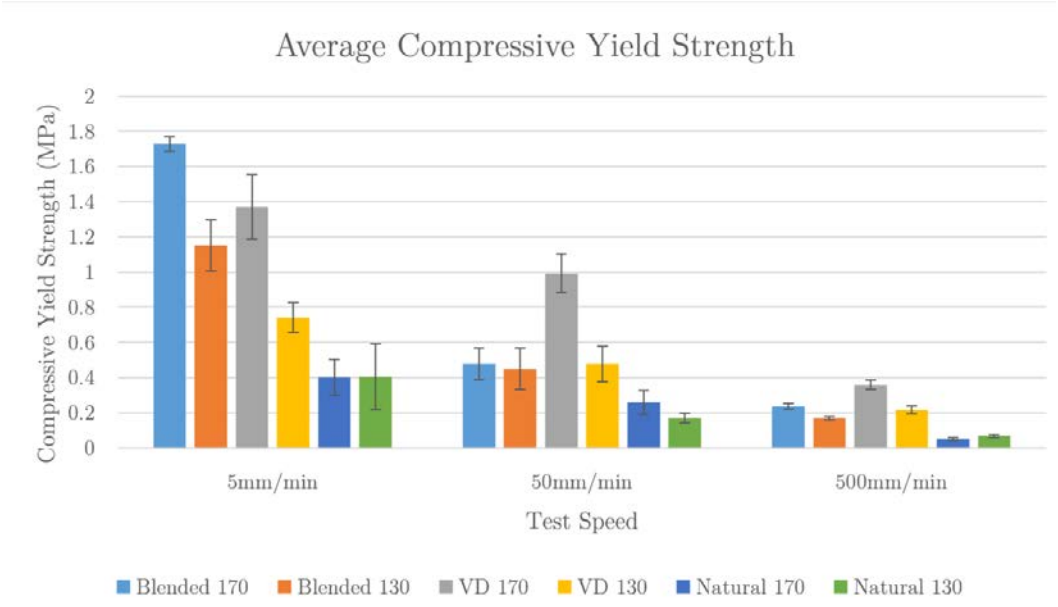

Figure 4.13 - Compressive yield strength for all snow types, error bars represent standard deviation

It should be noted that the strength of snow is strain rate dependent, so we see much higher strength when tested at lower strain rates. This is the opposite of ice which exhibits increased strength with increasing speeds (Petrovic (2003)).

As an example of the different curves, Figure 4.14 details a typical example from each of the snow types when tested at 5mm/min. It is possible to see some of the anomalies (partial yielding) in the linear region of the graph in the blended 170 example and the natural 170 example. When there is a levelling off within the linear region of the curve, it is treated as a lower yield point. Only if there is a notable drop in stress which would be a fracture is it considered the yield point to be selected.

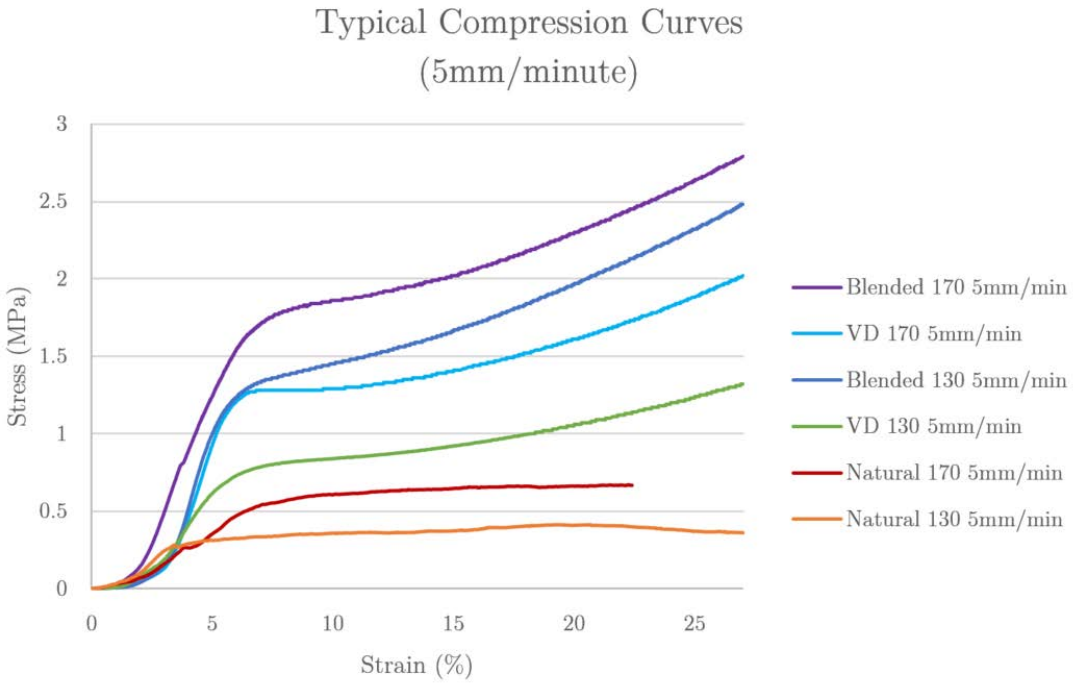

Figure 4.14 - Example curves for comparison of all snow when compressed at 5mm/min

In order to calculate the effective compressive modulus, a similar method was used with a Matlab script asking the user to select two different points within the linear region of the curve in order to calculate the gradient. The script then cycles through all the samples at all the speeds for all the snows, displaying each test twice. Giving two values for the gradient of each linear region which are then averaged. These are then averaged to give a value for the Young's modulus for a specific snow at a specific speed. These average values are presented in Figure 4.15.

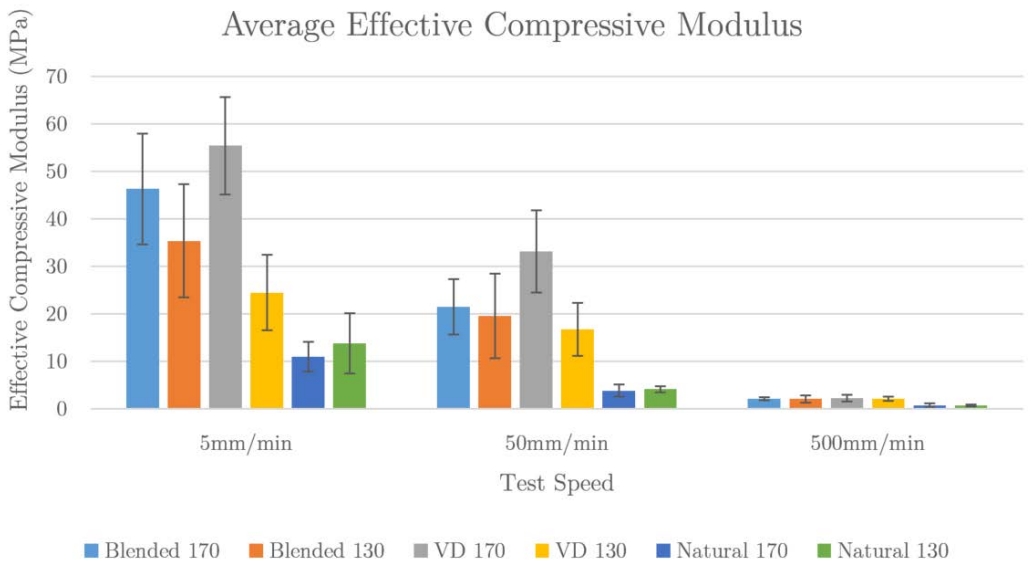

Figure 4.15 – Effective compressive modulus for all snow types, error bars represent standard deviation

When tested at 5mm/minute these snows have elastic modulus between 10MPa and 55MPa. When these values are compared to literature they appear to be lower than the established values for snow. The calculation of Young's modulus for snow appears to be more complex than initially thought. There are 4 main methods in use today to calculate Young's modulus for snow. Quasi-static, dynamic, derivation from X-ray microtomography with modelling of ice structures and finally penetration resistance measurements (Sigrist, 2006).

Quasi-static measurements are the most traditional and use uniaxial measurements in either compression or tension to calculate the Young's modulus. This type of measurement has been carried out by (Scapozza et al., 2004) and (Mellor, 1975).

The results of these experiments can be seen in Figure 4.16, alongside the results for all snows tested here at 5mm/min, 50mm/min and 500mm/min. Although the majority of these experiments from literature are carried out on snows with lower densities then

those tested here Figure 4.16 appears to show a general trend of increasing stiffness with increasing density which can be used to compare to the results presented above.

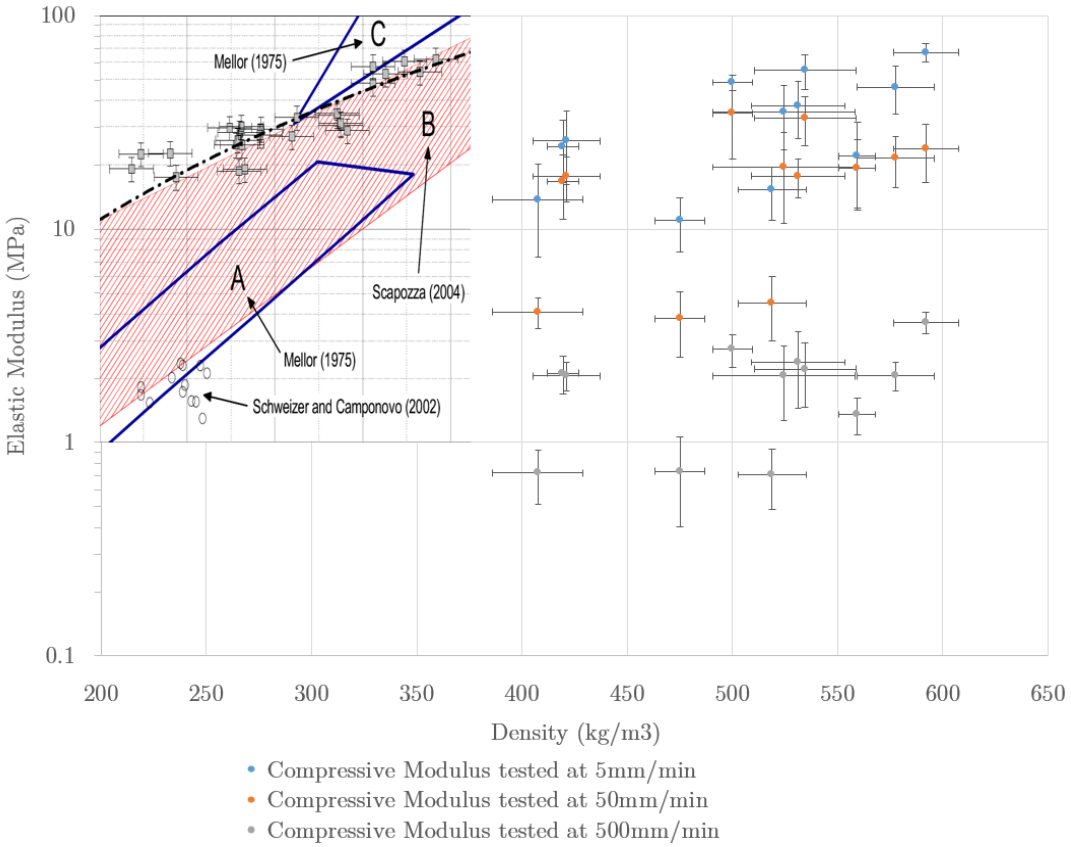

Figure 4.16 – Comparison of elastic modulus from literature with effective compressive modulus from all snows tested in this study. Full details of the tests performed in literature can be found in section 2.5.2.

The snows tested for this study which are presented in Figure 4.15 have densities ranging from 420kg/m^3 for vapour deposition 130 snow to 590kg/m^3 for blended 170 snow as shown in Figure 4.3. This puts them far above all the snows from literature, as shown in Figure 4.16 but the values for Young's modulus calculated for the snows tested at 5mm/min are in the range 10-50MPa. This corresponds to snows from Figure 4.16 in the density range 200kg/m^3 to 350kg/m^3. When the data in from literature is projected up to 600kg/m^3 the Young's modulus calculated here falls below this range. If the values

for the tests carried out at 500mm/minute are considered the calculated values for Young's modulus are 2 orders of magnitude lower.

From further investigation of the raw data, it appears that the linear region of the graphs extends up to 2.5mm into the compression test. When snow is compressed it is expected that the actual elastic region within which recovery to the original dimensions is possible is much smaller than this 2.5mm (8.5% strain). For this reason, the elastic modulus calculated will be referred to as the "effective elastic modulus" as it appears that it is not actually a calculation of the elastic properties of the material.

4.7 Profilometry

Profilometry was carried out on a freshly scraped track in order to investigate the surface of the snow which is actually about to be friction tested. The maximum peak to valley roughness that the Mitutoyo SJ-410 can measure is 1.2mm. This meant measuring of the roughness of the track post friction test was extremely difficult as the ploughing processes generally destroyed the surface so much that it was beyond the range of the profilometer. This also became an issue when attempting to measure the roughness of the natural snow. The grain size of the natural snow was far larger than that of the other snows meaning that the scraped surface of the snow generally un-measurable.

The roughness of the snow track was measured at 3 different locations (start middle and end of the track). A total of at least 20 individual measurements were taken across the 3 locations. Each trace was a measure of a 10mm length of snow. There was often a large variation in the results necessitating the large number of measurements for an average.

4.7.1 Raw Data

The profilometer reads the vertical position of the profilometer head and records the x position of the tip during the test. Figure 4.17, Figure 4.18 & Figure 4.19 are example profiles taken from blended and vapour deposition snows. It is possible to see that there are slight differences between the snows. In the blended 170 snow (Figure 4.17) it is possible to see two large lumps between 3mm and 8mm on the trace, each 2-3mm long. These are two ice crystals which make up the structure of the blended snow. On the vapour deposition snow, there are no such obvious features, this is due to the much finer grain structure of the starting material giving a much more uniform surface the main features being finer than those seen in the blended snow.

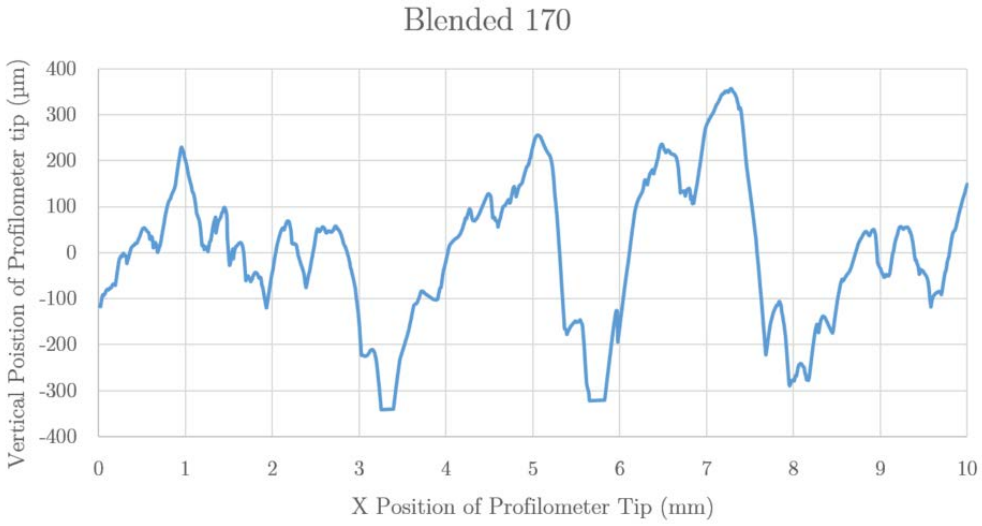

Figure 4.17 - Raw profile from blended 170 snow

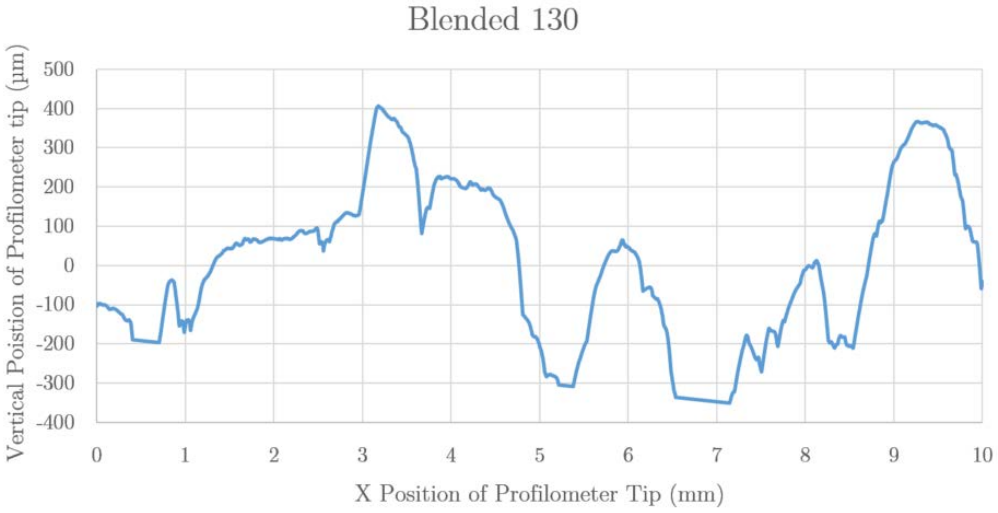

Figure 4.18 - Raw profile from blended 130 snow

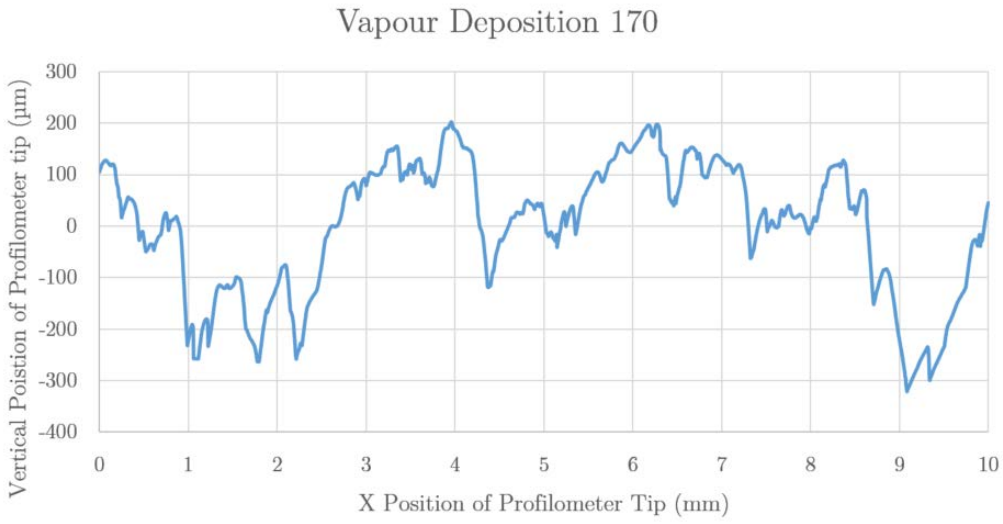

Figure 4.19 - Raw profile from vapour deposition 170 snow

4.7.2 Calculated surfaces roughness parameters

In order to interpret the roughness measurements, it is necessary to calculate different roughness parameters from the data. This allows for a direct quantitative comparison between the snows. Selecting the appropriate parameters for this comparison required a lot of careful thought and several options which were considered initially proved to have no helpful contribution to the understanding of the surface.

4.7.2.1 Average Roughness (Pa)

In order to initially investigate the differences in the surface a simple and commonly used measurement was required. By default this is the Ra, the average roughness based on a filtered roughness profile, the filtering applied to this profile within the Mitutoyo instrument is a long-wavelength cut-off filter (high-pass filter) to remove long wavelength segments. As the exact shape of the profile is important to the way the rubber interacts with the snow surface it was decided that a filtered profile was not appropriate for use as a roughness parameter. For this reason, the same calculation was done on the unfiltered profile to give the average roughness Pa.

The calculation of Pa was done within the software provided by Mitutoyo once the raw data had been uploaded to the computer. “Pa is the arithmetic mean of the absolute values of the evaluation profile deviations from the mean line.” (Degarmo et al., 2003).

Once Pa had been calculated, the 20 values for each snow were averaged and the standard deviation was calculated. These results can be seen in Figure 4.20. Natural snow is not presented as it was not possible to take roughness readings, as discussed above.

Figure 4.20 shows that the two blended snows have very similar roughness with a Pa values close to 140µm. Vapour deposition 170 snow has a much lower roughness with a Pa of 84µm. This was notable from observation of the scraped track during testing. The

vapour deposition tray was instantly visible by eye as being less rough then all the other tracks. Interestingly the vapour deposition 130 snow has a Pa of 120µm, giving it a roughness much closer to that of the blended snow then the high compression vapour deposition snow. Again this was visible when observing the tracks during testing, the vapour deposition 130 snow closely resembled the blended snow when scraped. It is unclear why the lower compression resulted in such a notable difference in roughness between the two vapour deposition snows.

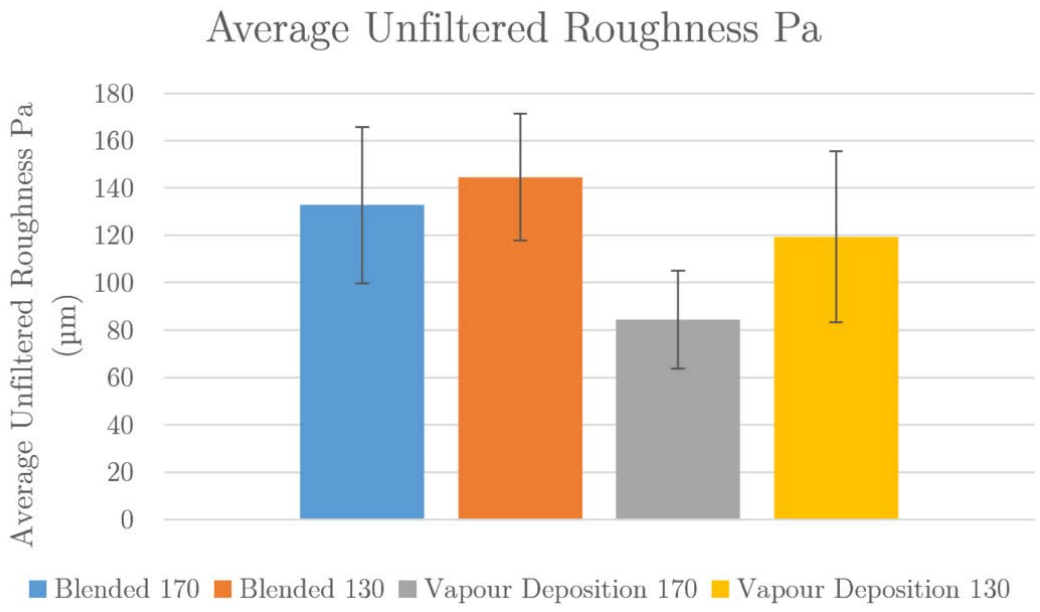

Figure 4.20 - Average unfiltered roughness Ra for all snows except natural snow. Error bars represent standard deviation

4.7.2.2 Kurtosis

Pa was not able to provide enough information about the snow profiles to quantify differences between the snows, especially between the two blended snows. It became necessary to investigate the shape of the features on the profile. Several options exist for investigating the shape of a roughness profile such as peak to valley heights, skewness and kurtosis. In this case, kurtosis was chosen as it describes a potentially important parameter of the roughness of the snow. Kurtosis can be calculated on either the averaged roughness trace or the unfiltered trace much in the same way as with Ra and Pa, for kurtosis, these are referred to as Rku and Pku. For the same reasons as before Pku will be used in this case.

The kurtosis is a measurement of the "spikiness" of the surface height distribution. "*If Pku < 3 the distribution curve is said to be platykurtoic and has relatively few high peaks and low valleys. If Pku > 3 the distribution curve is said to be leptokurtoic and has relatively many high peaks and low valleys."(Gadelmawla et al., 2002).* Examples of these two types can be seen in Figure 4.21.

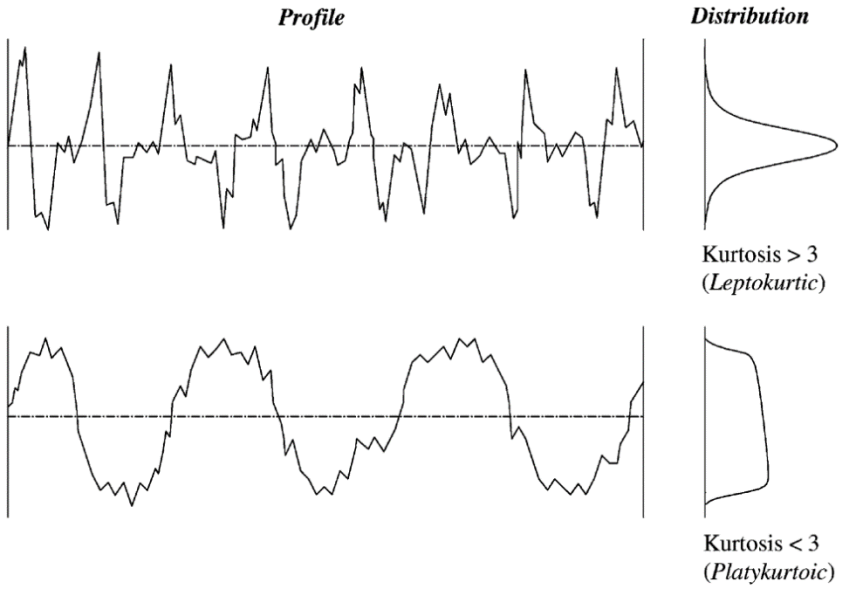

Figure 4.21 - Example traces to illustrate the definition of kurtosis parameter (Pku) (Gadelmawla et al., 2002)

The average kurtosis for each snow type was calculated using all 20 measurements taken on each tray. These are presented in Figure 4.22. It is possible to see that the blended snows have a lower kurtosis than the vapour deposition snows, but values tend to be within margin of error of each other so further investigation is required to identify differences between the snow roughness.

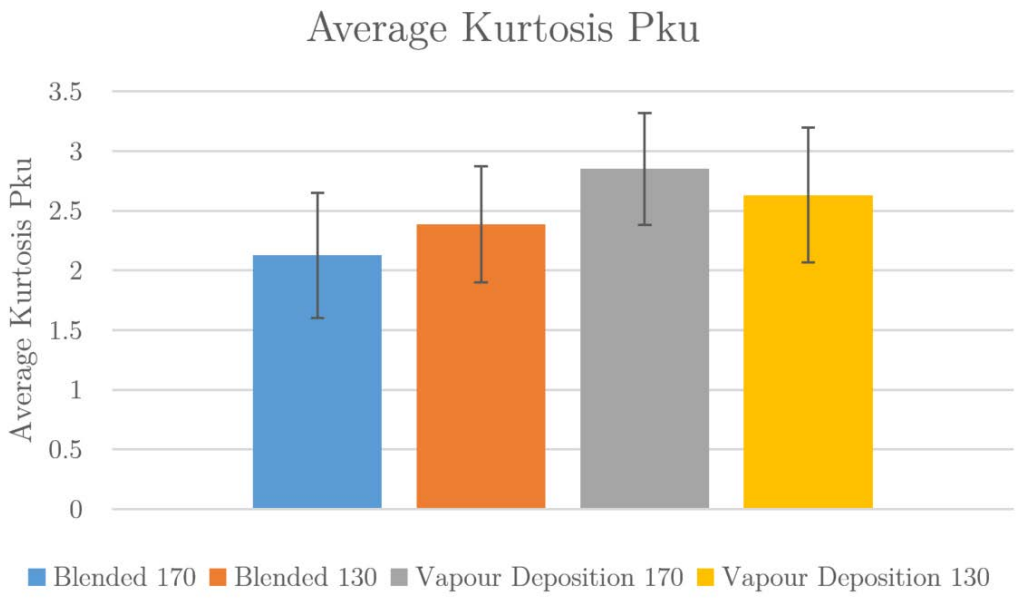

Figure 4.22 - Average kurtosis for all snows except natural. Error bars represent standard deviation

4.7.2.3 Peak count density

A final parameter was chosen to investigate the different roughnesses; this was the peak count density. It was clear from looking at that raw data that there is a difference in the number of individual peaks within each profile. The difficulty comes when trying to count these peaks as it is possible to count very different numbers by selecting different peak prominence (vertical distance between peak and nearest valley) to use as the method for defining a peak.

By using Matlab's signal processing toolbox it was possible to quickly adjust the prominence value to be used and re-evaluate all the roughness profiles. After much experimentation, a prominence of 7µm was selected. This meant that to be identified as a peak there must be a drop of at least 7µm on both sides of the peak. This allowed the software to pick up on the microscopic differences between the snow grain roughnesses.

It was also big enough to filter out any "noise" in the measurements as a result of the extreme resolution of the instrument (0.0125µm). This value of prominence also gave very similar results to when the peak count density was counted by eye.

The results of this measurement are presented in Figure 4.23 where we can see that again, vapour deposition 170 is different from the other three snows. Again there are relatively large standard deviations and the blended snow and VD130 snow are generally within margin of error of each other.

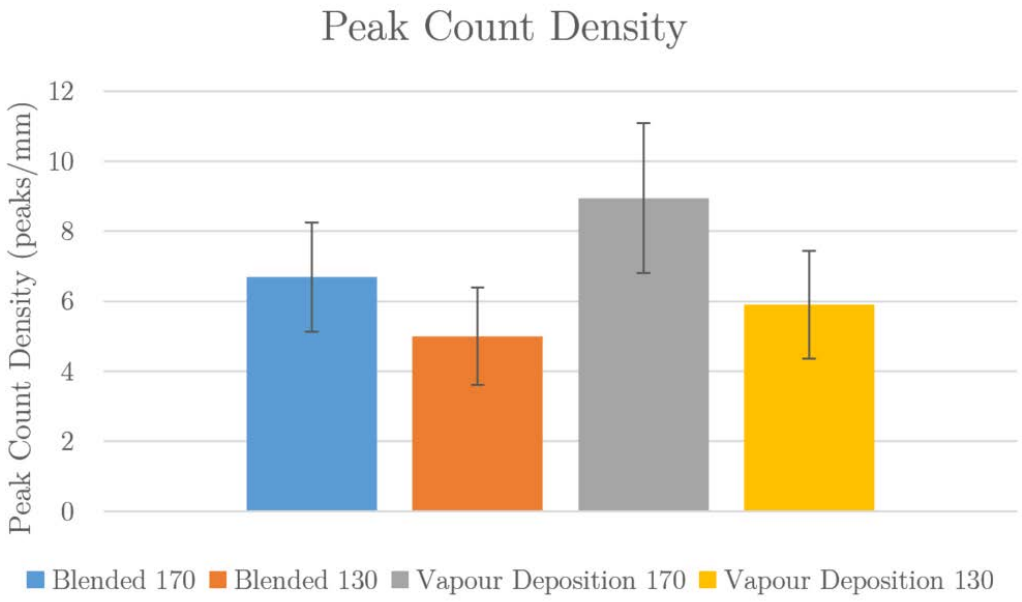

Figure 4.23 - Peak count density for all snows except natural. Error bars represent standard deviation

By looking at all 3 calculated parameters for surface roughness the same trends are present in all. That vapour deposition 170 stands out from the other 3 with significantly more peaks, those peaks are a reasonable amount "spikier" than those of the other snows but this snow still has a lower roughness. With some differences in roughnesses identified, it is now possible to look into how this roughness correlates with the difference in coefficient of friction on these snows; this is presented in section 6.6.

4.7.3 3D Profilometry

In addition to the work carried out on the individual roughness traces, several 3D profiles were generated. As discussed in section 3.8 they were created by taking 100 individual measurements of 5mm in length, next to each other with a gap of 0.05mm between them, gathering data over a 5mm x 5mm region of the snow. The 100 individual traces were then assembled using Matlab and a 3D surface plot was created.

Figure 4.24, Figure 4.25 Figure 4.26 show a visualisation for blended 170, blended 130 and vapour deposition 170 respectively. It was not possible to generate a 3D profile for the natural snow due to the large grain size as discussed earlier. The vapour deposition 130 snow exhibited a similar issue meaning it was not possible to get enough data to generate a VD130 3D profile either.

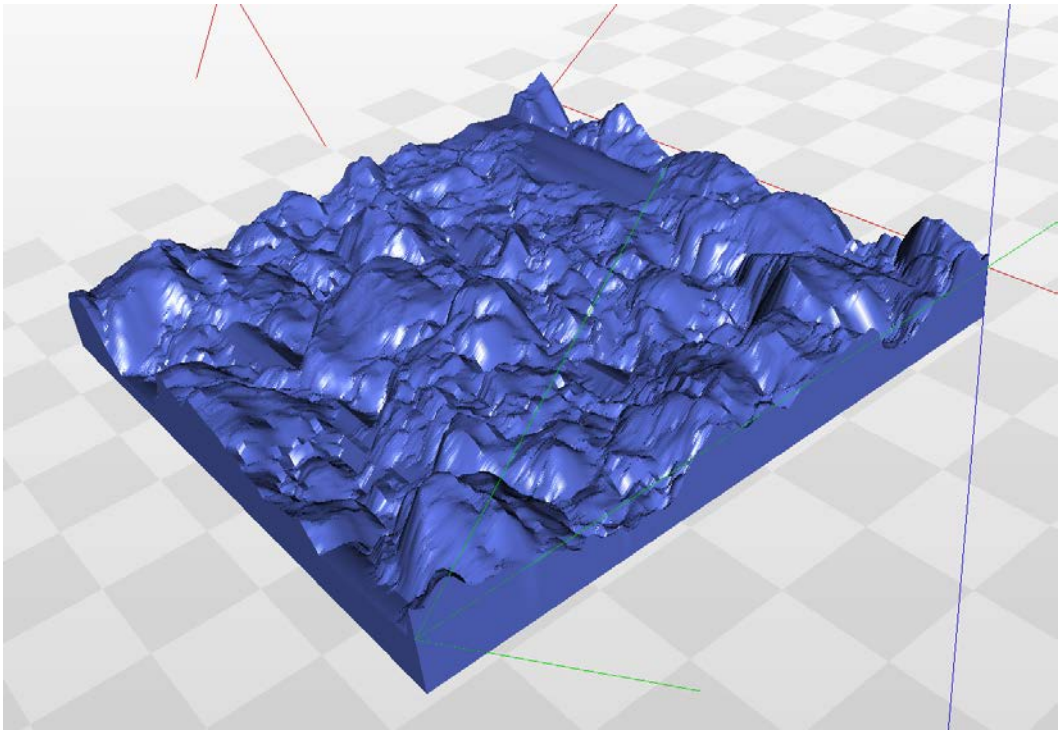

Figure 4.24 - 3D Profile generated from Blended 170 Snow. All axis scaled equally with edge dimensions are 5mm x 5mm

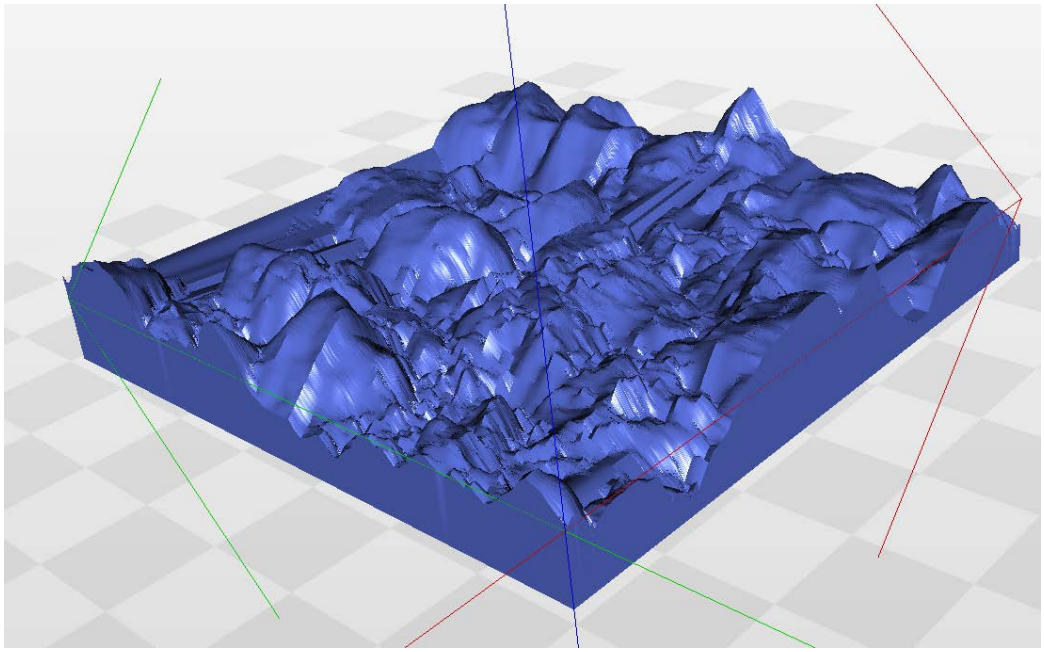

Figure 4.25 - 3D Profile generated from Blended 130 Snow. All axis scaled equally with edge dimensions are 5mm x 5mm

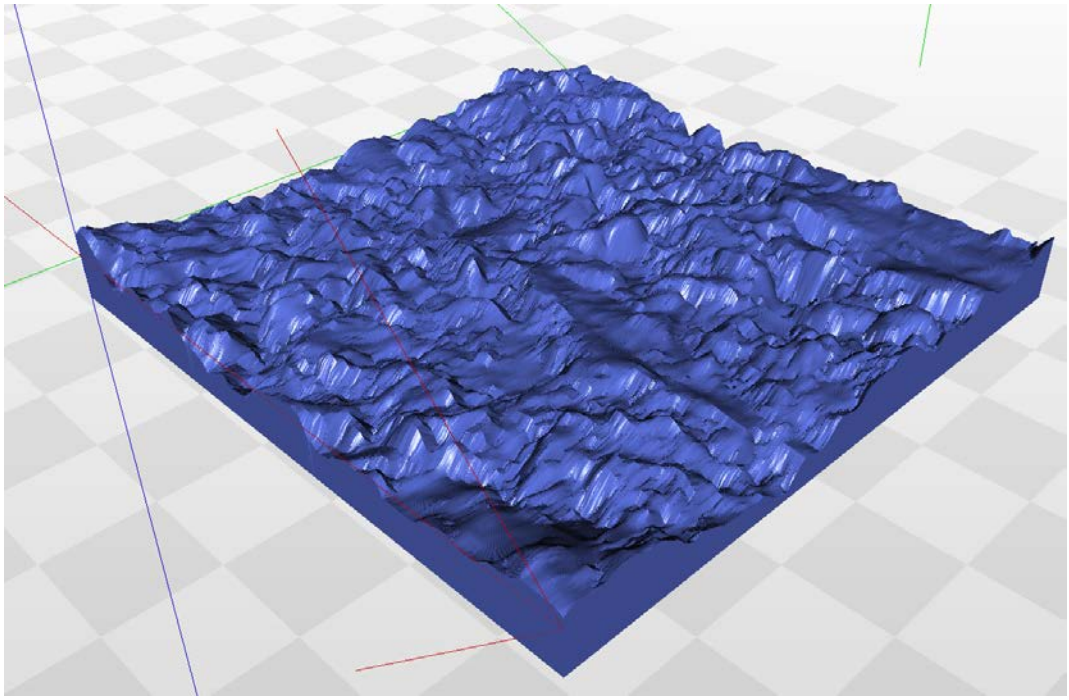

Figure 4.26 - 3D Profile generated from vapour deposition 170 snow. All axis scaled equally with edge dimensions are 5mm x 5mm

When comparing Figure 4.26 to Figure 4.24 and Figure 4.25 it is instantly obvious there is a difference between the surfaces. The VD170 snow appears to show a much finer grain structure with less extreme peaks and valleys then those of the blended snow.

It would be possible to carry out 3D roughness analysis on these surface maps, however, as the data for all the snows was not available and it would take considerable time to analyse the results it was decided not to attempt to analyse the 3D surfaces any further.

4.8 X-ray Microtomography

X-ray microtomography can be a very powerful technique for interpreting properties and characteristics of materials. The difficulty in utilising this data is that there are so many steps involved in the calculation of results from the images and 3D models. Each step in the process can have an effect on the calculations which can be performed such as grain size distribution. The following describes the steps which were taken to analyse the images from the XMT system.

The raw image files are taken from the XMT camera (Figure 4.27), they are then assembled to form a 3D greyscale model. The greyscale model is used for an initial visualisation but has limited use for performing analysis of the snow structure due to the difficulty the computer has interpreting the images.

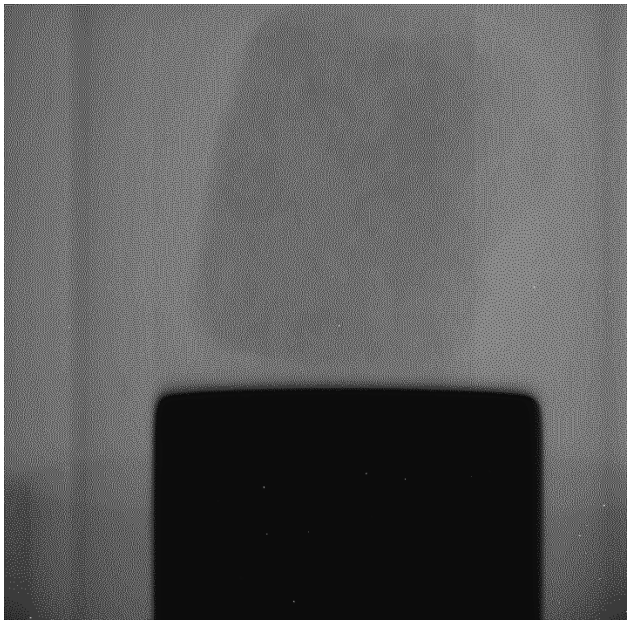

Figure 4.27 - Raw image from XMT scan. Black block is copper sample base, the grey structure above is snow sample, and vertical lines are edges of sample holder tubes.

Once the 3D greyscale model is created it is then broken down into individual image slices again. To perform an analysis of these images the grey scale 2D slices need to be converted to black and white. This is done using ImageJ software and a segmentation algorithm called Trainable Weka Segmentation. This requires the input of the user to identify areas of the 2D images which are definitely snow and areas which are definitely air/ pore space. The system will then use the input to attempt to identify all the snow and all the pore space, identifying one as black and one as white. This is a very iterative process with many attempts required to train the system to correctly identify which areas are snow and which areas are not. It is also very subjective as it relies on the user interpretation of whether the system is correctly identifying the different areas. An image of a grey scale 2D slice and the equivalent black and white 2D slice can be seen in Figure 4.28.

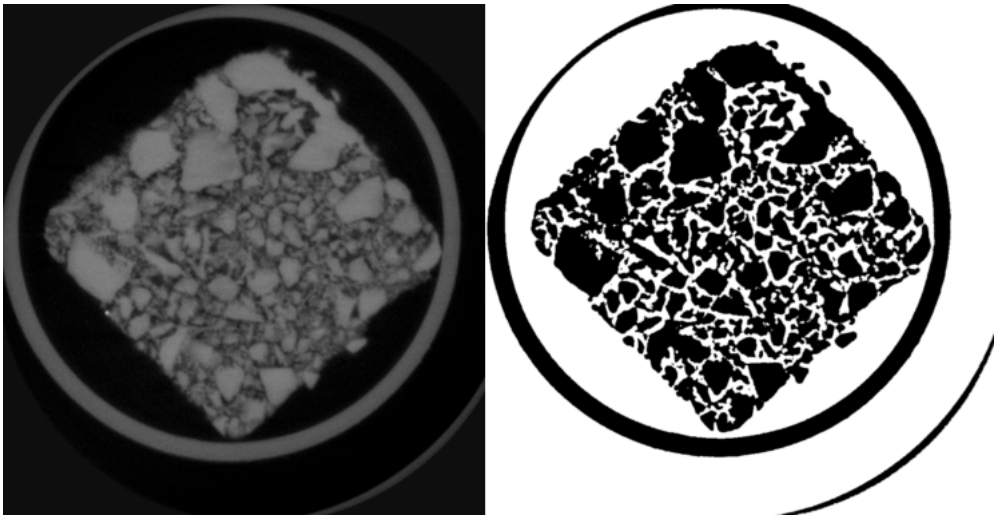

Figure 4.28 - Left - greyscale slice of snow structure. Right - Segmented slice of 2D structure.

The next stage in the analysis is to take the stack of 1500 segmented images from the ImageJ program into the 3D analysis software called Avizo. With the images separated into “snow” and “not snow” Avizo can now be used to identify one grain from another in 3D. This process could yield very different results based on the input parameters of the algorithm, which control the ways the program searches for the edge of grain structures. For the snows presented here a conservative grain separation was used, when a more extreme case was tried the program would separate the obvious large grains into many small ones. From examination of the microstructure and under a microscope it can be seen that the larger grains do remain whole after compaction in the snow press.

Once the grains have been identified it is then necessary to remove any grains which are too small to realistically be identifiable as snow. For this, any object less than 10 voxels were removed, this is equivalent to any object of 1.5×10^{-5} mm^3 or less. In addition, any grains touching the edge of the image were also removed, if a grain size distribution is to be performed, only complete grains should be included in the analysis. Finally, all the separated grains were analysed to determine their volume so a grain size distribution for each snow sample could be calculated.

Two snow types were fully analysed using the XMT system and the Deben cold stage. The results are indicative only, as mentioned earlier the results can change drastically based on the input variables at the different stages of the analysis. At this stage, the data is not going to be used in any further analysis or for investigating the relationship with friction as it is not possible to say definitively that these results are correct. The two snows presented below are Blended 170 and Vapour Deposition 170.

4.8.1 Blended 170 XMT Results

In order to analyse the grain size distribution of the snow, the grains are separated into ranges of volume. For visualisation purposes, the ranges are grains from 0.0015 mm^3 to 0.015 mm^3, grains from 0.015 mm^3 to 0.15 mm^3 and those grains above 0.15 mm^3. The visualisation and grain size distributions for Blended 170 snow are presented in Figure 4.29 and Figure 4.30 respectively.

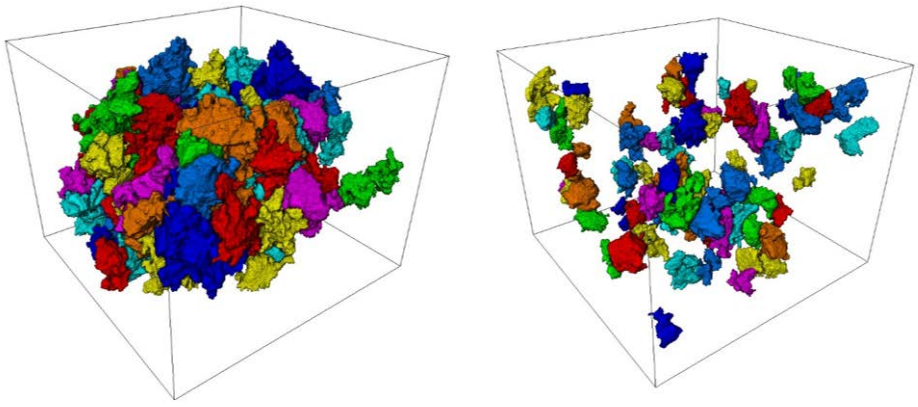

Figure 4.29 - Separated Blended 170 snow grains. Colours are only to identify one grain from another and do not refer to grain size. Left image - all grains above 0.15mm³. Right image - All grains between 0.015mm³ and 0.15mm³.

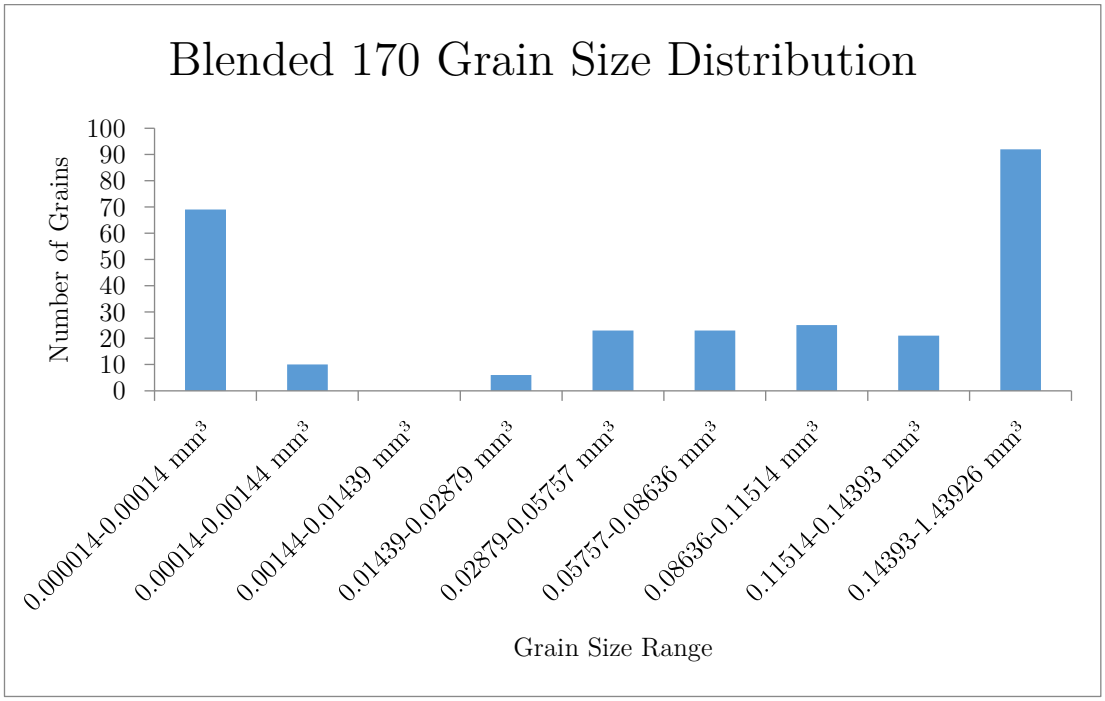

Figure 4.30 - Blended 170 Grain size distribution

From examination of the grain size distribution, it is possible to see that the majority of grains are relatively large (>0.15 mm^3). This matches well with a visual examination of the snow which shows a large proportion of the grains in the range of 0.1 to 1mm across. There are also a large number of grains also in the smallest range, this is most likely an issue with the analysis technique and more of the smaller grains should have potentially been discarded during the image analysis process as it is expected that most grains of this small size would have either sintered together or sublimed away between the time of blending and scanning with the XMT system.

4.8.2 Vapour Deposition 170 XMT Results

For Vapour Deposition 170 snow the same results are presented as with the Blended 170 snow. A visualisation of the different grain sizes along with a full render of the snow scan in Figure 4.31 and a grain size distribution analysis using the same bin sizes as with the blended 170 snow in Figure 4.32. From examination of Figure 4.32, it is possible to see that, as with the blended 170 snow there are a large number of very small grains. Again this can be put down to issues with the image analysis as it is unlikely grains of this size would survive long enough to be scanned without subliming or sintering together. Again a large proportion of the grains are in the largest size bin ($>0.15mm^3$), this again is to be expected based on the visual examination of the snow. The main difference compared to the Blended 170 snow is that there are a large number of snow grains in the range of 0.028 mm^3 to 0.05m mm^3. This is most likely due to the large dendritic vapour deposition grains being delicate and so breaking up during the snow preparation process whereas the blended snow grains are more like balls of ice and so would be much harder to break into smaller grains.

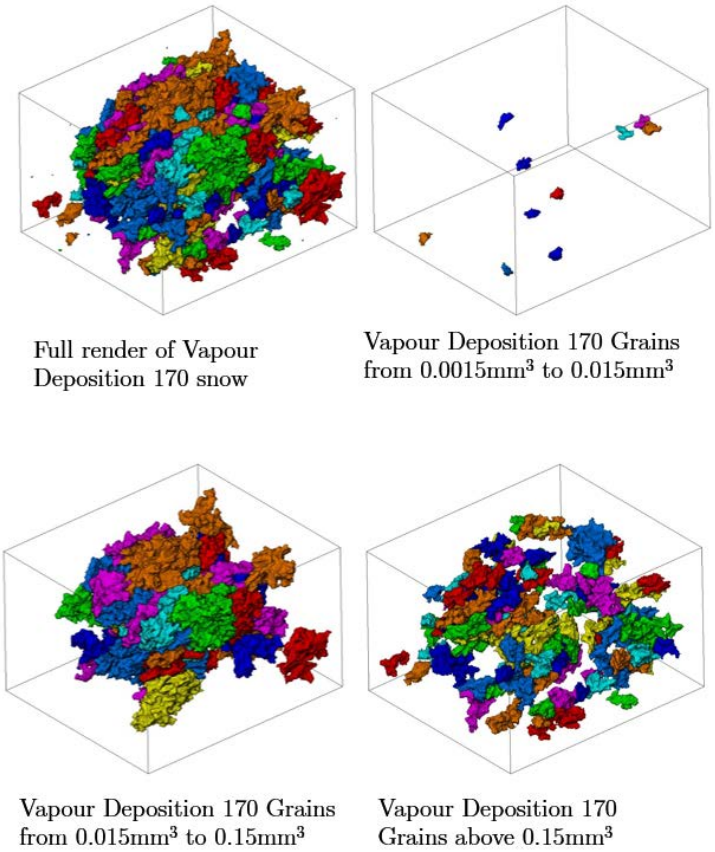

Figure 4.31 - Separated Vapour Deposition 170 snow grains. Colours are only to identify one grain from another and do not refer to grain size.

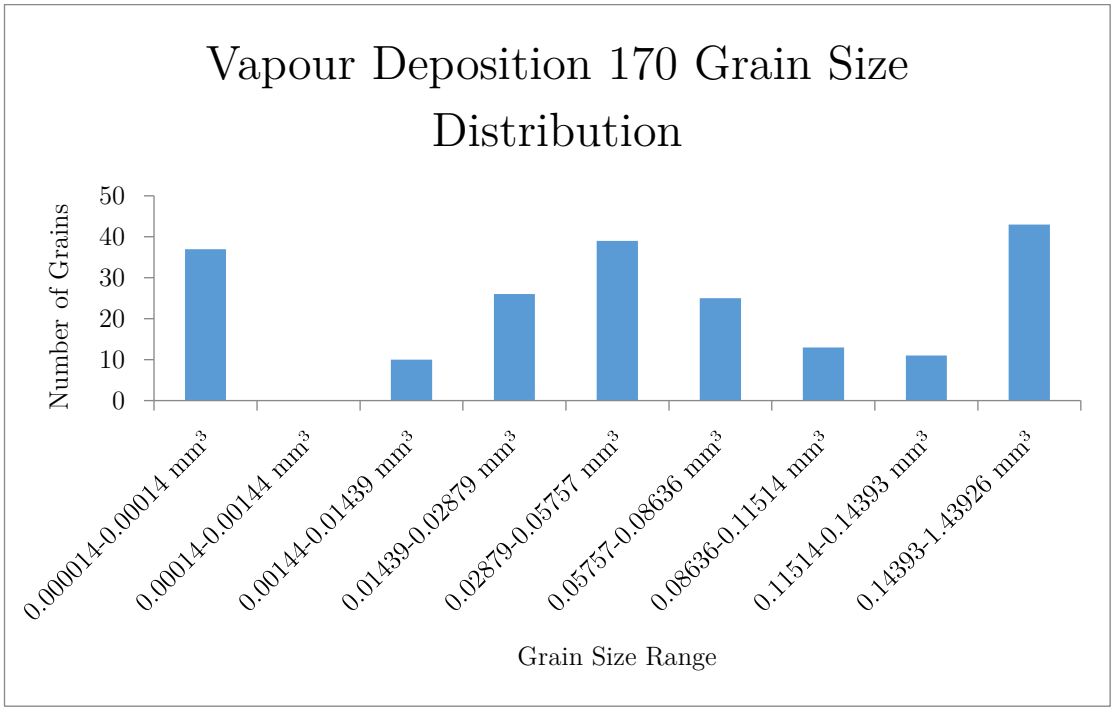

Figure 4.32 - Vapour Deposition 170 grain size distribution

XMT is a very powerful tool for analysis of granular materials such as snow and could be used to examine a lot of interesting factors about the snow such as grain shapes and coordination number (number of intergranular bonds per grain). However, due to the uncertainty surrounding the results gathered from a basic analysis of snow XMT scans, more work would be required to both develop the XMT scanning technique and cold stage further and to correctly analyse the images before committing to a more in-depth analysis of the snow microstructure. This sort of study falls beyond the scope of this PhD but would definitely be of interest for future work.

5 Friction Testing Results Analysis and Discussion

Summary

In this chapter, the results from friction testing six different snows using two analytical rubber samples (siped and smooth) are presented. The tests were carried out on a large-scale linear tribometer (FRIMA). Tests were carried out at 3 different speeds 0.01m/s, 0.1m/s and 1m/s. The chapter discusses raw data gathered for individual tests, some of the notable features of the friction curves and also the average friction taken from a region of the friction curves. The exact region over which the average is taken is important and the process of looking at how full-scale tyres on cars fitted with ABS behave has led to the selection of the region over which to take an average.

5.1 Introduction

All friction testing was carried out on the linear tribometer (FRIMA) within the cold laboratory and all tests were carried out at -10°C. Full details of the experimental setup and testing method can be found in section 3.4.

To summarise: the 2 main rubber samples (rounded edge and 4 sipes) were both tested at three velocities 0.01m/s, 0.1m/s and 1m/s. The tests at 0.01m/s and 0.1m/s were repeated 3 times in order to calculate average values for friction. Due to the need to use a longer snow track to allow the machine enough time to accelerate and decelerate when testing at 1m/s it was only possible to repeat each rubber twice at this speed.

From the data gathered by FRIMA, it was then necessary to calculate the coefficient of friction μ for the different combinations of speeds and rubbers. This was done by dividing the measured force in the X direction (opposing the movement of the rubber) by the normal force being applied to the slider, in this case, 0.82kN. A typical example of μ against distance for a rounded edge and a 4 siped sample can be seen in Figure 5.1.

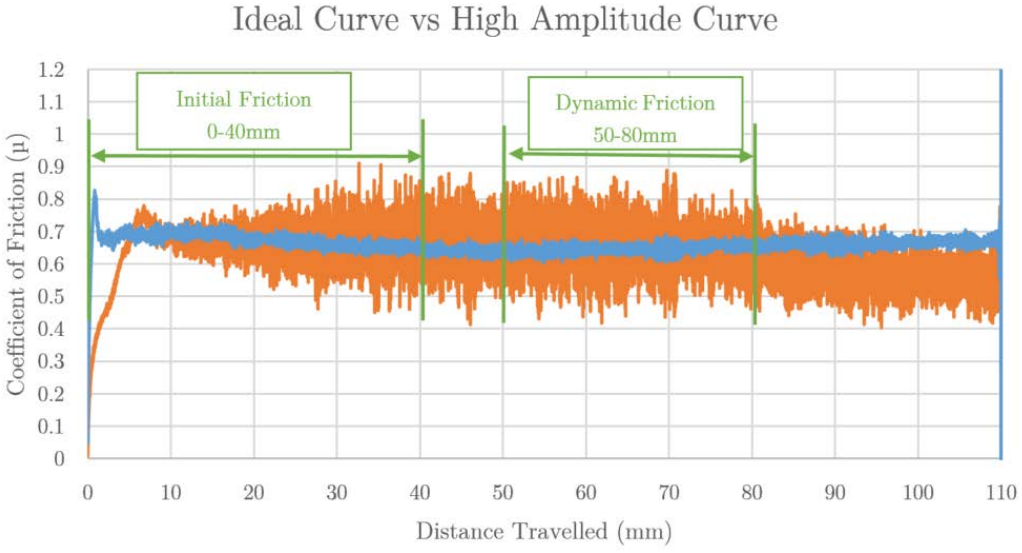

Figure 5.1 - Example μ-Distance curves for Rounded edge (Blue) and 4 Sipe samples (Orange) tested at 0.01m/s on Blended 170 snow.

The dynamic friction was calculated by taking the average μ over the distance range 50 to 80mm (as shown in Figure 5.1) where μ is stable and velocity is constant. This measurement is useful for comparing the different rubber/snow combinations analytically as velocity is constant in the distance range for all speeds.

When comparing the friction data to real-world examples such as the coefficient of friction measured during vehicle acceleration/deceleration the dynamic friction is not an applicable measurement. In a real-world scenario technologies such as anti-lock braking systems or traction control are used to control the tyre slip. This means it is necessary to look further into the reality of braking and acceleration in order to determine the most appropriate distance range over which to analyse the μ-distance curves.

5.2 Investigation of tyre interaction, allowing correct interpretation of μ-distance curves

A well-used approach to investigating tyre interactions is to use a brush model. A tyre brush model considers the tyre as rigid but with a series of bristles pointing outwards from the rim. Each bristle is able to move relative to each other (Mavros, 2005). The simplest example of this allows the elements to be sheared in one direction only (deceleration) with no cornering forces being considered (Pacejka, 2012). An example of a tyre brush model can be seen in Figure 5.2.

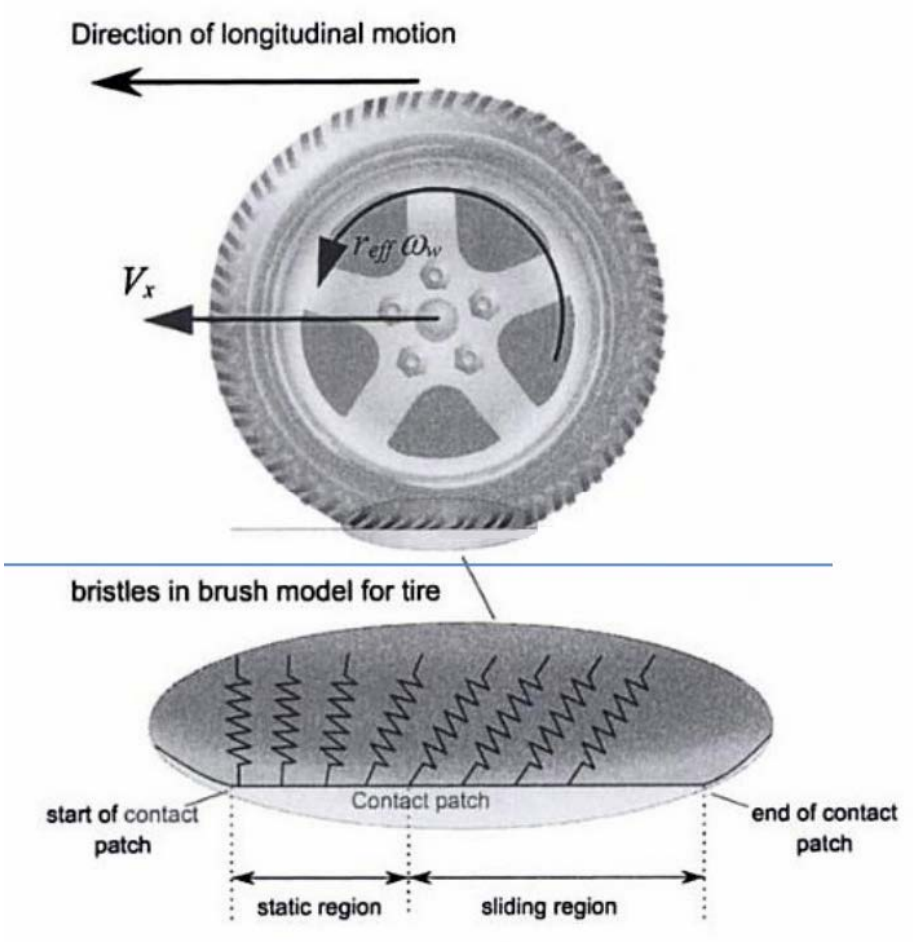

Figure 5.2 - Illustration of tyre brush model of a tyre during acceleration. V_x is the vehicle velocity, r_{eff} is the effective radius of the tyre and ω_w is the rotational speed of the tyre (Erdogan, 2009)

In order to calculate the displacement of a tread block within the sliding region of the tyre the sliding speed, slip ratio and sliding distance must first be calculated.

Initially we know:

Vehicle Speed = V_x

Tyre rotational speed = ω_W

Effective Tyre radius = r_{eff} (assumed to be a constant radius for this example)

Sliding speed = V_g

In order to find what area of snow a tyre will slide over during deceleration before an ABS system is enabled causing the tyre to rotate and therefore stop sliding, two values are required, the sliding speed of the tyre and the actual speed at which the vehicle is travelling over the ground. The sliding speed of the tyre is calculated using Equation (2)

$$V_g = \omega r_{eff} - V_x \tag{2}$$

The slip ratio (SR) is defined as the sliding speed divided by the vehicle speed (Equation (3))

$$SR = \frac{V_g}{V_x} \tag{3}$$

Contact patch length (length of tyre in contact with the ground when stationary) = L_x

The sliding distance d_x can be calculated from the slip ratio and the contact length, shown in Equation (4)

$$d_x = -L_x \frac{SR}{1 + SR} \tag{4}$$

Assuming a tyre contact patch length of 160mm and a slip ratio of -20% (Ella, 2014), the distance that the tyre tread block surface travels before leaving the contact patch is 40mm. In order to compare lab results directly with real-world tests, the coefficient of friction will be calculated over the distance 0-40mm as shown in Figure 5.1.

5.2.1 Interpreting μ-distance curves for rounded edge samples

This approach is used for investigation of siped sample friction, however, when friction tests are carried out using a rounded edge sample a different approach is required. Sipes in tyres will generally be no larger than 5mm wide. As each sipe slides over the snow it ploughs into the snow surface, revealing a new layer of snow below, effectively refreshing the snow surface. This means that as the tyre slides over the surface each sipe will be in contact with the snow for 5mm of sliding before it reaches the snow which has been refreshed by the sipe in front of it. As a result of this, it is expected that it is not necessary to investigate any surface friction mechanism such as fluid film lubrication or indentation for over a distance range greater than 0-5mm as the surface is refreshed and the process repeats itself after this distance. For this reason, when investigating the μ-distance curves for the rounded edge samples, the region of 0-5mm is investigated.

5.3 Friction Coefficient μ-Distance Graph Analysis

Before looking at the average μ for the various samples it is necessary to understand there is a lot more information about the friction tests and how the rubber and snow behave available if the time is taken to examine the μ-distance curves in detail. When the graphs are examined individually it is clear that there is depth and subtlety in the data which is not captured by reducing the curve to a pair of values.

This section considers the curves in more detail, identifying the similarities and differences and explores ways to quantify the complexity of this behaviour by identifying features that capture the essence of the data.

5.3.1 Graph overview

The various combinations of rubber sample geometry, snow types and speeds have resulted in different shapes and features being seen in the μ-distance curves. The analysis of the curves was carried out before completing the final testing of the snow this ensured the correct tests were being carried out when moving to test on the natural snow (of which there were very few good quality samples) and it would be possible to understand what differences we would see.

The combinations of samples include three different rubber samples:

- 4 sipes
- Rounded blocks

The four different snows used are:

- Vapour deposition 170
- Blended 170
- Vapour deposition 130
- Blended 130

The 3 different speeds used are

- 0.01m/s
- 0.1m/s
- 1m/s

5.3.2 The Ideal Curve

In order to explain the differences that can be seen, an ideal curve has been defined, this allows all anomalies with the other graphs to be compared to a consistent reference. In this case, the most suitable curve is from the rounded sample on blended 170 snow at 0.01m/s (Figure 5.3).

The features that led to this choice are described below.

1 Very steep initial gradient to reach clearly defined static friction peak

2 Obvious drop from static peak to reach steady dynamic friction

3 Low amplitude of fluctuations throughout dynamic region

4 Dynamic friction remains steady throughout test (no decrease with distance)

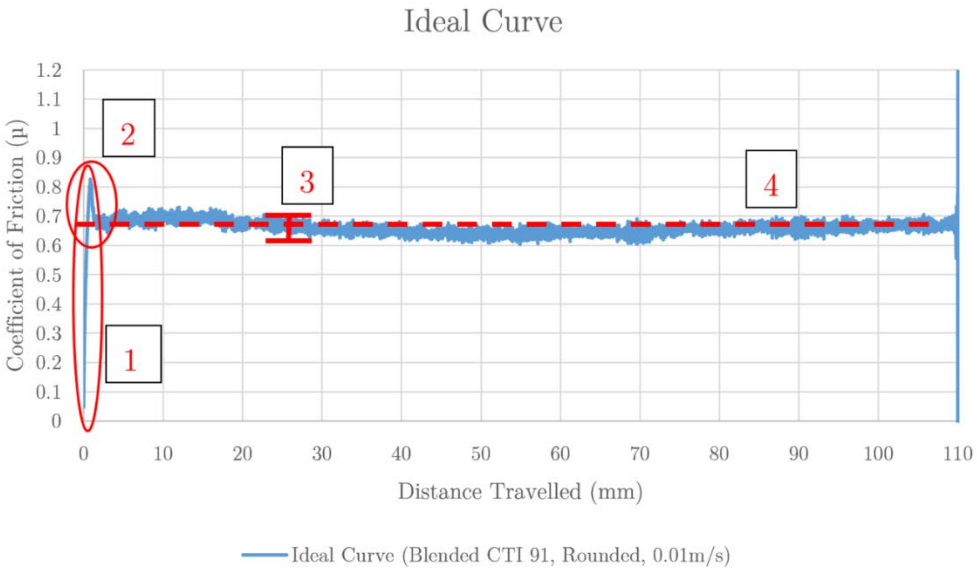

Figure 5.3 - μ - distance curve of the representative ideal curve. Tested with rounded rubber sample on blended 170 snow at 0.01m/s.

5.3.3 Description of graph variations

Here the various differences which have been noted are identified, in some cases, the variations in curve shape will have little influence on the average friction which is calculated later. However, it is necessary to understand that not all of the tests behaved in the same manner and as such, introduced errors into the results which it is not possible to correct for. This is the main point to take away from the analysis of these graphs.

5.3.3.1 Varying amplitude of different traces

Figure 4 shows a comparison between the ideal curve and a trace with an especially high amplitude

The amplitude is being identified as the average peak to valley distance measured throughout the dynamic friction region (50-80mm) as shown in Figure 5.3.

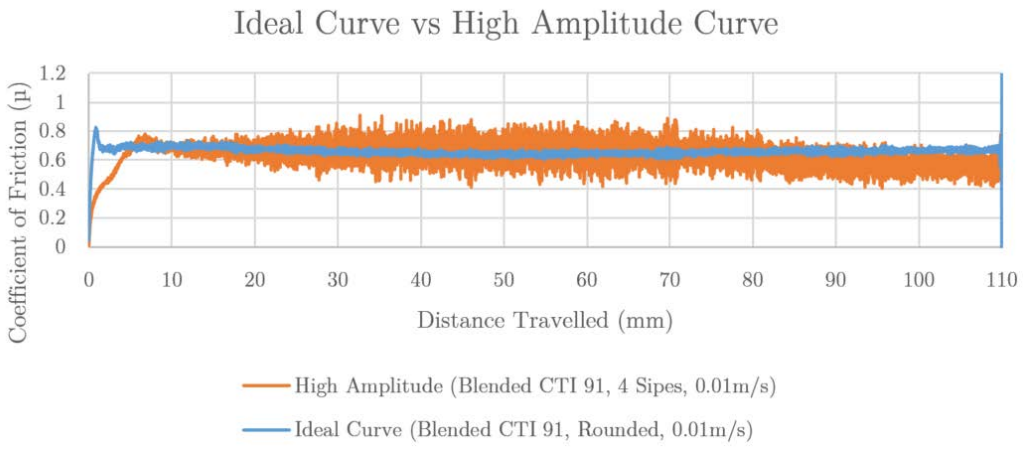

Figure 5.4 - Ideal curve vs High Amplitude Curve

The high amplitude of the 4 siped sample is due to the flexing of the sipes and the fracturing of the snow grains during the ploughing process, all of which is picked up by the load cells.

5.3.3.2 Static friction variation through test repeats

As can be seen in Figure 5.5 the static friction peak of test 1 (orange line in Figure 5.5) (μ of 0.83) is quite different to the peaks of the second and third test (yellow and grey lines in Figure 5.5) (μ of 0.7). Despite this relatively large difference, the average μ between 50mm and 80mmfor all three tests is approximately 0.4.

This drop is most likely due to snow being caught between the sipes of the rubber samples, which is not cleared fully between tests.

A similar drop in static friction from the first of a group of tests to the 2nd and 3rd tests can be seen in several different snow/rubber/speed combinations.

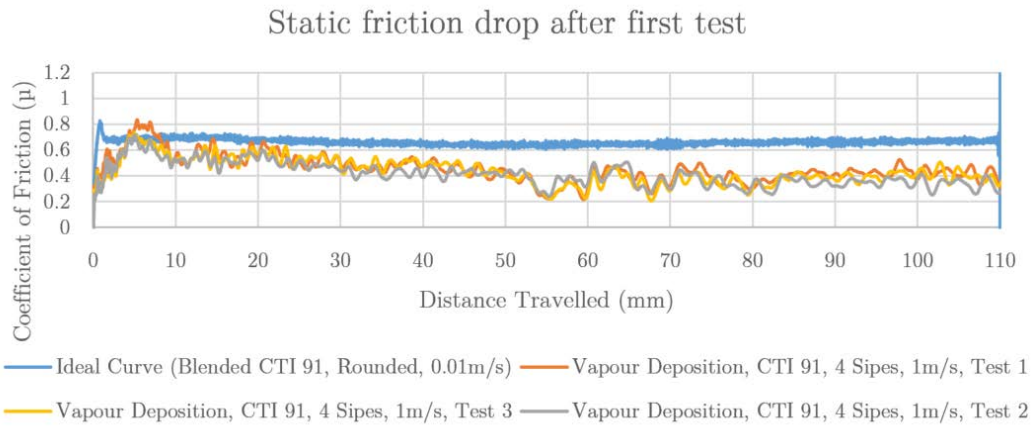

Figure 5.5 - Ideal curve vs dropping static friction peaks

5.3.3.3 μ decreases with distance

On certain tests, the average μ can be seen to decrease with distance travelled. It appears to be a relatively uniform decrease in μ over the entire test distance as seen in Figure 5.6 represented by the red line. The decrease does not tail off near the end of the test but continues all the way across the full distance. The most likely explanation for this decrease is due to the properties of the snow being different across the tray, resulting in a variation in friction seen along the length of the tray.

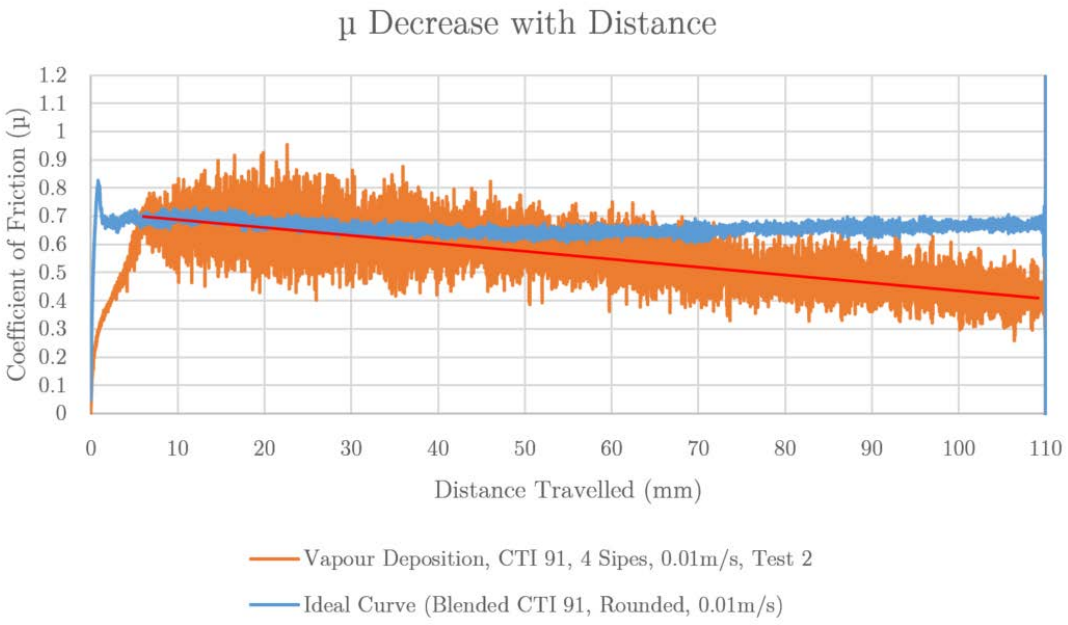

Figure 5.6 - Ideal Curve vs Dynamic friction decrease. Red line represents the decrease in friction with distance.

This effect appears to only be prominent during tests on vapour deposition snow, both CTI 91 & 86. With very little evidence of this decrease on blended snow tests. This seems to indicate that something different is happening when testing on vapour

deposition snow. Potentially something related to the snow grains, which do not orientate themselves as uniformly during tray preparation, potentially resulting in an anisotropic material, at this stage this is only a best guess and future work would be required in order to investigate further.

5.3.3.4 Flex of sipes

There is quite a noticeable difference in the distance a siped sample travels before the static friction peak is reached. This appears to be due to the flex of the sipes. The 4 siped sample travels the furthest (4 to 5mm), and the rounded sample the shortest distance (<0.5mm) as shown in Figure 5.7. This flexing region appears to be the same on all snow samples for the same speeds.

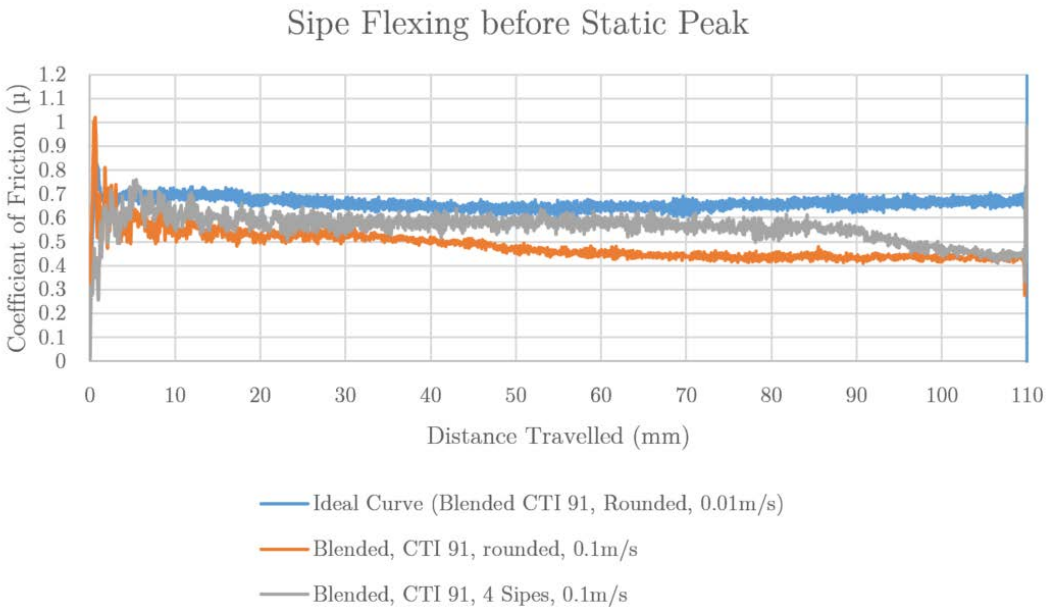

Figure 5.7 - Ideal curve vs flexing sipe examples

5.3.3.5 Levelling before static peak

Although the flex of the sipes to the static peak appears to be a constant across all snow samples there is sometimes an initial "levelling" before the static peak is reached as shown in Figure 5.8. At 1-2mm µ begins to fluctuate in a similar way to when dynamic steady state friction has been reached, then after a further 2-3mm µ continues to rise, reaching a peak and entering steady-state friction mode.

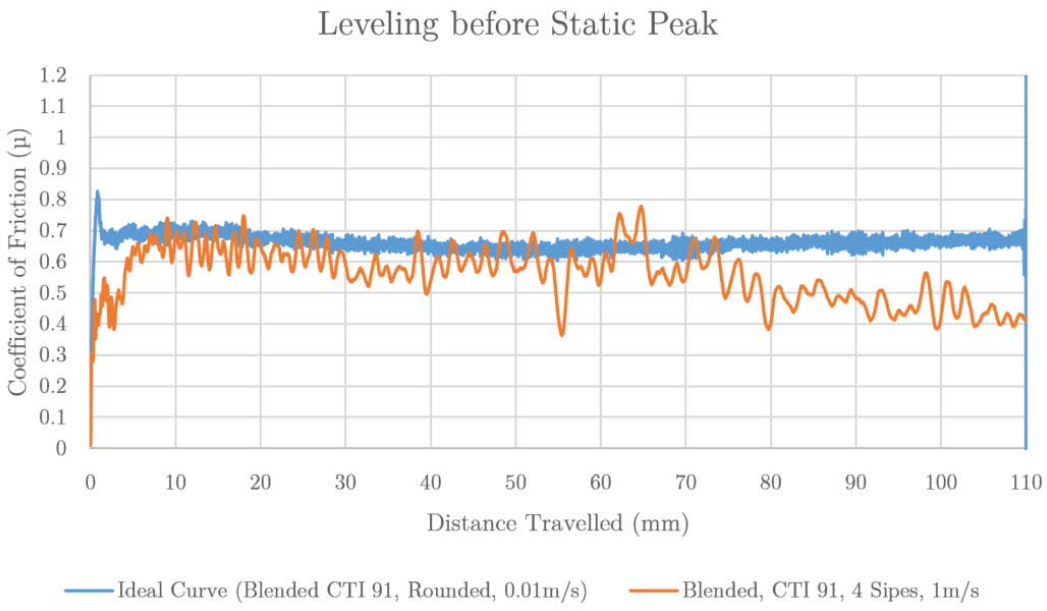

Figure 5.8 - Ideal curve vs levelling before static peak

This effect is only present when testing with the 4 siped sample and is most notable when testing at 1m/s, however, the effect is still present during testing at lower speeds and it is also present on all snow types and does not appear to be related to test repeats. It is most likely due to a non-uniform flexing of the sipes, for example when there is snow in between the sipes this may cause the sipes to deform differently to when there is no snow in between. The only way around this would be to clean the snow from between the sipes after each individual test which would treble the time to carry out

tests. This would not be possible during the extremely tight schedule for each testing day.

5.4 Investigation of Average μ

As discussed above the μ-Distance curves can be very complex and rich in data, however in order to make comparisons and more easily observe the differences between the rubber-snow interactions it is necessary to simplify the curves. As discussed in section 5.2 this is done by calculating the average μ between 0 and 40mm as a comparable performance indicator to the tests carried out with tyres in the field.

Friction data is presented in graphs below. Each graph details a different combination of snow and rubber tests. One data point is present for each rubber and snow sample at each speed. Error bars are the standard deviation of the test repeats. The software was provided by Michelin in order to calculate the average μ and standard deviations.

5.4.1 High compression snows

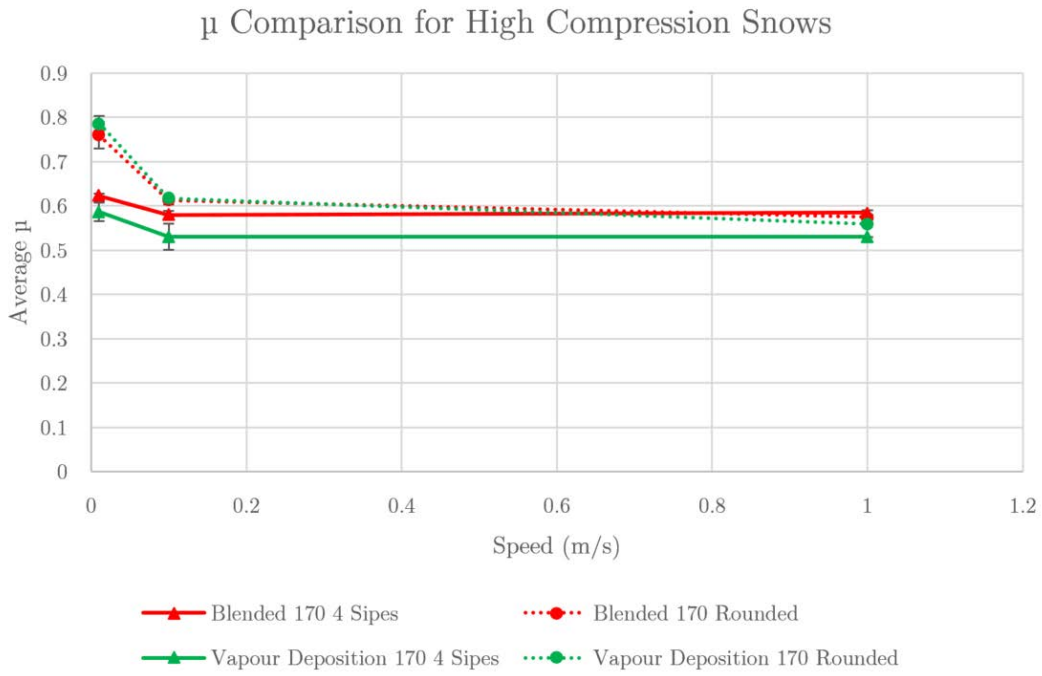

Figure 5.9 - Average μ between for high compression snows. Red lines represent blended snow, Green lines represent vapour deposition snow. Dashed lines represent rounded edge rubber samples, solid lines represent 4 siped sample

Rounded samples and siped samples behave differently during the friction tests. Siped samples have a large amount of ploughing at all speeds giving them an almost constant μ across all tested speeds. There is a slight increase in friction when tested at 0.01m/s which is explained by reduced frictional melting of the surface at lower speeds.

This effect is exaggerated further when testing with rounded samples as the majority of the friction comes as a result of surface interactions rather than ploughing. This can be seen in Figure 5.9 where the rounded samples have a higher μ at 0.01m/s than the siped samples which is explained by the higher real surface contact area of the sample.

When the speed increases, resulting in higher frictional heating and therefore meltwater lubrication, μ lowers to a very similar μ to the 4 siped samples. There is almost no ploughing occurring during the rounded edge tests this means if meltwater is present μ drops rapidly compared to the siped samples. The siped samples are not as dependent on the surface interactions as they are on energy dissipation through grain bond fracturing. This explains the relatively constant response to speed for the siped samples. Extensive work has been carried out investigating this by both (Ella, 2014) & (Skouvaklis, 2010) and the effect is identical here to what they observed.

When testing using the siped sample the vapour deposition snow has a slightly lower μ than the blended snow. As the friction mechanism appears to be mainly ploughing it is likely that this effect comes as a result of a variation in the mechanical properties of the snows. From examination of the measured properties for these two snows it appears a likely reason for this difference is the lower density of the vapour deposition snow meaning that less energy is being expended to move the lighter snow during the ploughing process.

The rounded edge sample shows the opposite effect at the lower speeds with vapour deposition snow exhibiting a higher μ than the blended snow. These measurements converge at the higher speed to give almost identical values. As the dominant mechanism for friction at these low speeds for rounded samples is mainly surface interactions it is likely this difference comes as a result of a difference in the surface structure. From looking at the measured surface parameters of the two snows, the most likely reason for this difference is that the vapour deposition snow is much smoother with a Pa of 84μm compared to blended snow with an average Pa of 132μm. This gives a greater real area of contact for the vapour deposition snow and while there is very little fluid film lubrication, a higher μ.

5.4.2 Low compression snows

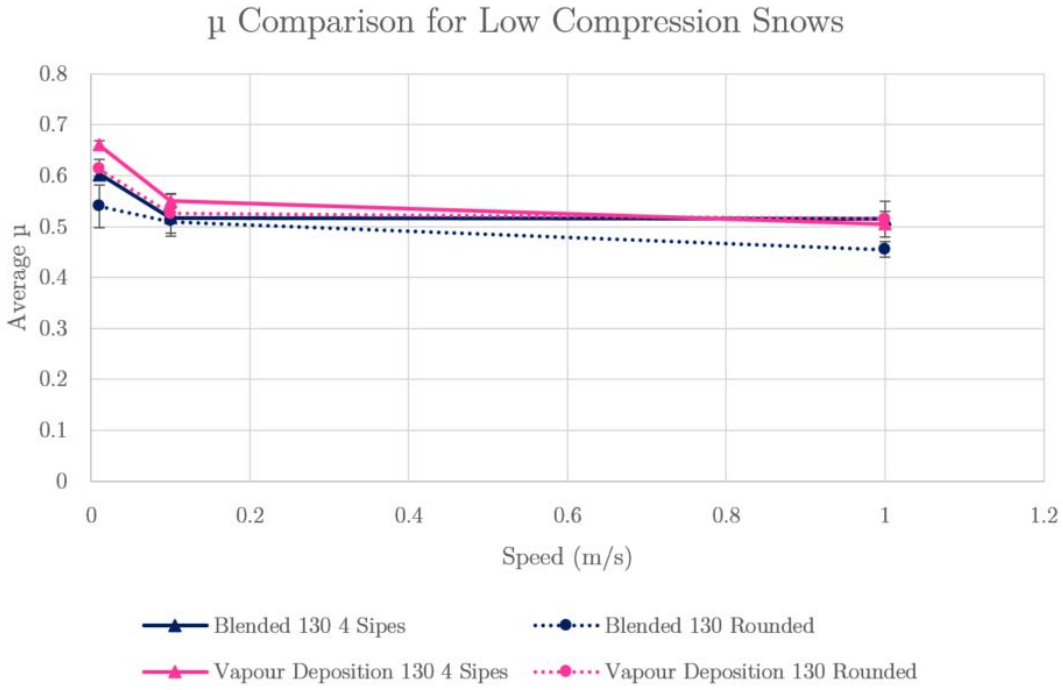

Figure 5.10 - Average μ between for low compression snows. Blue lines represent blended snow, Pink lines represent vapour deposition snow. Dashed lines represent rounded edge rubber samples, solid lines represent 4 siped sample

Figure 5.10 compares the 4 siped rubber sample with the rounded edge rubber sample when tested on snow prepared using the low compression method.

When investigating snow prepared using the low compression procedure we can see some similarities with the high compression snow such as the drop in μ as the speed is increased above 0.01m/s.

When looking at the comparison of the rounded sample with the siped sample, the rounded sample exhibits a lower μ at all speeds on both snow types. The rounded sample also has a much lower μ on the low compression snow (0.55 for blended snow at 0.01m/s) than the high compression snow (0.74 for blended sow at 0.01m/s). The initial

explanation is that this difference is due to the surface differences between the two snows. However, when comparing the high and low compression snows, the differences are not that extreme. With a Pa value of 133µm and a peak count density of 6.7peaks per mm for high compression snow and a Pa of 144µm and 5 peaks per mm for low compression snow, they appear to be very similar in terms of roughness. In contrast, the high compression vapour deposition snow has a Pa of 84µm and a peak count density of 8.9 peaks per mm. This is a 58% decrease in Pa and a 33% increase in peak count density compared to the high compression blended snow. For this change, an 8.1% increase in friction is observed.

Comparing this to the difference between high and low compression blended snow, there is an 8.2% increase in Pa and a 34% decrease in peak count density of the low compression snow. This corresponds with a 35% decrease in coefficient of friction.

The difference in roughness between high compression vapour deposition and high compression blended snow is much more apparent in both visual observations of the track and raw data, meaning the difference observed in µ can be attributed to the difference in surface roughness. The large difference in friction between the two blended snows must be explained another way.

To do this the friction for the siped samples are examined to see if there is a difference in the siped sample results which could explain the difference with the rounded samples.

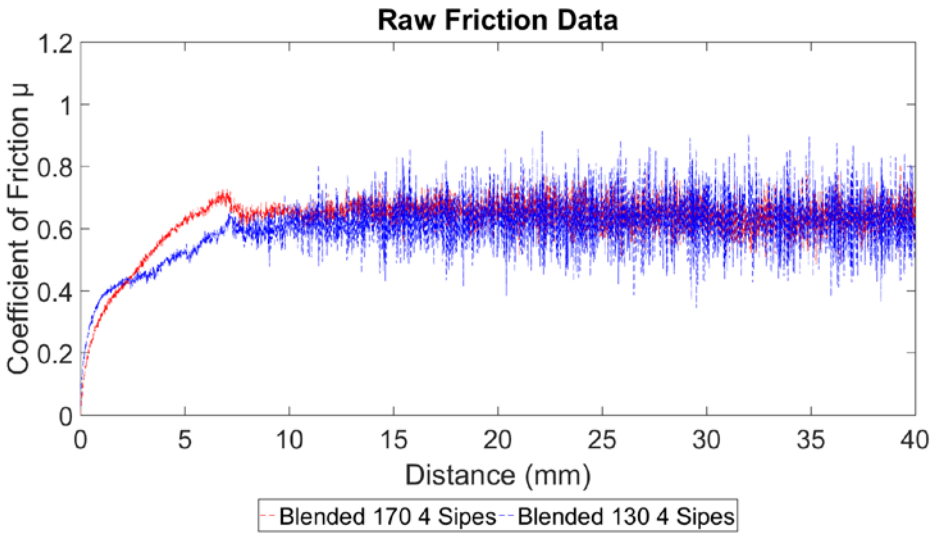

Figure 5.11 - Raw friction data for high and low compression blended snow using a 4 siped sample tested at 0.01m/s

Figure 5.11 shows the region of the μ-distance curve over which the average reading is taken (0-40mm). It can be seen that past the initial peak (7mm distance) when ploughing is the dominant mechanism the frictional behaviour is very consistent between the two snows with average values and amplitude variations being very similar.

When examining the initial area of the curve (0-10mm) it is clear that there is a difference between the two snows, with the low compression snow appearing to behave differently during the interactions before the static peak is reached. This altered behaviour occurs after approximately 1mm of travel, causing μ to stop rapidly rising at a μ of 0.4. After this point, it would appear the sipes begin to dig into the snow and bring μ back up to be in line with the high compression snow.

When this is compared to Figure 5.12 which shows the μ distance curves for the rounded samples it is clear that there is a distinct difference between the low and high compression snows which also occurs after approximately 1mm of travel. This difference

presents itself as the beginning of dynamic friction at a much lower μ for the low compression snow then the high compression snow. The hypothesis is that for both the siped sample and the rounded sample, there is a de-cohesion of the top layer of grains due to the applied loading through the rubber. This failure occurs at lower forces with the low compression snow due to the grains being less strongly bonded due to being given less time and less pressure during the forming of the snow tray. This failure initiates the movement of the rubber sample which then moves into dynamic friction.

A similar mechanism is likely to be occurring in the vapour deposition snow which exhibits similar behaviour.

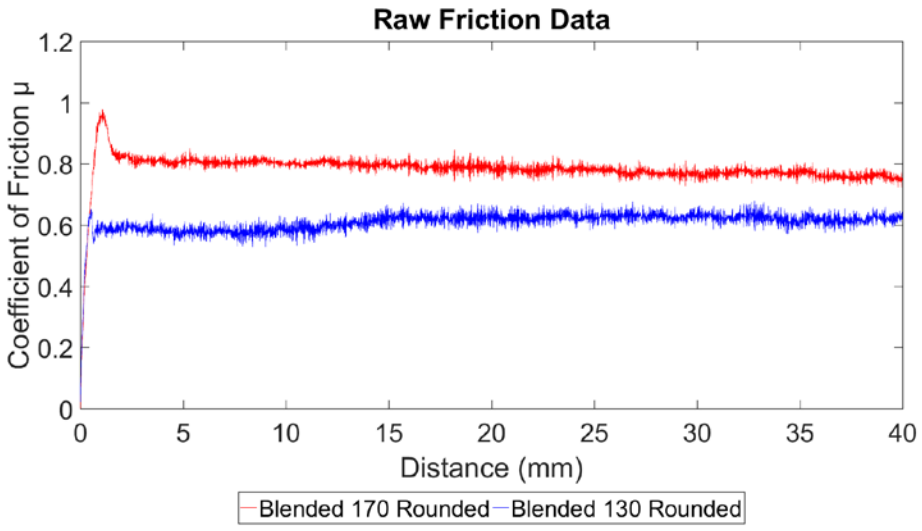

Figure 5.12 - Raw friction data for high and low compression blended snow using a rounded sample tested at 0.01m/s

5.4.3 Natural Snow

The last type of snow that was tested was natural snow collected from the Cairngorm Mountains. The natural snow was tested for comparison and validation of the results from the artificial snows. This shows that the artificial snow being created within the lab is applicable to the real snow in the field. Unfortunately, it was very difficult to achieve consistent snow properties across the entire tray area, this caused larger errors in several measurements including friction as seen by the error bars in Figure 5.13. Also, the large grains (approx. 3-5mm as opposed to 1mm for the blended snow) making up the structure were bigger than the maximum measurement of the profilometer so it was not possible to measure the roughness.

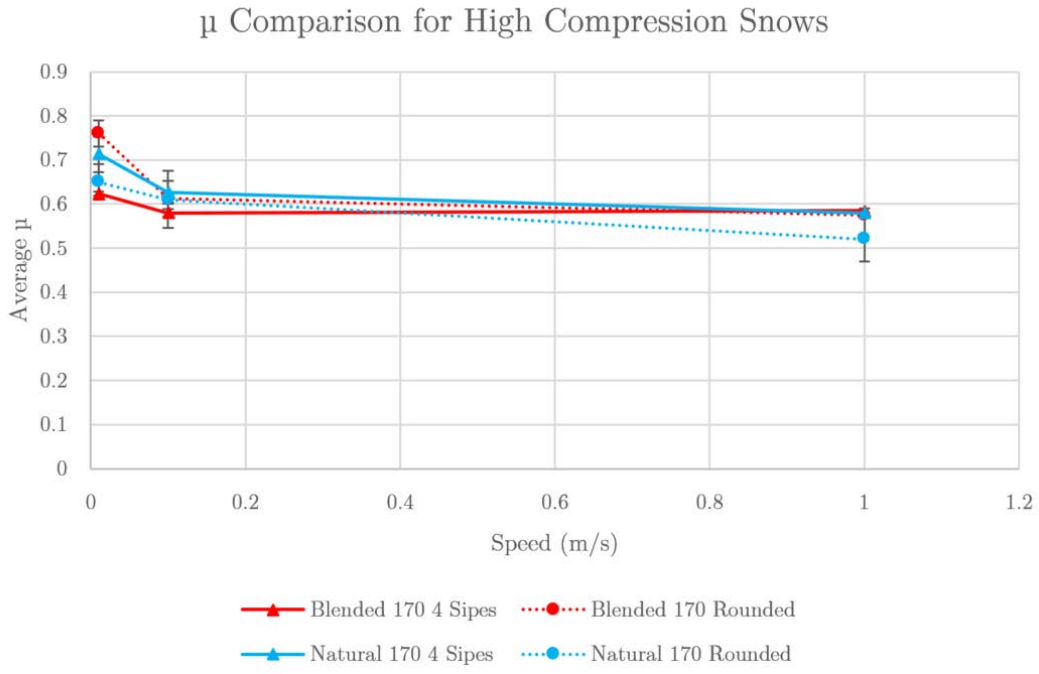

Figure 5.13 - Average μ between for high compression snows. Red lines represent blended snow, light blue lines represent natural snow. Dashed lines represent rounded edge rubber samples, solid lines represent 4 siped sample

In general, the natural snow follows the same trends Figure 5.14 shows these, with a notable drop in friction as the speed increases above 0.01m/s and a cross-over of the rounded and siped samples with rounded samples having higher friction than the siped samples at 0.01m/s and siped samples having higher friction than the rounded samples at all higher speeds. It was hypothesised that the natural snow would behave very similarly to the blended snow as the microstructure is much closer to the blended snow then the vapour deposition snow. Although a lot of similarities are seen between the blended and natural snow, there were also similarities between the blended and vapour deposition snow. This means that the artificial snow created in the lab is comparable to natural snow.

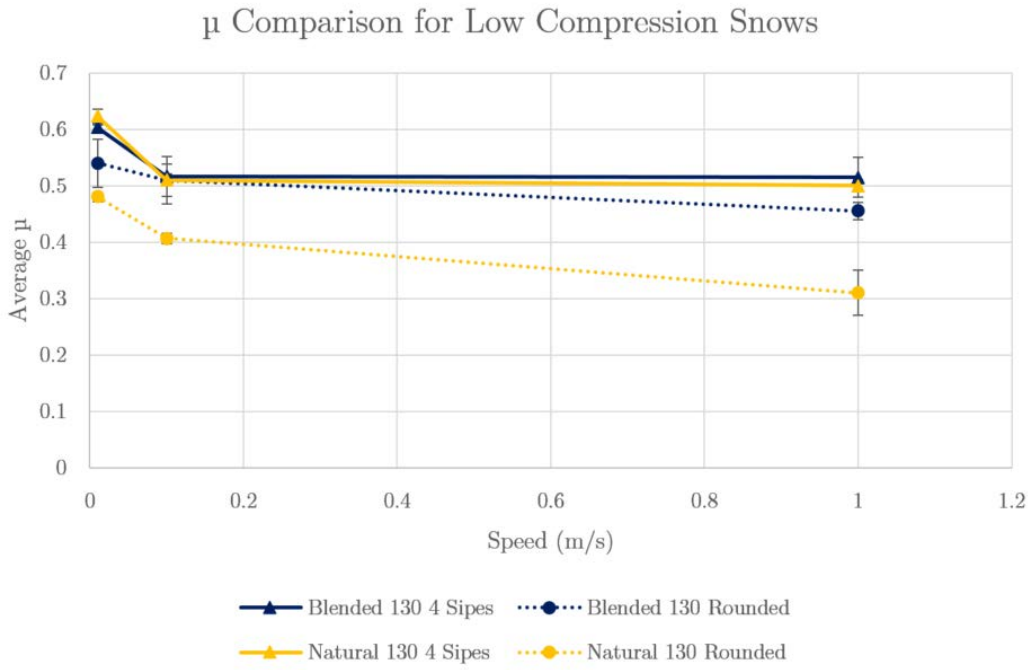

Figure 5.14 - Average μ between for low compression snows. Blue lines represent blended snow, yellow lines represent natural snow. Dashed lines represent rounded edge rubber samples, solid lines represent 4 siped sample

As expected Figure 5.14 shows that the low compression natural and blended snow behave very similarly when tested with the siped sample. However, there is a very significant drop in friction over the blended snow when looking at the rounded samples tested at 0.1m/s and 1m/s. It is hypothesised that this is due to the large reduction in real contact area as a result of the larger snow grains, therefore an increase in pressure and frictional heating causing a large fluid film effect to occur. However, it was not possible to measure the surface roughness with available instruments so this hypothesis is based only on observation of the experiments.

5.5 Conclusions

Friction testing was carried out on different snows, the differences between them are often subtle. By using two analytical rubber samples (rounded and siped) it was possible to investigate these differences. The subtlety in the data is not always obvious when looking at an average value for the friction, for this reason, all the individual friction curves were looked at individually to identify features of them which may be of use when interpreting these results. This led to an understanding of features such as how the sipes behave before steady-state friction begins and why there are large amplitudes in some test runs and not others.

In order to take the data further, it did become necessary to reduce the curves down to average values. By careful selection of the region over which the average coefficient of friction is taken it is possible to use values which correspond to those measured by Michelin in full car scale tests and provides a value that is appropriate to use to investigate the relationship between snow properties and friction in the next stages of work.

6 Estimating Coefficient of Friction

Summary

This chapter details how all the data was investigated in an attempt to understand the friction mechanisms occurring under the various testing conditions. This was done by examining how the measured snow characteristics correlate with the coefficient of friction. In order to do this a Matlab script was developed which could calculate the correlation coefficient for a given mechanical property and friction parameter for a selection of snows. By interpreting the correlations and investigating the raw data it is possible to hypothesise about what mechanisms are occurring in certain situations. With an understanding of the mechanisms, it has then been possible to develop an empirical formula which can be used to predict μ in the specific cases which have been investigated in the lab.

6.1 Introduction

To start understanding how the snow characteristics affect the friction. A basic idea of where the overall μ comes from is required. The initial assumption is that there are two main factors contributing to the total friction achieved by a siped sample on snow. The first factor being a combination of the various surface interactions (adhesion, indentation and fluid film lubrication) and the second being all energy dissipated as a result of the ploughing interactions.

$$\mu_{Total} = \mu_{Surface} + \mu_{Ploughing} \tag{5}$$

With the aim of estimating μ_{Total} it is necessary to hypothesize where the different frictional forces within the system are coming from within both $\mu_{Surface}$ and $\mu_{Ploughing}$. For example, $\mu_{Ploughing}$ may be higher on one snow because the snow is exhibiting a higher shear strength than another snow. This will allow the determination of how big a contribution each of the mechanisms have on the total friction and the ratio of $\mu_{Surface}$ to $\mu_{Ploughing}$.

Once we understand where the friction is coming from, it is then possible to start finding which snow properties measured in the testing plans could represent the friction mechanism, and could, therefore, be used to represent that mechanism in the calculation of total friction.

6.2 Estimating $\mu_{Ploughing}$

This section aims to separate out the different contributions to total friction by investigating the fiction measurements carried out using the two different rubber samples. The two friction measurements which were carried out (one using a 4 siped sample, one using a smooth sample) represent 2 of the terms in the equation. The siped

sample represents μ_{Total} as there are both ploughing and surface interactions occurring in this measurement. The smooth sample represents $\mu_{Surface}$ as there should be no ploughing occurring so we are only measuring the surface interactions.

If Equation (5) is correct it is possible to subtract $\mu_{Surface}$ from μ_{Total} and arrive at $\mu_{Ploughing}$. Once $\mu_{Ploughing}$ is calculated it is possible to begin substituting snow property measurements for both $\mu_{Ploughing}$ and $\mu_{Surface}$ with the aim of calculating μ_{Total} from snow property measurements.

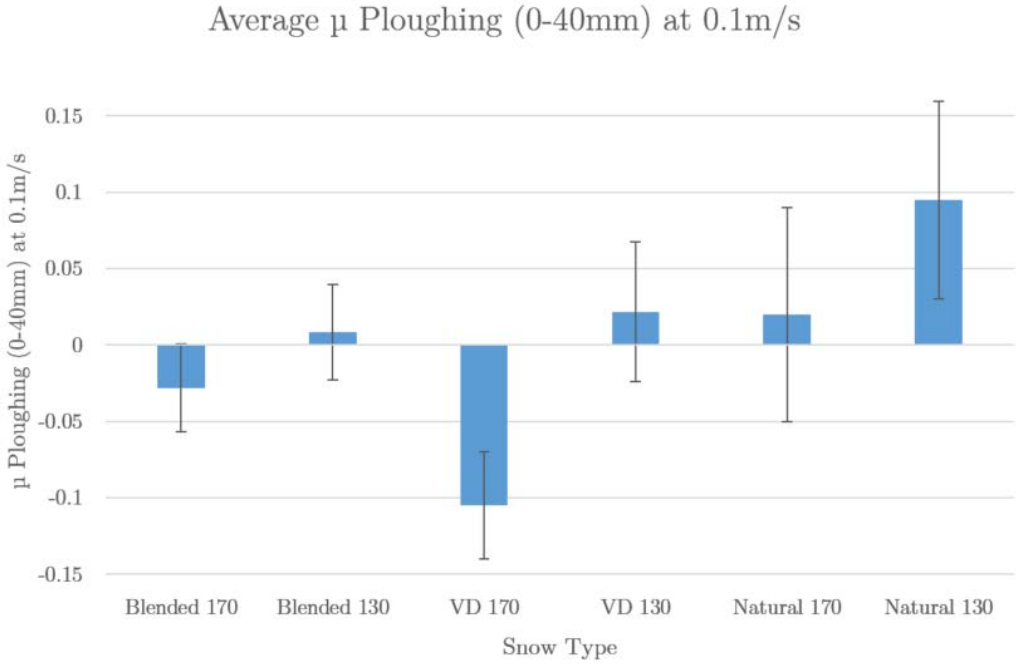

Figure 6.1 - μ Ploughing at 0.1m/s, calculated from Equation (5). Data for μ total and μ surface is averaged from 2 tray repeats.

Figure 6.1 shows the results of the calculation of $\mu_{Ploughing}$ at 0.1m/s. This calculation has resulted in negative values for ploughing friction. The blended 170 and Vapour Deposition 170 snows both exhibit higher friction with the smooth rubber sample then

the siped sample at almost all speeds. This leads to the situation where when the smooth sample is subtracted from the siped sample a negative value for $\mu_{Ploughing}$ is reached.

Two main possibilities exist to explain this:

Assumption 1:

The numbers are correct and that there are other mechanisms going on within ploughing mechanism which actually reduce the coefficient of friction when sipes are used. For example, powder snow created during the ploughing process building up under the sipes, acting like ball bearings and reducing friction.

Assumption 2

There cannot be a negative contribution from ploughing. The negative value is not necessarily coming from a reduction in the friction when looking at the siped sample friction, instead, the fact that the tests are not comparable as they are not measuring the same things. For example, the contact area of the siped sample is not the same as the rounded edge sample to start with and will be modified greatly as a result of the ploughing and bending of the siped segments of the rubber. This causes a reduction of the surface contribution term meaning that μ_{Total} which is being measured does not correspond directly to the $\mu_{Surface}$ term being measured by the rounded edge sample. This means an attempt must be made to correct Equation (5) so that a negative ploughing value is not reached. This can be done by multiplying $\mu_{Surface}$ in Equation (5) by a constant coefficient. In addition, it is assumed that the friction mechanisms will change as the siped sample progresses further into the snow altering the way the sipes interact with the surface.

In order to determine which assumption to use, the different possibilities have to be investigated.

6.2.1 Investigation of Assumption 1 (Additional mechanisms within ploughing process)

From observation of the actual test while it is being carried out along with the high-speed video footage of the tests, an additional mechanism presents itself which could contribute to the ploughing mechanism, potentially resulting in a lower coefficient of friction when ploughing is occurring.

- Mechanism – Debris thrown up by the sipes is not ejected to the sides of the sipes, it is instead forced beneath the sipes giving a "ball bearing" effect which means the sipes do not interact with the firmly bonded snow below, effectively rolling on the loose snow grains, reducing the friction.

From consideration of this mechanisms, it appears unlikely that this mechanism could reduce the coefficient as much as seen in Figure 6.1 for vapour deposition 170 snow. If the "ball bearing" effect was taking place, the sipes would no longer be interacting with the firm snow base below the powder, meaning no more powder is produced. If this was the case it would only be for a brief period of time, then the sipes would manage to eject the powder and coefficient of friction would return to normal.

As no other mechanisms present themselves which could cause a reduced friction compared to the siped sample assumption 1 will be perused no further.

6.2.2 Investigation of assumption 2 (Correcting Equation (5))

The second assumption, that the two tests are not equal due to the effect of the sipes and the way the ploughing mechanism changes as the sipes plough deeper into the snow can be corrected in 2 ways.

Firstly, the surface area of the base of the siped sample is not equal to the surface area of the smooth sample which is being used for the measured μ of $\mu_{Surface}$. This would normally not be an issue as μ is generally considered independent of surface area. Any reduction in contact area would give an increase in pressure and these effects perfectly cancel each other out thus giving a constant friction force (Bhushan, 2013). However, when dealing with snow and rubber the actual pressure is very important. A higher pressure can have an influence on fluid film lubrication (Evans et al., 1976). A higher pressure can also result in more concentrated force on individual grains, resulting in fracture of intergranular bonds and therefore more ploughing.

In addition to the surface area discrepancies, there are additional factors to consider such as the flexing of the sipes. This flexing affects pressure distribution beneath the sipe as it moves. This flexing can result in extremely high pressures at the leading edge of each sipe and a further altered real area of contact. The more rigid rounded edge sample does not exhibit this behaviour; the pressure distribution remains steady during testing. This is illustrated in Figure 6.2.

This discrepancy between the surface areas of the two different rubber samples justifies the use of a constant coefficient to compensate for the fact that the siped sample and the rounded edge sample are not directly comparable in this equation and can therefore be used to alter the relative contributions of $\mu_{Surface}$ and $\mu_{Plouging}$ to the total friction.

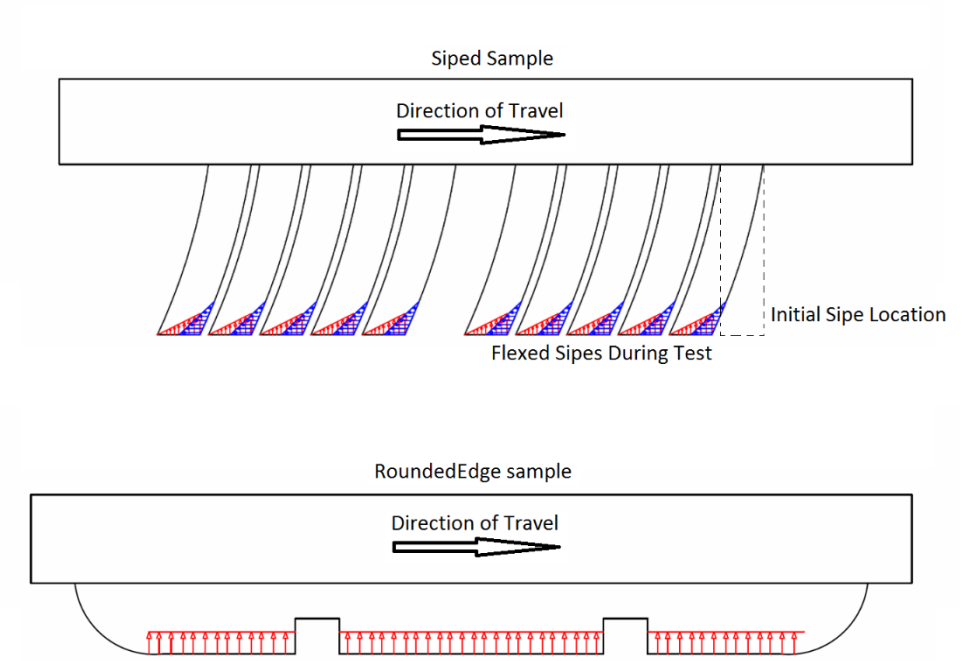

Figure 6.2 - Comparison of Pressure distribution in rubber samples during friction testing. Red arrows represent normal pressure. Blue arrows represent pressure applied laterally as a result of ploughing. Initial sipe location is shown before friction test begins.

In addition, it is hypothesised that the friction mechanism will be changing as the sipes plough further into the snow. It is assumed that this is a greater effect than simply a reduction in the surface area effect and so must also be taken into account in the formula. For this reason, z depth will be used as a coefficient in Equation (5). Z-depth is a measure of how far the siped sample penetrates into the snow surface between 0-40mm during a friction test.

Z-depth will be used to alter the $\mu_{Surface}$ contribution in Equation (5). Using z-depth as a coefficient will allow us to compensate for the altered mechanism as the ploughing sample digs deeper into the snow surface. In addition, using a constant coefficient will

allow us to compensate for the discrepancies between the two samples in terms of surface area and behaviour of the sipes (flexing).

Initially, it was attempted to use z-depth and constant coefficients to alter the $\mu_{Ploughing}$ term of Equation (5). However, after multiple iterations it was found that this did not work as when the resulting equation was used to calculate friction, it did not correlate with the measured friction.

Instead of altering the contribution of the ploughing mechanism as penetration into the snow increases, z depth will be used as a coefficient of the surface component of the total friction. If $\mu_{Surface}$ is divided by z depth, the increase in penetration will correspond to a decrease in surface contribution. Again after many iterations of the formula it was found that this gave results which correlate far better with the measured values of friction.

6.2.3 Calculating correct $\mu_{Ploughing}$

From multiple observations during the testing and examination of the high-speed camera footage of a selection of tests, it appears the snow with the lowest $\mu_{Ploughing}$ is the vapour deposition 170 snow, as there was the least amount debris left behind after each test and the measured z-depth for VD 170 is the lowest out of all the snows. In order to work out the correct coefficient to use vapour deposition snow will be used with an aim of choosing a coefficient which brings the calculated value of $\mu_{Ploughing}$ close to zero.

The ploughing behaviour varies depending on the speed at which the test is carried out. This means the speed where vapour deposition 170 exhibits the lowest coefficient of

friction with a siped sample is used in order to calculate the coefficient which brings $\mu_{Ploughing}$ as low as possible without deviating from the expected trends in the data (VD 170 exhibiting the lowest ploughing at all speeds and the 130 snows exhibiting higher ploughing in general than the 170 equivalents). In this case that speed is 0.01m/s.

From altering the coefficient manually and re-plotting the data to confirm $\mu_{Ploughing}$ is never negative, a constant coefficient of 0.8 was decided upon. This meets the requirements of bringing the calculated vapour deposition ploughing value at 0.01m/s as low as possible, giving a coefficient of friction for $\mu_{Ploughing}$ of 0.18 for vapour deposition 170 snow.

$$\mu_{Ploughing} = \mu_{Total} - \frac{0.8 \times \mu_{Surface}}{Zdepth + 1} \tag{6}$$

In the denominator of the $\mu_{Surface}$ component of the equation a "+1" is included. This is to remove the issue of z-depth being below 1 and would therefore have increased the contribution of $\mu_{Surface}$ rather than decrease it.

At this stage Equation (6) is not dimensionally correct. It is presented this way for simplicity while developing the formula and is corrected by introducing further constant coefficients at a later stage in order to result in a dimensionally correct formula for total friction.

This equation could then be applied to all other snows and all other speeds to give the data presented in Figure 6.3. Although the vapour deposition 170 snow at 0.01m/s is being set close to zero in order to choose the constant coefficient for the formula, when tested at 1m/s the vapour deposition snow has the highest level of ploughing. This is attributed to the drastic reduction in friction of the rounded edge sample, from 0.8 at 0.01m/s to 0.55 at 1m/s.

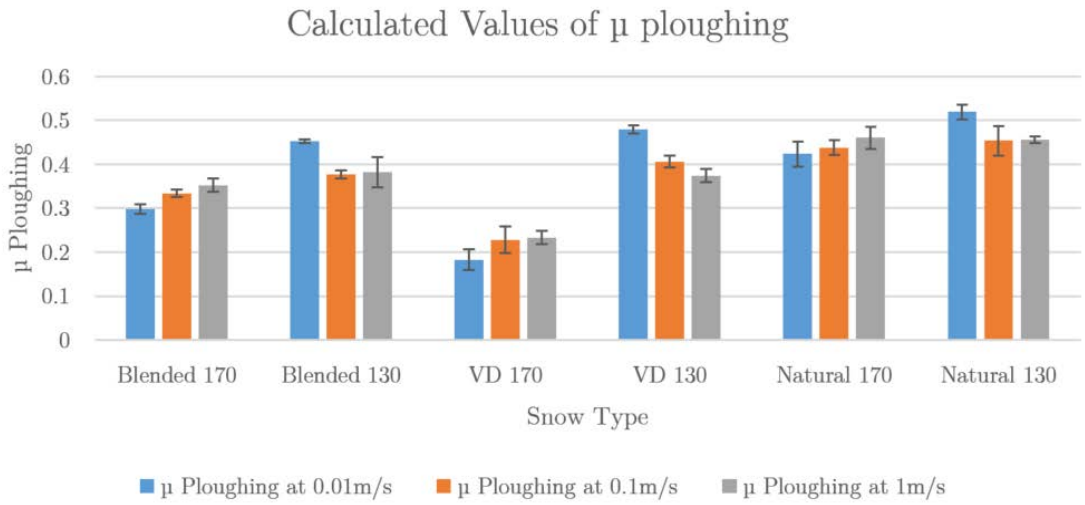

Figure 6.3 - Calculated values of µ ploughing using Equation (6). Error bars represent the standard deviation of the measured values of both the smooth samples and the siped samples.

Figure 6.4 shows the values measured during testing with the rounded edge rubber sample. These values correspond to the $\mu_{Surface}$ component of Equation (6).

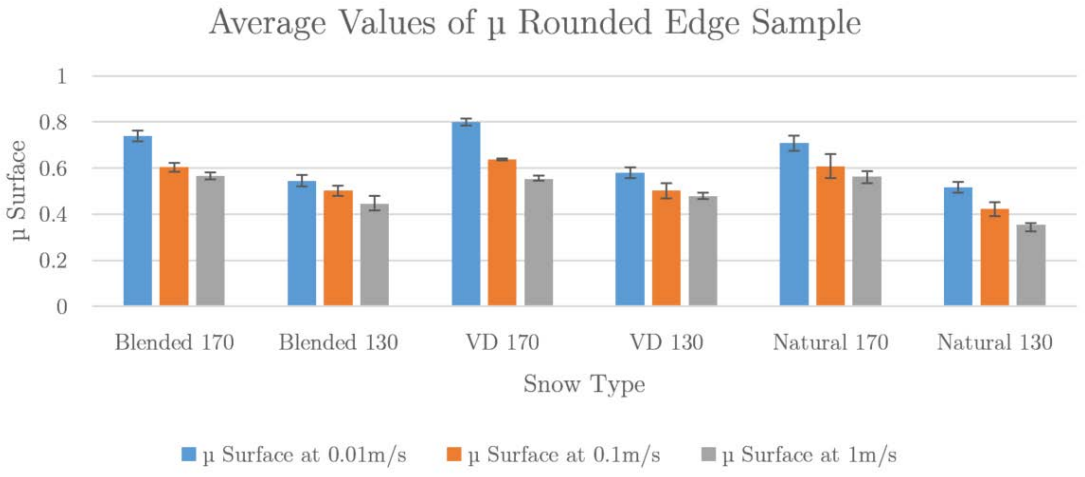

Figure 6.4 - Measured values of friction from testing with the rounded edge rubber sample. This corresponds to the value of $\mu_{Surface}$ in Equation (6). Error bars represent the standard deviation of the measured values of µ.

6.3 Determining relationships between friction and snow properties

Now that a starting point has been established, using Equation (6) as a base to work from in order to understand what mechanisms are contributing to the total friction. The next step is to look at the individual components $\mu_{Ploughing}$ and $\mu_{Surface}$ and how the variations in the snow affects them.

This section concentrates on correlating the observed snow characteristics with either $\mu_{Ploughing}$ or $\mu_{Surface}$ with the aim of replacing them within the equation. This will lead to an empirical formula which can be used to estimate total friction.

In order to choose which characteristics can be used to replace the terms in Equation (6), it is necessary to make some guidelines and assumptions. Firstly no measurements taken on FRIMA should be used. Ideally, these measurements could be done in the field while characterising snow for full-scale tests. FRIMA would not be present in the field so any measurements made using it such as Z-Depth and cohesion are not going to be used.

Secondly, as $\mu_{Surface}$ does not include any ploughing it is assumed that the only influence on this part of the friction is directly from the surface of the snow. This means that $\mu_{Surface}$ is only going to be correlated with measurements of the surface from the profilometer.

Finally, $\mu_{Ploughing}$ is expected to encompass all contributions to total friction which are not directly related to the surface interactions. Correlations will only be made with measurements made on the snow which are not related to the surface and were not taken on FRIMA.

6.4 Correlation Methodology

This section describes the process of correlating the snow characteristics and properties with the friction measured on FRIMA for $\mu_{Surface}$ and the friction calculated in section 6.2.3 using Equation (6) for $\mu_{Ploughing}$.

In order to carry out correlations all the key results that were calculated chapter 4 and 5 were assembled into a database. The tray repeats were averaged in order to provide one result to work with for the correlations. The database also listed the associated errors in the form of standard deviations.

In order to correlate mechanical properties of the snow with the measured $\mu_{Surface}$ and calculated $\mu_{Ploughing}$, a MATLAB correlation script was made. This allowed a quick selection of two properties to be compared in order to look for a correlation and which snows to use when looking for a correlation. For example it is possible to select $\mu_{Ploughing}$ and shear strength as the properties to look for a correlation between. It would then be possible to select all the low compression snows (blended 130 vapour deposition 130 and natural 130) and the program would display the results on a graph and list the correlation coefficient.

The correlation coefficient was calculated within MATLAB using the built-in correlation function. This gives a number between -1 and 1 with 1 being a strong positive correlation, -1 being a strong negative correlation and 0 having no relationship.

Instead of individually selecting what properties to compare to what, a script was then created to compare every property to every other property. It was then possible to perform a search for any correlations with a coefficient of >0.75 or <-0.75. Although in many fields of study this would be considered a poor correlation, the large errors and difficulties associated with working with snow mean it is very difficult to get perfect measurements which can be used to definitively calculate correlation coefficients. A

Correlation of 0.75 was chosen as this appeared to be a strong enough correlation to be worthy of further investigation.

6.5 Correlation with $\mu_{Ploughing}$

This section details the process of taking all the snow properties which have been shown to correlate with $\mu_{Ploughing}$ (correlation coefficient >0.75 or <-0.75), examining the correlation plots to determine which property is most appropriate to replace $\mu_{Ploughing}$ in Equation (6). This was also based on the mechanisms involved in the ploughing friction and careful consideration of how the chosen snow property influences the mechanisms.

The first step is to pick out all the properties which correlate with $\mu_{Ploughing}$. The correlations may be different for the different speeds of $\mu_{Ploughing}$ so this must be taken into account when looking for the best correlation.

Table 6.1, Table 6.2 &Table 6.3 detail the options that were found to correlate with $\mu_{Ploughing}$ which have a correlation coefficient >0.75 or <-0.75 for the three different speeds. Now a check is made to see which options provide a correlation at all speeds.

Table 6.1 - Snow properties found to correlate with μ ploughing at 0.01m/s

$\mu_{Ploughing}$ @ $0.01m/s$ Correlates well with:	Correlation Coefficient
Compressive Elastic modulus tested at 5mm/min	-0.79
Compressive Elastic modulus tested at 50mm/min	-0.9
Compressive Yield Stress tested at 5mm/min	-0.75
Compressive Yield Stress tested at 50mm/min	-0.84
Compressive Yield Stress tested at 500mm/min	-0.78
CTI	-0.91

Table 6.2 - Snow properties found to correlate with μ ploughing at 0.1m/s

$\mu_{Ploughing}$ @ $0.1m/s$ Correlates well with:	Correlation Coefficient
Compressive Elastic modulus tested at 5mm/min	-0.81
Compressive Elastic modulus tested at 50mm/min	-0.95
Compressive Yield Stress tested at 5mm/min	-0.79
Compressive Yield Stress tested at 50mm/min	-0.91
Compressive Yield Stress tested at 500mm/min	-0.95
CTI	-0.85

Table 6.3 - Snow properties found to correlate with μ ploughing at 1m/s

$\mu_{Ploughing}$ @ $1m/s$ Correlates well with:	Correlation Coefficient
Compressive Elastic modulus tested at 50mm/min	-0.91
Compressive Yield Stress tested at 50mm/min	-0.96
Compressive Yield Stress tested at 500mm/min	-0.98

From looking at which properties correlate at all speeds it is possible to see that there are three options: Compressive Elastic modulus tested at 50mm/min, Compressive Yield Stress tested at 50mm/min and Compressive Yield Stress tested at 500mm/min. In order to determine which one is most appropriate, the data for each option is plotted against $\mu_{Ploughing}$ with a line of best fit plotted. The correlations can then be investigated by looking at the distribution of data along and around the mean line and thinking about which property makes the most sense to represent $\mu_{Ploughing}$ in Equation (6).

6.5.1 Investigation of $\mu_{Ploughing}$ correlations at 0.1m/s

In order to simplify the process of investigating the correlations, only the correlations relating to $\mu_{Ploughing}$ at 0.1m/s are being presented here. The speeds of 0.01m/s and 1m/s were investigated in the same manner and showed very similar distributions to those presented here for 0.1m/s.

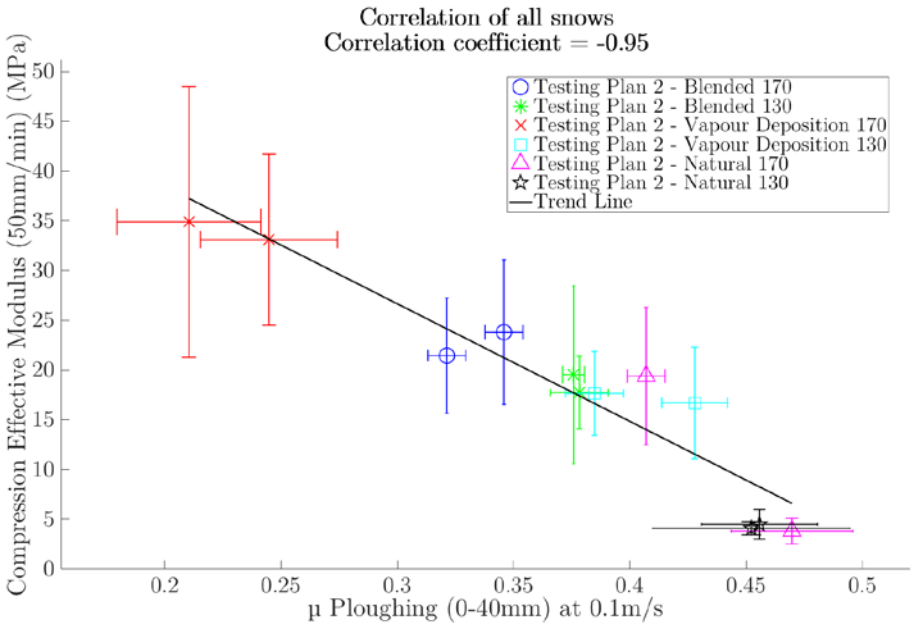

Figure 6.5 - μ Ploughing at 0.1m/s vs Compressive Elastic modulus tested at 50mm/min

As shown in Figure 6.5, the correlation of elastic modulus tested at 50mm/min is strong, there is a good distribution of data along and around the mean line. The majority of the points are close to the mean line, within margin of error. There are no extreme outliers which could cause the mean line to be displaced and the correlation coefficient to become unrealistic. Natural snow 170 is the least correlated, this is due to the difficulty in getting consistent samples when testing with natural snow. This all means the elastic modulus is a strong contender to be used to replace $\mu_{Ploughing}$.

The correlation of $\mu_{Ploughing}$ and yield strength tested at 50mm/min is shown in Figure 6.6. When examining the yield strength correlation it is possible to see that although the error bars are smaller than those of the elastic modulus correlation the actual data is spread further away. This indicates that the correlation is worse as the more precise results less accurately represent $\mu_{Ploughing}$, this can also be seen in the slightly lower correlation coefficient. In addition, the manual way in which the yield strength is selected involves more human error then the method used for selecting the elastic modulus as discussed in section 4.6. At this point the elastic modulus is the preferred option to use replacing $\mu_{Ploughing}$.

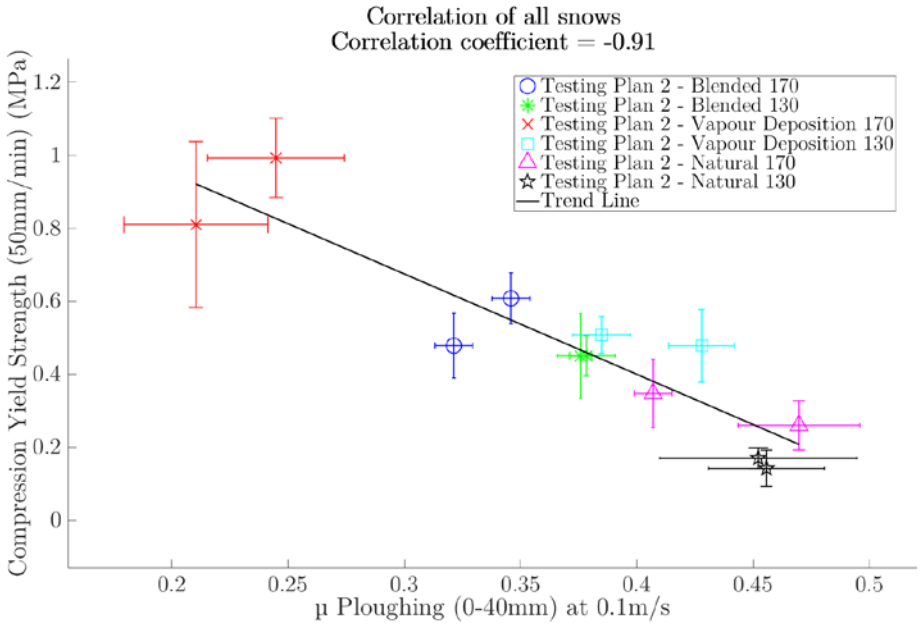

Figure 6.6 - μ Ploughing at 0.1m/s vs Compressive yield strength tested at 50mm/min

Looking at the data for the yield strength when tested at 500mm/min as shown in Figure 6.7 it is possible to see that several of the issues associated with the yield strength when tested at 50mm/min are avoided. The measurements appear to match the mean line more accurately will still maintaining their precision, this has given a higher correlation coefficient of -0.95 then the -0.93 of the yield strength at 50mm/min.

However, when looking at the area where $\mu_{Ploughing}$ is the highest, the results are more spread out. If vapour deposition 170 snow were not included in the data there would be little to no correlation of the results. Whereas if the same was done with Figure 6.5 for the yield strength there would still be some correlation. For this reason yield strength tested at 500mm/min will not be used to replace $\mu_{Ploughing}$ in Equation (6).

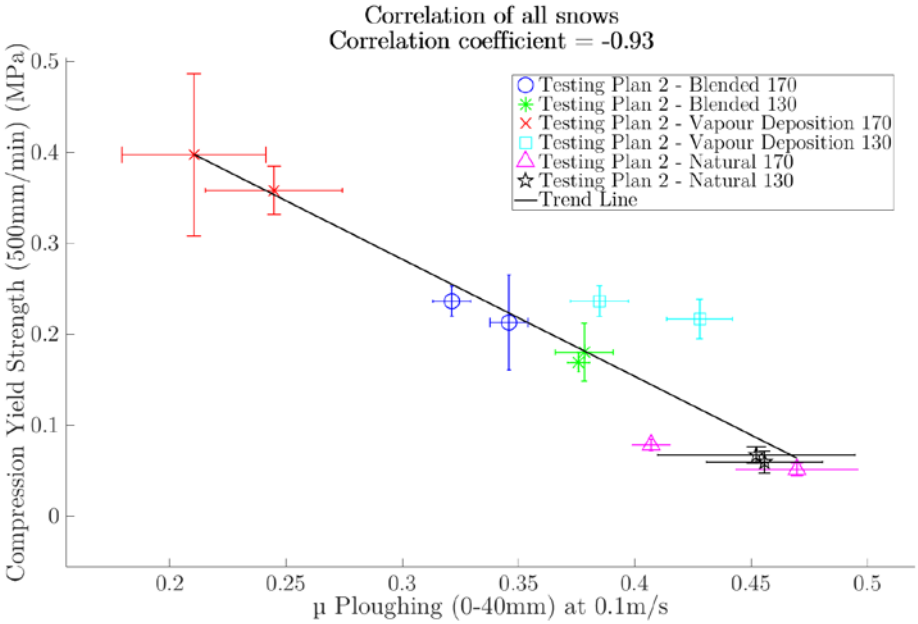

Figure 6.7 - μ Ploughing at 0.1m/s vs Compressive yield strength tested at 500mm/min

6.5.2 Understanding the link between $\mu_{Ploughing}$ and Effective Modulus

$\mu_{Ploughing}$ is the friction resulting from the permanent deformation of the snow. This deformation can come in the form of fracturing of intergranular bonds, ejection of snow grains to the front and sides of the sipes and compaction of the snow below the sipes.

As can be seen in Figure 6.5 as effective modulus decreases, $\mu_{Ploughing}$ increases. This initially seems counter intuitive as one might expect a stiffer material to be stronger and therefore exhibit more resistance to ploughing. However, because $\mu_{Ploughing}$ results from the movement of snow grains, if the snow is less well bonded it will exhibit a lower stiffness, the weaker bonds also exhibit lower strength allowing the sipes to dig further into the snow ultimately resulting in a larger volume of snow being displaced. This can be seen in Figure 6.8 which shows that for a higher z-depth there is a lower effective modulus.

The number of grain bonds being fractured increases with z depth due to the greater volume of snow being displaced. In this case, the energy dissipation from multiple weaker bonds is greater than a fewer number of stronger bonds being fractured on the surface.

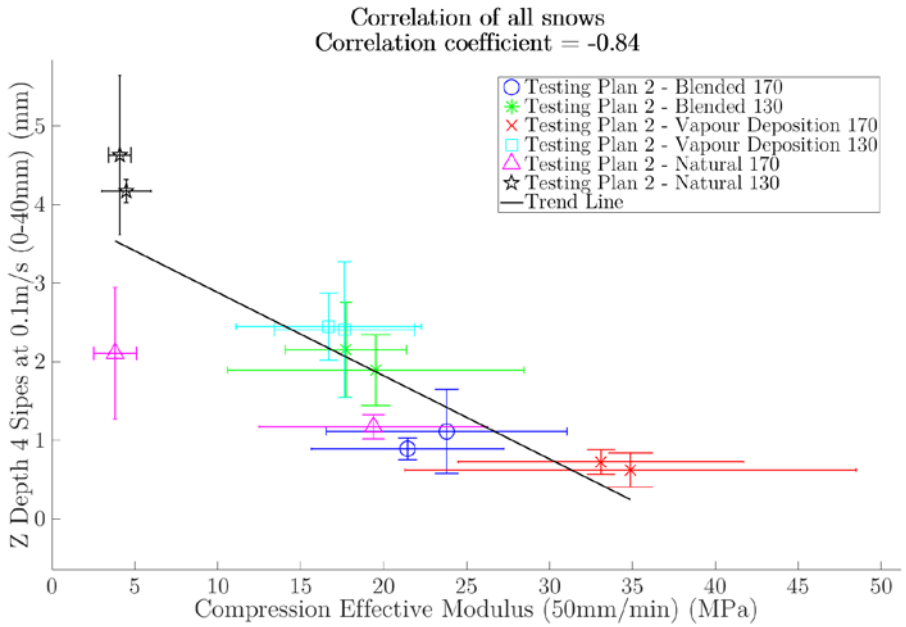

Figure 6.8 - Correlation of Z-depth (4 sipes at 0.1m/s) and compressive modulus tested at 50mm/min

6.5.3 Replacing $\mu_{Ploughing}$ in Equation (6)

In this section Equation (6) will be altered by replacing $\mu_{Ploughing}$ with effective modulus. This is the first of two replacements which will be carried out based on the correlations of snow properties with the friction data. Equation (6) has been rearranged to place μ total as the subject of the equation as shown in Equation (7)

$$\mu_{Total} = \mu_{Ploughing} + \frac{0.8 \times \mu_{Surface}}{ZDepth + 1} \tag{7}$$

Before $\mu_{Ploughing}$ can be replaced Equation (7), the relationship of $\mu_{Ploughing}$ to yield strength at 50mm/min must be calculated. This is done by finding the equation of the line of best fit of the correlation and re-arranging to find $\mu_{Ploughing}$. This equation is provided by MatLAB when the correlations are plotted. The equation is slightly

different for each friction test speed. For simplicity during this discussion, the 0.1m/s will be used as, an example. The complete equations for the friction tests at 0.01m/s and 1m/s are presented in section 6.7.3

$$\mu_{Ploughing} = -0.0076 \times E + 0.5093 \tag{8}$$

Equation (8) can now be used combined with Equation (7) to complete the first replacement. However, a key part of developing an empirical formula is a "sanity check" to confirm that the formula makes logical sense. In this case there is a problem that $\mu_{Ploughing}$ is unit less but E has units of Pascals. The simplest way to correct this issue is to introduce a constant value in the equation which has the same units as E, if these values are divided, the units cancel out leaving both sides of the equation unit less.

In this case, it makes sense to use a constant which is related to the test being carried out. The most obvious option is to use the Young's modulus of Ice. Ice is better understood then snow and the literature generally agrees well on the value of E_{Ice}. Snow is generally described as being made up of a lattice of ice crystals. For these reasons using the Young's modulus of ice as a constant is an appropriate choice.

The Young's modulus of polycrystalline ice (E_{Ice}) at -16°C is 9.33GPa (Petrenko et al., 1999)

When this is included in the equation it must be compensated for by multiplying E by the same value giving the formula:

$$\mu_{Ploughing} = -70.908 \times \frac{E}{E_{Ice}} + 0.2394 \tag{9}$$

Where:

E_{Ice} = 9330 MPa

E = Compressive effective modulus measured at 50mm/min (MPa)

Equation (9) can now be substituted into Equation (7) to give the following equation for μ_{Total}:

$$\mu_{Total} = \left(\frac{-70.908 \times E}{E_{Ice}} + 0.2394\right) + \frac{0.8 \times \mu_{Surface}}{ZDepth + 1} \quad (10)$$

6.6 Correlation with $\mu_{Surface}$

This section follows the same method as was used in 6.5. This time taking all the surface measurements which have been shown to correlate with $\mu_{Surface}$ (correlation coefficient of >0.75 or <-0.75) and examining the correlation plots to determine which measurement is most appropriate to replace $\mu_{Surface}$ in the newly developed Equation (10).

As before, the first step is to pick out all the surface measurements which correlate with $\mu_{Surface}$. The correlations may be different for the different speeds of $\mu_{Surface}$ so this must be taken into account when looking for the best correlation.

In this case, natural snow was too rough to measure any roughness parameter so correlations with all snows were not possible hence, the correlations are with the available data for blended and vapour deposition snow.

The roughness measurements available for correlation are Ra, Kurtosis & Peak count density. Table 6.4, Table 6.5 and Table 6.6 detail the options that were found to correlate with $\mu_{Surface}$. With ploughing it was necessary to look for which measurements correlate at all three speeds. In this case that is not necessary as there is only one parameter which correlates at any of the speeds.

Table 6.4 - Snow properties found to correlate with μ surface at 0.01m/s

$\mu_{Surface}$ @ $0.01m/s$ Correlates well with:	Correlation Coefficient
Peak Count Density	0.92

Table 6.5 - Snow properties found to correlate with μ surface at 0.1m/s

$\mu_{Surface}$ @ $0.1m/s$ Correlates well with:	Correlation Coefficient
Peak Count Density	0.88

Table 6.6 - Snow properties found to correlate with μ surface at 1m/s

$\mu_{Surface}$ @ $0.1m/s$ Correlates well with:	Correlation Coefficient
Peak Count Density	0.75

6.6.1 Investigation of peak count density correlations

Although peak count density is the only parameter which correlates at all speeds it is necessary to investigate the correlations further to explore if it makes sense to represent $\mu_{Surface}$ with peak count density in Equation (10). In this case, instead of investigating the parameters which correlate at 0.1m/s as was done with ploughing in section 6.5.1, the correlations of $\mu_{Surface}$ and peak count desnity at all speeds (0.01m/s, 0.1m/s and 1m/s) are investigated.

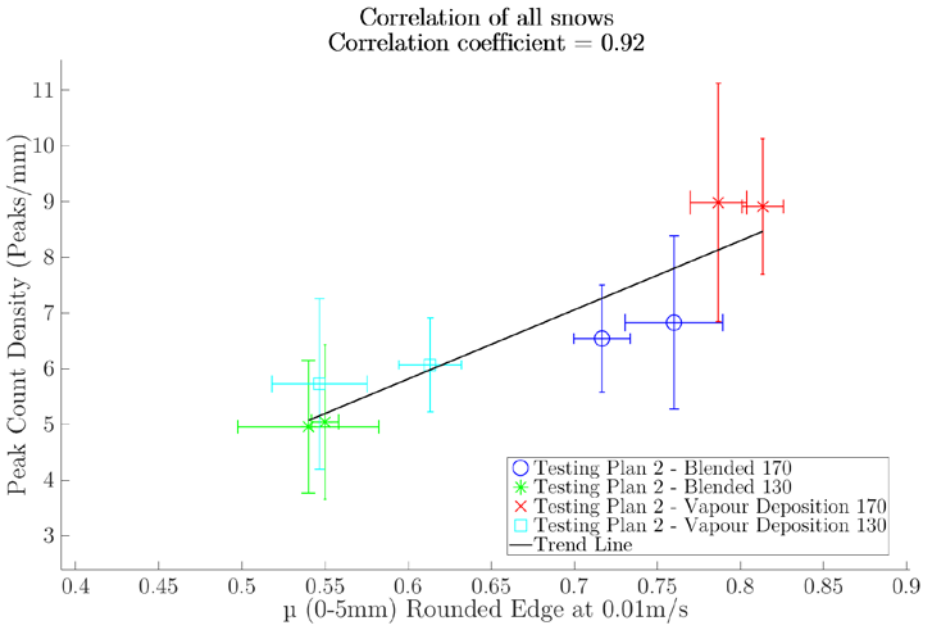

Figure 6.9 - μ surface at 0.01m/s vs Primary Peak Count Density

The correlation of peak count density with $\mu_{Surface}$ is the best at 0.01m/s as shown in Figure 6.9. Although there are large errors in peak count density, in general the correlation is good with no extreme outliers. Looking at Figure 6.10 & Figure 6.11 the correlations appear significantly worse even though the correlation coefficient is still above the threshold of 0.75. One if the reasons it appears this way when looking at the plots is due to the much smaller spread of friction data then that seen in Figure 6.9. This makes the data appear more clustered and with the large errors it starts to become harder to interpret the general trend of the data. The reduced correlation as the speed increases can be attributed to the change in mechanism which occurs at higher speeds. As discussed in section 2.2.4, a meltwater layer begins to form at higher speed, this alters the friction mechanism, reducing the dependence on peak count density.

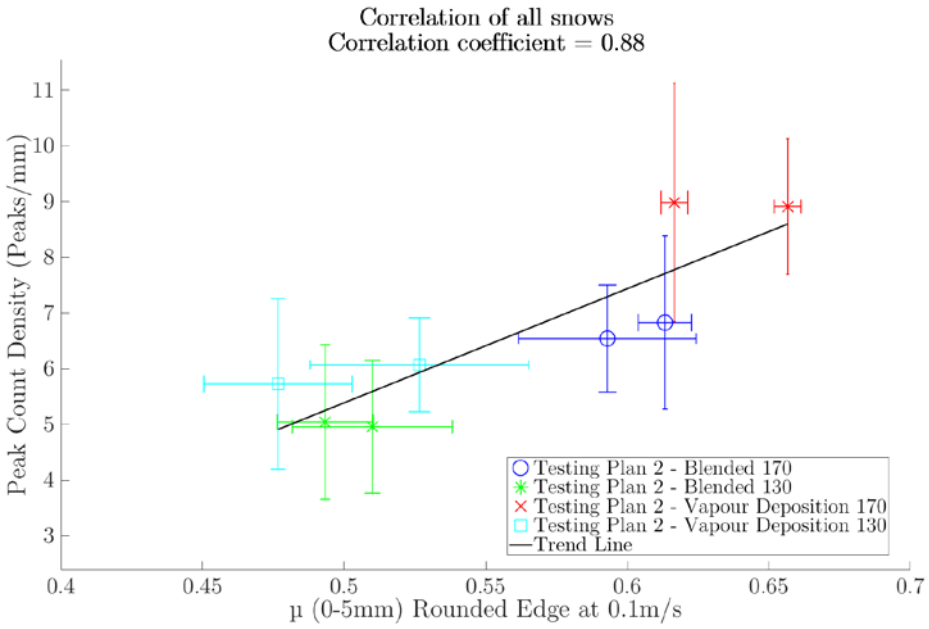

Figure 6.10 - μ surface at 0.1m/s vs Primary Peak Count Density

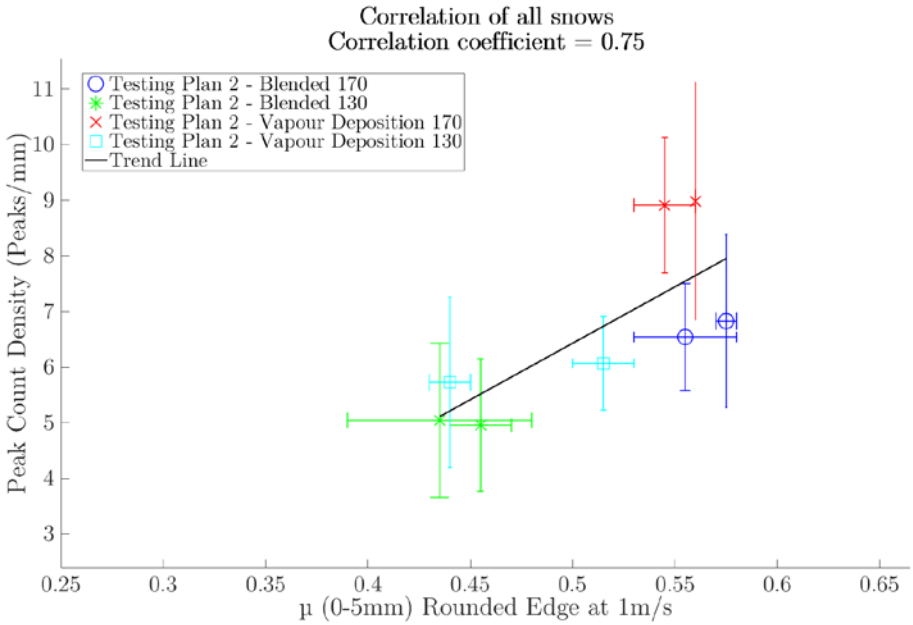

Figure 6.11 - μ surface at 1m/s vs Primary Peak Count Density

The large errors and spread of the peak count density correlations is not ideal for using to correlate with $\mu_{Surface}$, however the data does fall within the criteria of having correlation coefficient of >0.75 also, being the only surface measurement which correlated with $\mu_{Surface}$ it is the only option available to use.

6.6.2 Understanding the link between $\mu_{Surface}$ and peak count density

$\mu_{Surface}$ is the friction resulting from the indentation of the rubber and adhesion to the snow, fluid film lubrication will also have a large influence if the test speed is high enough for melting to occur. As discussed in section 6.6.1, as the test speed increase the dependence on peak count density decreases. This indicates that at the higher speeds the friction mechanism is changing however it does appear to still have some dependence on the peak count density.

As can be seen in Figure 6.10 as peak count density increases, $\mu_{Surface}$ also increases. My hypothesis is that this is due to larger number of contact points indenting the rubber giving more real area of contact and thus more energy dissipation in the rubber through the indentation mechanism.

6.6.3 Replacing $\mu_{Surface}$ in Equation (10)

In this section Equation (10) will be altered by replacing $\mu_{Surface}$ with peak count density.

After $\mu_{Ploughing}$ was replaced in section 6.5.3 the partially finished Equation (10)was:

$$\mu_{Total} = \left(\frac{-70.908 \times E}{E_{Ice}} + 0.2394\right) + \frac{0.8 \times \mu_{Surface}}{ZDepth + 1}$$

Before $\mu_{Surface}$ can be replaced in Equation (10) the relationship of $\mu_{Surface}$ to Peak count density must be calculated. This is done by finding the equation of the line of best fit of the correlation and re-arranging to find $\mu_{Surface}$. As before MatLAB provides this equation when the correlations are calculated. Once again the equation is different at the three different speeds, only 0.1m/s is presented here as an example The complete equations for the friction tests at 0.01m/s and 1m/s are presented in section 6.7.3.

$$\mu_{Surface} = 0.0374 \times PCD + 0.3128 \tag{11}$$

As discussed in section 6.5.3 it is necessary to consider if the equation being created makes sense. In this case, the inclusion of peak count density brings the units of peaks/mm. These units must also be cancelled out in a similar way as presented in section 6.5.3, however as "peaks" is simply a numerical value it is only necessary to remove the "mm" part of the unit.

In order to achieve this the measurement is multiplied by the length over which the measurement is taken (L_0). In this case 10mm. This alters the formula and must be corrected back to its original form. This is done by dividing by 10, this will cancel out any effect of including the 10mm test length.

This gives the formula:

$$\mu_{Surface} = \frac{0.0374}{10} \times L_0 \times PCD + 0.3128 \quad (12)$$

Where:

L_0 = 10mm

Equation (12) can now be included in the overall formula for μ total (Equation (10)). The resulting equation is presented below (Equation (13)).

$$\mu_{Total} = \left(\frac{-70.908 \times E}{E_{Ice}} + 0.2394\right) + \frac{0.00374 \times L_0 \times PCD + 0.3128}{ZDepth + 1} \quad (13)$$

Where:

E_{Ice} = 9330 MPa

E = Compressive effective modulus measured at 50mm/min (MPa)

L_0 = 10mm

PCD = The measured peak count density (Peaks/mm)

6.7 Correlation with Z-Depth

This section follows the same method as was used in section 6.5 & section 6.6. This time taking all the measured snow properties which have been shown to correlate with Z-Depth (correlation coefficient of >0.75 or <-0.75) and examining the correlation plots to determine which measurement is most appropriate to replace Z-Depth in the newly developed Equation (13).

As before, the first step is to pick out all the snow properties which correlate with Z-Depth. The correlations may be different for the different friction test speeds so this must be taken into account when looking for the best correlation.

Table 6.7, Table 6.8 & Table 6.9 detail the options that were found to correlate with Z-Depth which have a correlation coefficient >0.75 or <-0.75 for the three different speeds. Now a check is made to see which options provide a correlation at all speeds.

Table 6.7 - Snow properties found to correlate with z-depth at 0.01m/s

$\boldsymbol{Z-Depth\ Siped\ @\ 0.01m/s}$ Correlates well with:	Correlation Coefficient
CTI	-0.79
Compressive Elastic modulus tested at 50mm/min	-0.8
Peak Shear Stress	-0.86

Table 6.8 - Snow properties found to correlate with z-depth at 0.1m/s

$\boldsymbol{Z-Depth\ Siped}$ **@ 0.1*m/s* Correlates well with:**	**Correlation Coefficient**
CTI	-0.8
Compressive Elastic modulus tested at 50mm/min	-0.84
Compressive Yield Stress tested at 5mm/min	-0.75
Compressive Yield Stress tested at 50mm/min	-0.77
Peak Shear Stress	-0.82

Table 6.9 - Snow properties found to correlate with z-depth at 1m/s

$\boldsymbol{Z-Depth\ Siped}$ **@ 1*m/s* Correlates well with:**	**Correlation Coefficient**
CTI	-0.88
Compressive Elastic modulus tested at 5mm/min	-0.88
Compressive Elastic modulus tested at 50mm/min	-0.92
Compressive Elastic modulus tested at 500mm/min	-0.78
Compressive Yield Stress tested at 5mm/min	-0.91
Compressive Yield Stress tested at 50mm/min	-0.88
Compressive Yield Stress tested at 500mm/min	-0.83

From looking at which properties correlate at all speeds it is possible to see that there are two options: Compressive Elastic modulus tested at 50mm/min, and CTI. In order to determine which one is most appropriate the data for each option is plotted against Z Depth with a line of best fit. The correlations can then be investigated by looking at

the distribution of data along and around the mean line and thinking about which property makes the most sense to represent Z-Depth in Equation (6).

6.7.1 Investigation of Z-Depth of siped samples at 0.1m/s Correlations

In order to simplify the process of investigating the correlations, only the correlations relating to Z-Depth at 0.1m/s are being presented here. The speeds of 0.01m/s and 1m/s were investigated in the same manner and showed very similar distributions to those presented here for 0.1m/s.

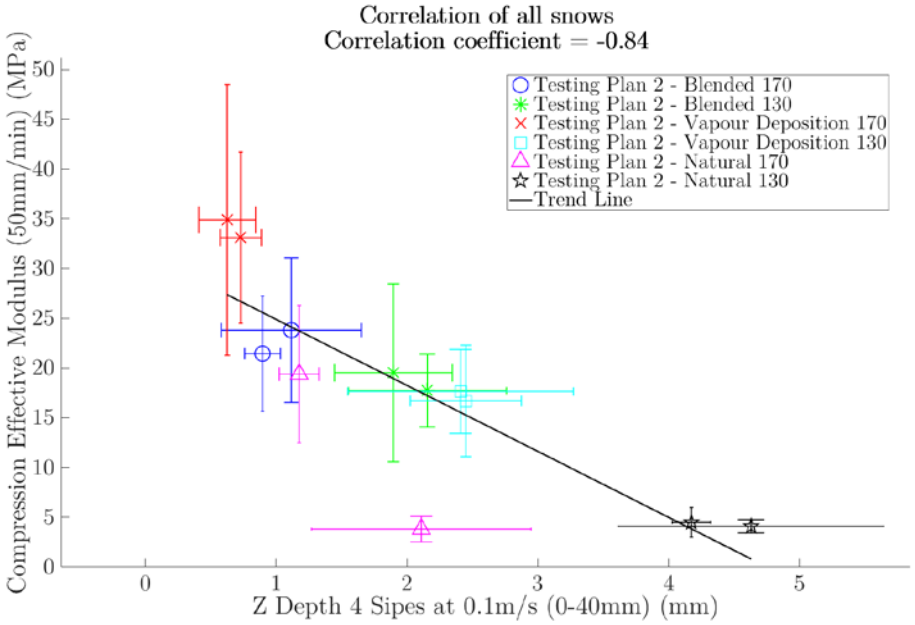

Figure 6.12 - Z-Depth of 4 Siped sample at 0.1m/s vs Compressive Effective Modulus tested at 50mm/min

Figure 6.12 shows the correlation of z-depth of the siped sample at 0.1m/s and effective compressive modulus tested at 50mm/min. The correlation coefficient of -0.84 is well within the range of properties suitable to represent Z-Depth, however one of the measurements of the natural 170 snow is positioned away from the trend line, this causes

the line to be pulled downward more than expected, this causes the data calculated when using the equation of the line of best fit to calculate Z-Depth to be thrown off. This means that when the data is included in the complete empirical equation (Equation (13)) the results no longer match the measured results for total friction.

Figure 6.13 shows the correlation of z-depth of the siped sample at 0.1m/s and CTI (penetration test of the snow). Here the results are clustered in groups, this is due to the preparation and compaction of the snow which was designed to achieve constant CTI values for each different preparation. However, the correlation is still within the usable limit and the relationship between CTI and Z-depth appears to be consistent with the full range of CTI's tested.

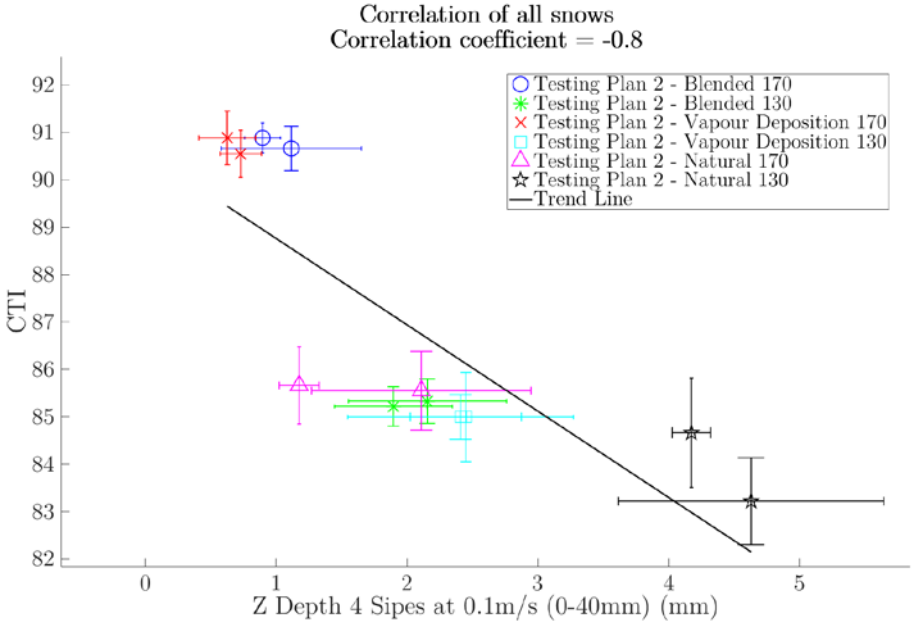

Figure 6.13 - Z-Depth of 4 Siped sample at 0.1m/s vs CTI

Ideally, it would be possible to use the effective modulus to replace z-depth in Equation (13) as effective modulus is also being used to represent $\mu_{Ploughing}$ which would have meant only two measurements of snow properties would be required. However, after extensive iterations of the formula, this was not possible as the specific way z-depth and

effective modulus correlate means it was not possible to achieve the correct calculated values for μ_{Total}. This leave the other option of using CTI to represent Z-Depth in Equation (13).

6.7.2 Understanding the link between Z-Depth and CTI

The correlation between Z-Depth and CTI was to be expected. Z-Depth is a measure of the depth a siped sample is able to penetrate into the snow by fracturing intergranular bonds during the ploughing process. CTI is a measure of the depth a spike can penetrate into the snow, also by fracturing intergranular bonds as a result of being dropped onto the snow surface. Both of these processes involve multiple different processes such as compression and fracture but the main processes of fracturing intergranular bonds to make progress into the depth of the snow exist in both tests. This indicated that a correlation between the two measurements was to be expected.

6.7.3 Replacing Z-Depth in Equation (13)

In this section Equation (13)will be altered by replacing Z Depth with CTI. This replacement will complete the equation at which point it can be used to estimate the friction expected in the specific cases used in the laboratory. It is also possible to estimate the relative contributions of both the ploughing and surface mechanisms.

After $\mu_{Ploughing}$ was replaced in section 6.5.3 and $\mu_{Surface}$ was replaced in section 6.6.3 the partially finished Equation (13)was:

$$\mu_{Total} = \left(\frac{-70.908 \times E}{E_{Ice}} + 0.2394\right) + \frac{0.00374 \times L_0 \times PCD + 0.3128}{ZDepth + 1}$$

Before Z-Depth can be replaced in Equation (13) the relationship of Z-Depth to CTI must be calculated. This is done by finding the equation of the line of best fit of the correlation and re-arranging to find Z-Depth. As before Matlab provides this equation when the correlations are calculated. Once again the equation is different at the three

different speeds. Only 0.1m/s is presented here as an example. The complete equations for the friction tests at 0.01m/s and 1m/s are presented in section 6.7.3

$$ZDepth = -0.3445 \times CTI + 32.825 \tag{14}$$

As discussed in section 6.5.3 it is necessary to consider if the equation being created makes sense. In this case, the inclusion of CTI does not cause any issues as it is a Unitless measurement so will not affect the relationship between the measured properties of the snow and the coefficient of friction which is also unitless. This means Equation (14) can now be included in the overall formula for µ total (Equation (13)). The resulting equation is presented below (Equation (15)). This is the completed equation for µ total at a testing speed of 0.1m/s.

$$\mu_{Total} = \left(\frac{-70.908 \times E}{E_{Ice}} + 0.2394\right) + \frac{0.00374 \times L_0 \times PCD + 0.3128}{-0.3445 \times CTI + 33.825} \tag{15}$$

Where:

E_{Ice} = 9330 MPa

E = Compressive effective modulus measured at 50mm/min (MPa)

L_0 = 10mm

PCD = The measured peak count density (Peaks/mm)

CTI = The measured CTI of the snow

The same process was carried out for all friction test speeds, the resulting equations are presented below Equation (16) & Equation (17)represent 0.01m/s and 1m/s test speeds respectively.

$$\mu_{Total} = \left(\frac{-105.429 \times E}{E_{Ice}} + 0.2394\right) + \frac{0.00676 \times L_0 \times PCD + 0.2172}{-0.2911 \times CTI + 27.972} \quad (16)$$

$$\mu_{Total} = \left(\frac{-67.176 \times E}{E_{Ice}} + 0.5059\right) + \frac{0.00277 \times L_0 \times PCD + 0.3262}{-0.3707 \times CTI + 35.304} \quad (17)$$

Where:

E_{Ice} = 9330 MPa

E = Compressive effective modulus measured at 50mm/min (MPa)

L_0 = 10mm

PCD = The measured peak count density (Peaks/mm)

CTI = The measured CTI of the snow

6.8 Comparison of calculated µ Total with Measured µ

In order to confirm Equations (15), (16) & (17) are of practical use, it is necessary to attempt to calculate the coefficient of friction achieved for each snow. If the calculated values correlate well with the measured values of friction using the 4 siped rubber sample it confirms the equation can be used to estimate the coefficient of friction by measuring three properties of the snow.

Presented below are the comparisons of calculated friction with measured friction for the artificial snows. As stated before it was not possible to measure the roughness of

the natural snow using the current profilometer so conclusions must be made without this data.

Figure 6.14 shows the comparison of the measured friction from the 4 siped sample and the calculated μ total for the same snows at 0.1m/s. There are some variations in the actual values for the measured and calculated friction, this is to be expected when multiple variables each with relatively large errors and non-perfect correlations are combined and could potentially be corrected by fine-tuning the equation to be more specific to the test speed it is relating to.

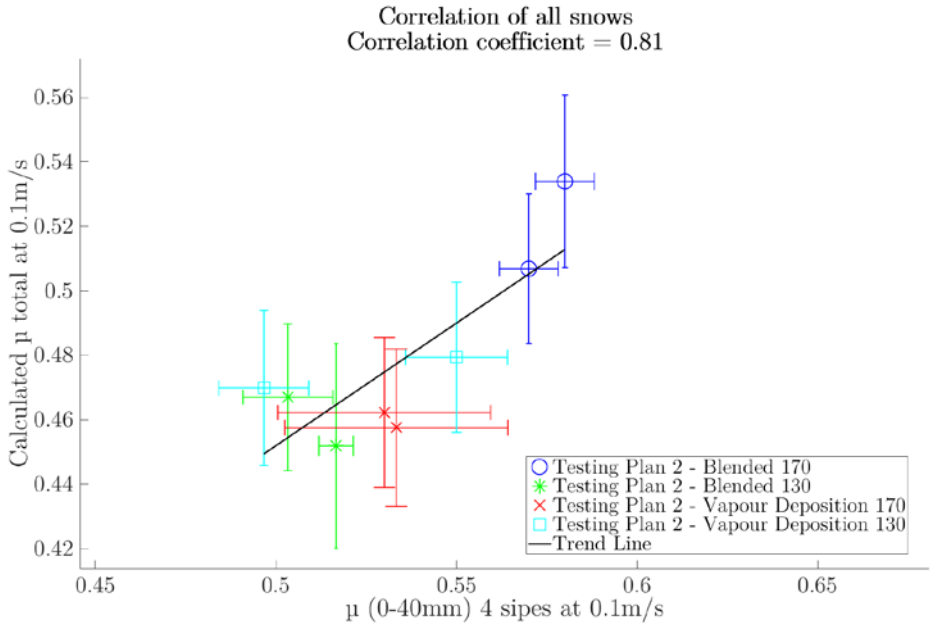

Figure 6.14 - Correlation of Coefficient of friction calculated from overall formula and measured friction when tested at 0.1m/s

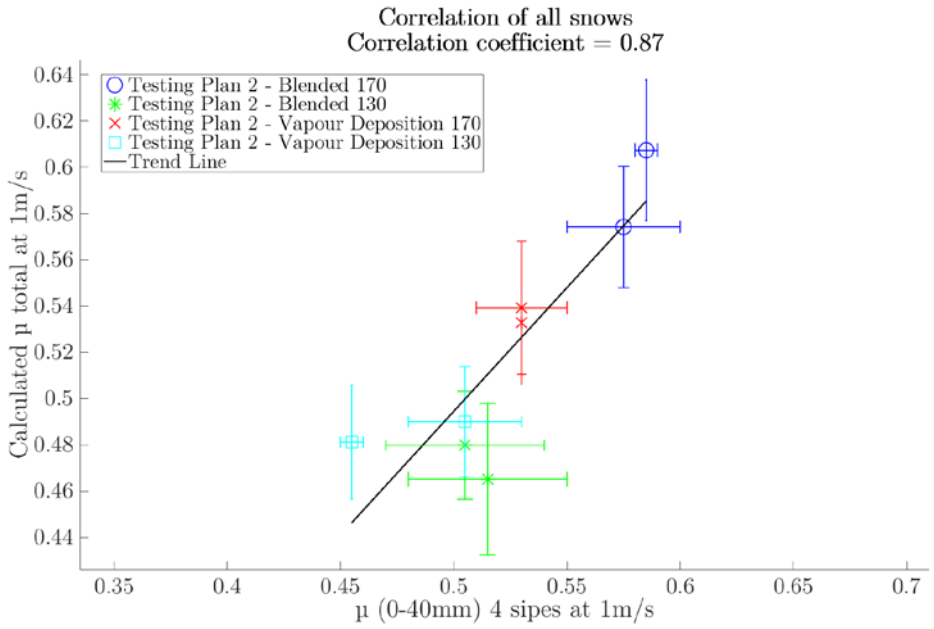

Figure 6.15 - Correlation of Coefficient of friction calculated from overall formula and measured friction when tested at 1m/s

Figure 6.15 shows the comparison of the measured friction from the 4 siped sample and the calculated μ total for the same snows at 1m/s. It shows a very similar level of correlation to the 0.1m/s results, again there are some variations in the specific values being calculated compared to the measured ones.

At speeds of 0.1m/s and 1m/s, the correlation of the calculated values of friction and the measured values correlate well, this is not the case when looking at the results at 0.01m/s. Figure 6.16 shows these results, it is clear there is almost no correlation between the measured and calculated values and the specific values being calculated are very different from those being measured. This is most likely due to a change in friction mechanism which is occurring at this lower speed. It is likely that there is little to no fluid film lubrication occurring at this speed. This means an entirely different formula would be required when attempting to calculate the friction when there is no fluid film lubrication. An additional complexity to add to this is the fact that the speed at which

this transition occurs will vary with the ambient temperature. This is beyond the scope of what is being considered here. What is presented here is only one possible interpretation of these results. Without further data and understanding of the mechanisms, it would be fruitless to continue countless iterations of the formulas.

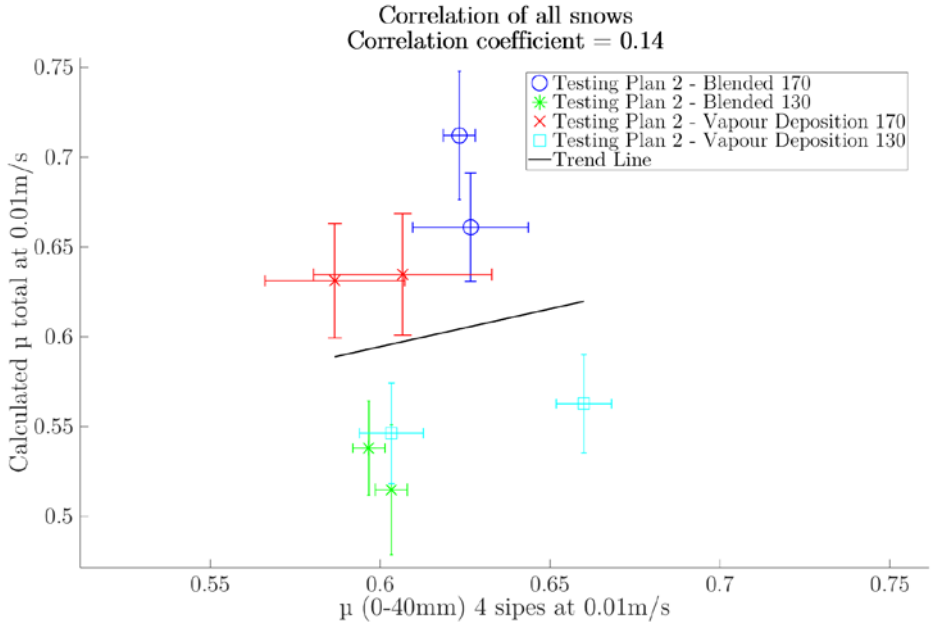

Figure 6.16 - Correlation of Coefficient of friction calculated from overall formula and measured friction when tested at 0.01m/s

6.9 Summary

This chapter details the process of comparing the snow properties to the measured coefficient of friction. Carrying out this work means it is now possible to estimate the coefficient of friction of a specific rubber sample on our artificial snows. In addition, by examining the relative contributions of effective modulus, peak count density and CTI it is possible to estimate the relative contribution of the different friction mechanisms. For example if one snow had a high peak count density and a high effective modulus, it may have the same total friction as snow which had a low peak count density and a low effective modulus, except now it is possible to understand that although the total friction is the same the mechanisms relating to the friction are different with one snow exhibiting a much higher surface contribution than the other.

There are many challenges and potential sources of error throughout this chapter, however, the key discussion which affected the overall correlations and the success of the formula was the starting point: the selection of the initial formula for calculating μ ploughing. There are many different ways this can be interpreted by selecting different coefficients with the aim of achieving different starting conditions. Each change which is made to the calculation of μ ploughing has a profound effect on the outcome of the equation.

7 Conclusions and Future Work

7.1 Conclusions

The aim of this work was to identify which snow properties contribute to the friction of tyres on snow and the mechanisms by which they do so. This was achieved by completing a comprehensive study of the mechanical properties, examination of the microstructure and measurement of the friction behaviour on both artificial and natural snows. Extensive work has been carried out developing new testing methods: shear testing and surface profilometry, and using existing test methods: compression testing, density testing, friction testing and X-ray microtomography to examine high-density snow (420kg/m^3 to 600kg/m^3) of different microstructures. For the first time, all these results are drawn together, to further understanding of friction mechanisms and to develop an empirical formula for predicting the coefficient of friction of rubber on snow.

Key conclusions drawn from this work are:

1. An empirical formula was developed which allows the prediction of total friction at 0.1m/s and 1m/s from measurement of a snow's compressive effective modulus, peak count density and snow compaction (CTI). In addition, by examining the relative values of these measurements it is now possible to predict the relative contribution of both surface and ploughing mechanisms.
2. A new method of using a contact profilometer to measure surface roughness properties has been developed. This avoids the labour intensity of hand tracing the profiles as was done by (Ella, 2014) but also avoid the cost and complexity of calculating roughness from optical or X-ray measurements. This contact profilometry method is able to pick up subtle differences between different snow surfaces that relate to the friction behaviour of the snow.
3. By using a newly developed 3 axis mount for the profilometer it is now possible to create a 3D profile of the snow surfaces, this provides a clearer visualisation

of the differences that snow microstructure has on the surface characteristics of the snow and can allow for different surface analysis procedures to be carried out computationally.

4. Further microstructure characterisation is now possible using a newly developed cold stage. This allows imaging of the snow using X-ray microtomography. With resolutions as low as 10µm XMT allows a more in-depth examination of various features of the snow microstructure such as porosity, grain coordination number and grain size distribution.
5. The simplification of an established method of manufacturing artificial snow by vapour deposition has proved to be successful at creating a snow with very different properties and microstructure to artificial snows previously created in our group.
6. A successful method of collecting natural snow from the field was developed. This allows the comparison of artificial snows to natural snows in order to confirm the relevance of laboratory testing to real-world environments.
7. An in-depth analysis of the frictional behaviour of analytical rubber samples was carried out. By examining features of the friction curves such as the flexing of the sipes and the way friction alters over various test lengths a better understanding of how different rubber samples interact with the snow is achieved.
8. There is a strong correlation of ploughing friction with the compressive strength of snow, specifically the effective modulus of the snow when tested at 50mm/min is the best measurement to correlate with ploughing friction.
9. There is a strong correlation of surface friction with the surface roughness of the snow, specifically the peak count density.

10. There is a strong correlation between the penetration of siped samples into the snow and the CTI penetration test.

7.2 Future Work

In addition to the work carried out relating snow microstructure and properties to the grip of winter tyres, it is clear that there are many possibilities for additional research in many of the areas which have been explored in this PhD.

All the snow testing carried out was completed at a temperature of -10°C. This was done to try to keep the snow properties as consistent throughout the day and from tray to tray. By testing at different temperatures it is would be possible to gain a better understanding of how the mechanical properties will vary with temperature. In addition, it will be possible to investigate the friction mechanism change occurring between speeds of 0.01m/s and 1m/s at -10°C to determine if the mechanism change is temperature dependent. In addition to testing at different temperatures, testing the friction at different speeds would give a clearer understanding of the change in mechanisms (fluid film lubrication becoming more dominant at higher speeds).

A more in-depth study of the surface roughness of the snow would aid in the understanding of surface friction. By examining both the large protuberances made up of grains as a whole and the much smaller features seen on the surface of the individual grains it would be possible to investigate which feature is having the greatest effect on surface friction. In addition, if measurement of surface roughness was carried out both before and after friction testing it would be possible to examine the changes to specific areas or even specific grains as a result of the friction. If the measurement of 3D surface profiles could be automated in order to rapidly generate a 3D surface it would mean more samples could be analysed and compared giving the opportunity to perform more in-depth analysis and comparisons of the 3D surfaces which are not possible when examining 2D traces.

A significant proportion of the time spent working on the X-ray microtomography for this study was spent on developing the required cold stage and the protocol for its use. Only limited examination of the snow microstructure was carried out, there is far more to be gained from examining the 3D structure of the snow, for example examining a piece of the snow test track both before and after friction testing, it could be possible to see features such as changes to the surface roughness, compression of the snow and how that had affected the intergranular bonds.

The behaviour of snow in compression is complex, especially when looking at different compression rates. Snow exhibits a ductile to brittle transition at a certain compression rate, which depends on the snows microstructure (approximately 20mm/min). A study into the way the compression mechanisms change with various microstructure and a comparison to natural snow would bring greater understanding of the link between compressive failures and snow microstructure.

Finally, carrying out further study on snows with a wide variety of microstructures, especially concentrating on natural snows could verify the results of the six different snows presented in this study.

8 Appendices

8.1 Appendix 1 - Mechanical Tests used on snow

Reference	Test Method	Temperature	Density	Snow Details	Further Details	Results	Discussion
(Salm, 1982)	Uniaxial Compression	-10	335kg/m3	Faceted grain surfaces & weak intergranular bonding		Graph of free energy dissipation vs time. Varying deformation rate for 3 different load paths	Thermodynamic theory meaning the deformation and failure can be expressed in terms of energy
(Ramseier et al., 1963, Mellor, 1964)	Unconfined compression	-50	200 - 700 kg/m3	Snow samples taken and tested at south pole	cylindrical samples in manually controlled press (proving ring + dial gauge)	Graph of Density vs compressive strength (kg/cm2)	All samples less than 420kg/m3 had very low strength. Above 420 approximate linear relationship
(Butkovich, 1956)	Unconfined compression	-10	350-600kg/m3		cylindrical samples in manually controlled press (proving ring + dial gauge)	Graph of Density vs compressive strength (kg/cm2)	All samples less than 400kg/m3 had very low strength. Above 400 approximate linear relationship represented by the empirical eq $\sigma c = 1418\ (\gamma - 0.39)$ where

							σc is unconfined compressive strength, γ = density
Mellor 1964	Tensile Test	-10	200 - 700kg/m3		Beam test	Graphs of Tensile strength as a function of density	Widely differing grain textures found in low density snow lead to considerable strength variations for a given density. Low strength below 420kg/m3
Mellor 1964	Tensile Test	-10	200 - 420kg/m3	No common grain form between snow samples or tests	Test carried out by Bucher, Butkovich, Haefeli, Bader et al.	Graphs of Tensile strength as a function of density	No correlation between density and strength below 400kg/m3
(Butkovich, 1956)	Centrifugal Tensile test	-10	300 - 440kg/m3	Different density's as a result of extraction from different depths of snowpack	any tests on higher density snows limited by rpm of centrifuge	Table of Average density and average tensile strength	Other study at the university of Minnesota confirmed these results

(Butkovich, 1956)	Ring Tensile Test	-10	450-727kg/m3	Different densities as a result of extraction from different depths of snowpack		Table of average density and average ring tensile strength	
(Butkovich, 1956)	Double Shear Test	-10	420 - 730 kg/m3	12 inch length 3 inch diameter core of snow from 100ft pit		Sketches of failure mechanisms. Table + graph of density vs Shear strength	Different failure mechanisms for different densities of snow. Below 500kg/m3 failure occurred on one shear plane, above failure occurs on both planes. Lateral pressure on the sample influence the shear strength (seen in graphs). Significantly lower shear strength and high rates.
(Butkovich, 1956)	Torsional Shear Test	-10	500-640 kg/m3	3 Inch diameter cores	Base had to be packed with slush and refrozen to form square torsion mount	Images of failed samples, table of results and graph of density vs torsional strength	Fast rate used to produce plastic response. Failure as a typical 45° helical torsion break, usually seen in brittle materials

(Perla et al., 1982)	Shear Frame Test	-2 to -25	18 - 531kg/m3	Multiple different snow types with multiple densities for each		Table of Density/shear index for 6 different snow types	
(Butkovich, 1956)	Disaggregation of Snow	-10	340 - 570 kg/m3	3 inch diameter snow core from various depths		Graph and table of results of disaggregation	Rotating spiked wheel measuring giving the work per unit volume to disaggregate the snow in lbs/in3
(Mellor, 1964)	Penetration Resistance	-3	70 - 320kg/m3			Pictures of failure mechanisms. Graphs of depth vs plate stress	Flat surface forced into snow with a large depth and lateral extend compared to the indenting plate. Notes different failure mechanisms based on loading rate and density. Shearing at plate edges for ULD snow. Stress bulb on medium density.

8.2 Appendix 2 - Design for Deben XMT Coolstage

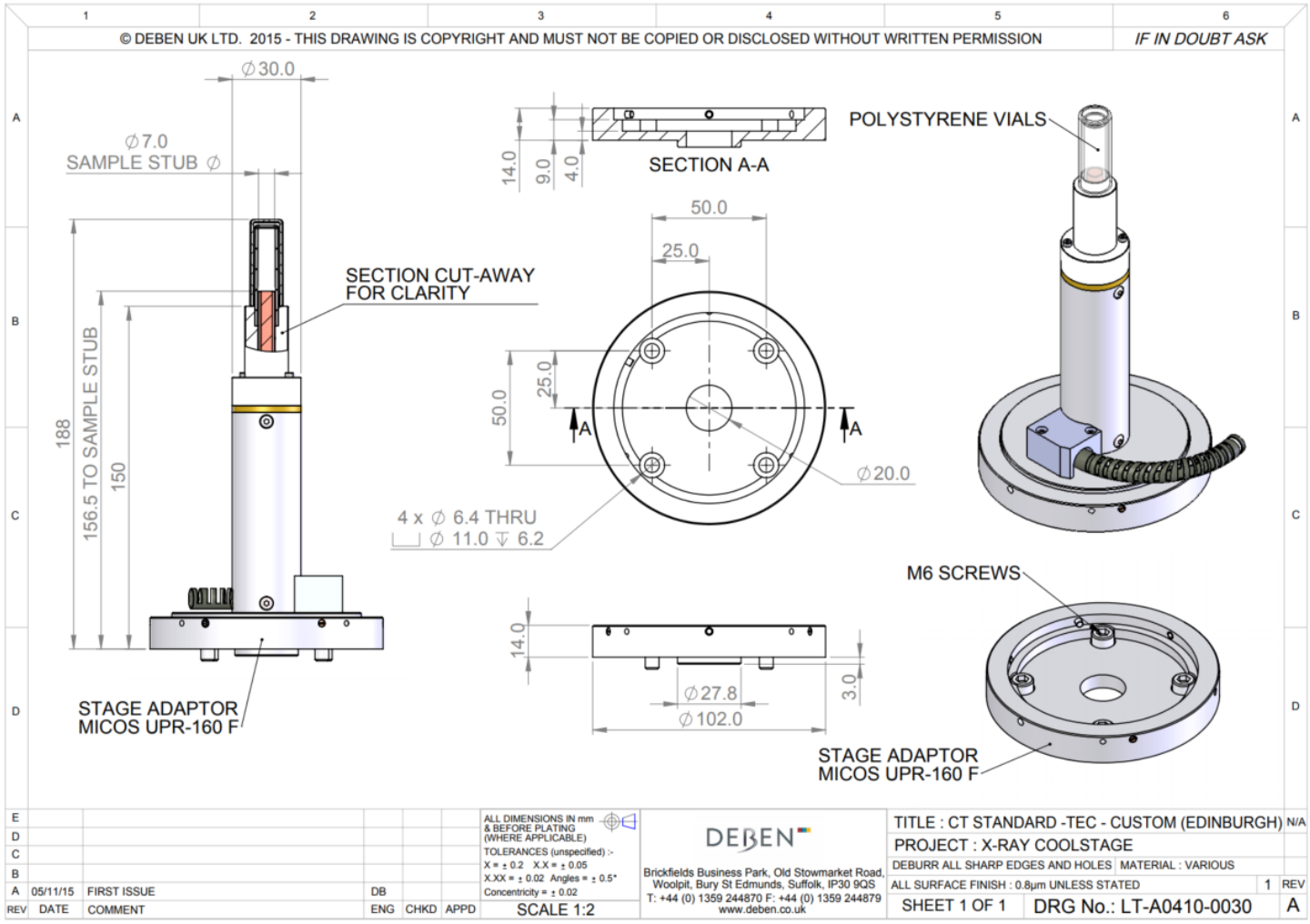

9 Literature References

Barnes, P., D. Tabor and J. Walker, C, F. (1971). "The Friction and Creep of Polycrystalline Ice." Procedings of the Royal Society of London Series A, Mathematical and Physical Sciences **324**(1557): 127-155.

Bäurle, L., T. U. Kaempfer, D. Szabó and N. Spencer, D. (2007). "Sliding friction of polyethylene on snow and ice: Contact area and modeling." Cold Regions Science and Technology **47**(3): 276-289.

Bhushan, B. (2013). Introduction to tribology Second Edition. Tribology series, John Wiley & Sons, Ltd: 1 online resource.

Blackford, J., R., G. Skouvaklis, M. Purser and V. Koutsos (2012). "Friction on ice: stick and slip." Faraday Discussions **156**: 243.

Bowden, F., P. (1953). "Friction on Ice and Snow." Procedings of the Royal Society of London Series A, Mathematical and Physical Sciences **217**(1131).

Bowden, F., P. and T. Hughes, P. (1939). "The Mechanism of Sliding on Ice and Snow." Proceedings of the Royal Society A: Mathematical, Physical and Engineering Sciences **172**(949): 280-298.

Bruker. (2011). "SkyScan2011 X-Ray nanotomograph." Retrieved 04/08/2017, 2017, from http://bruker-microct.com/products/2011.htm.

Brun, E. and L. Rey (1987). "Field Study on Snow Mechanical Properties." Avalanche Formation, Movement and Effects **162**: 183 - 192.

Butkovich, T., R. (1956). "Strength Studies of High-Density Snow." Snow Ice and Permafrost Research Establishment **Research Report 18**.

Camponovo, C. and J. Schweizer (2001). "Rheological measurments of the viscoelastic properties of snow." Annals of Glaciology **32**: 44-50.

Choi, J., H., J. Cho, R., J. Woo, S. and K. Kim, W. (2012). "Numerical investigation of snow traction characteristics of 3-D patterned tire." Journal of Terramechanics **49**(2): 81-93.

Colbeck, S., C. (1992). "A Review of Processes that control snow friction." Cold Regions Research & Engineering Laboratory **92-2**.

Coléou, C., B. Lesaffre, J. Brzoska, W. Ludwig and E. Boller (2001). "Three-dimensional snow images by X-ray microtomography." Annals of Glaciology **32**(1): 75-81.

Degarmo, E., J. Black, T. and R. Kohser, A. (2003). Materials and Processes in Manufacturing.

Domine, F., J. Bock, S. Morin and G. Giraud (2011). "Linking the effective thermal conductivity of snow to its shear strength and density." Journal of Geophysical Research **116**(F4).

Ella, S. (2014). Rubber snow interface and friction. PhD, The University of Edinburgh.

Ella, S., P.-Y. Formagne, V. Koutsos and J. Blackford, R. (2013). "Investigation of rubber friction on snow for tyres." Tribology International **59**: 292-301.

Erdogan, G. (2009). "Tire Modeling: Lateral and Longitudinal Tire Forces." Retrieved 13/01/2017, 2017, from http://www.menet.umn.edu/~gurkan/Tire%20Modeling%20%20Lecture.pdf.

Evans, D., C, B., J. Nye, F. and K. Cheeseman, T. (1976). "The Kinetic Friction of Ice." Procedings of the Royal Society of London Series A, Mathematical and Physical Sciences **375**(1651): 493-512.

Gadelmawla, E. S., M. M. Koura, T. M. A. Maksoud, I. M. Elewa and H. H. Soliman (2002). "Roughness parameters." Journal of Materials Processing Technology **123**(1): 133-145.

Hagenmuller, P., T. Theile, C. and M. Schneebeli (2014). "Numerical simulation of microstructural damage and tensile strength of snow." Geophysical Research Letters **41**(1): 86-89.

Kennedy, F., E., E. Schulson, M. and D. Jones, E. (2000). "The friction of ice on ice at low sliding velocities." Philosophical Magazine A **80**(5): 1093-1110.

Ketcham, R., A. and W. Carlson, D. (2001). "Acquisition, optimization and interpretation of X-ray computed tomographic imagery: applications to the geosciences." Computers & Geosciences **27**: 381-400.

Lang, T., E. and J. Dent, D. (1982). "Review of Surface Friction, Surface Resistance and Flow of Snow." Review of Geophysics and Space Physics **20**(1): 21-37.

Lee, J., H. (2009). "A new indentation model for snow." Journal of Terramechanics **46**.

Lee, J., H. (2011). "Finite element modeling of interfacial forces and contact stresses of pneumatic tire on fresh snow for combined longitudinal and lateral slips." Journal of Terramechanics **48**(3): 171-197.

Libbrecht, K., G. (2005). "The physics of snow crystals." Reports on Progress in Physics **68**(4): 855-895.

Lintzen, N. (2013). "Mechanical Propeties of Artificial Snow." Licentiate Thesis, Lulea University of Technology.

Marmo, B., A., J. Blackford, R. and C. Jeffree, E. (2005). "Ice friction, wear features and their dependence on sliding velocity and temperature." Journal of Glaciology **51**(174): 391-398.

Mavros, G. (2005). Tyre Models for Vehicle Handling Analysis under Steady-State and Transient Manoevers. PhD, Loughborough University.

Mellor, M. (1964). "Properties of Snow." Cold Regions Research & Engineering Laboratory **Monograph 3-A1**.

Mellor, M. (1975). "A Review of Basic Snow Mechanics." 251-291.

Michelin (2001). The tyre GRIP. Société de Technologie Michelin 23, rue Breschet, 63000 Clermont-Ferrand, Société de Technologie Michelin.

Mössner, M., G. Innerhofer, K. Schindelwig, P. Kaps, H. Schretter and W. Nachbauer (2013). "Measurement of mechanical properties of snow for simulation of skiing." Journal of Glaciology **59**(218): 1170-1178.

Muro, T. and R. Yong, N. (1980). "Rectangular plate loading test on snow." Journal of the Japanese Society of Snow and Ice **42**(1): 17-24.

Murthy, V., N, S. (2002). Principles and Practices of Soil Mechanics and Foundation Engineering, CRC Press.

Nakajima, Y. (2003). "Analytical model of longitudinal tire traction in snow." Journal of Terramechanics **40**(1): 63-82.

Pacejka, H. B. (2012). "Tire and Vehicle Dynamics, 3rd Edition." Tire and Vehicle Dynamics, 3rd Edition: 1-632.

Perla, R., T. Beck, M, H. and T. Cheng, T. (1982). "The Shear Strength Index of Alpine Snow." Cold Regions Science and Technology **6**: 11-20.

Petrenko, V., F. and R. Whitworth, W. (1999). Physics of Ice. Oxford Oxford University Press.

Petrovic, J., J. (2003). "Review Mechanical Properties of Ice and Snow." Journal of Materials Science **38**: 1-6.

Rabinowicz, E. (1984). Wear Coefficients. E. Booser, D. Boca Raton, Florida, CRC Press: 201-208.

Ramseier, R., O. and T. Pavlak, L. (1963). "Unconfined Creep of Polar Snow." Journal of Glaciology **5**(39): 325-332.

Ripka, S., S. Mihajlovic, M. Wangenheim, K. Wiese and B. Wies (2009). Tread blockmechanics on ice & snow surfaces studied with a new

high speed linear friction test rig. 12 Int Congress Reifen-Fahrwerk Fahrbahn Hannover, VDI-Berichte Nr. 2806: 239-254.

Salm, B. (1982). "Mechancial Properties of Snow." Reviews of Geophysics 20(1): 1-19.

Scapozza, C., F. Bucher, P. Amann, W. J. Ammann and P. Bartelt (2004). "The temperature-and density-dependent acoustic emission response of snow in monoaxial compression tests." Annals of Glaciology, Vol 38 2004 38: 291-298.

Schleef, S., M. Jaggi, H. Lowe and M. Schneebeli (2014). "An improved machine to produce nature-identical snow in the laboratory." Journal of Glaciology 60(219): 94-102.

Schleef, S. and H. Löwe (2013). "X-ray microtomography analysis of isothermal densification of new snow under external mechanical stress." Journal of Glaciology 59(214): 233-243.

Shapiro, L., H., J. Johnson, B. , M. Sturm and G. Blaisdell, L. (1997). "Snow Mechanics - Review of the State of Knowledge and Applications." Cold Regions Research & Engineering Laboratory 97(3).

Shoop, S. (1993). "Terrain characterization for trafficability." CRREL report 93-6.

Shoop, S., R. Haehnel, K. Kestler, K. Stebbings and R. Alger (1999). "Finite Element Analysis of a wheel rolling in snow." Cold Regions Engineering: Putting Research into Practice: 519-530.

Shoop, S., K. Kestler and R. Haehnel (2006). "Finite Element Modeling of Tires on Snow." Tire Science and Technology **34**(1): 2-37.

Sigrist, C. (2006). "Measurement of Fracture Mechanical properties of snow and application to avalanche realease." University of Bern PhD Thesis.

Skouvaklis, G. (2010). Rubber Friction on Ice and Snow Surfaces. PhD, The University of Edinburgh.

Steiakakis, C. (2013). "The Mohr-Coulomb strength criterion." Retrieved 19/10/2014, 2014.

Suga, N. (2016). Metrology Handbook: The Science of Measurment, Mitutoyo (UK) Ltd.